

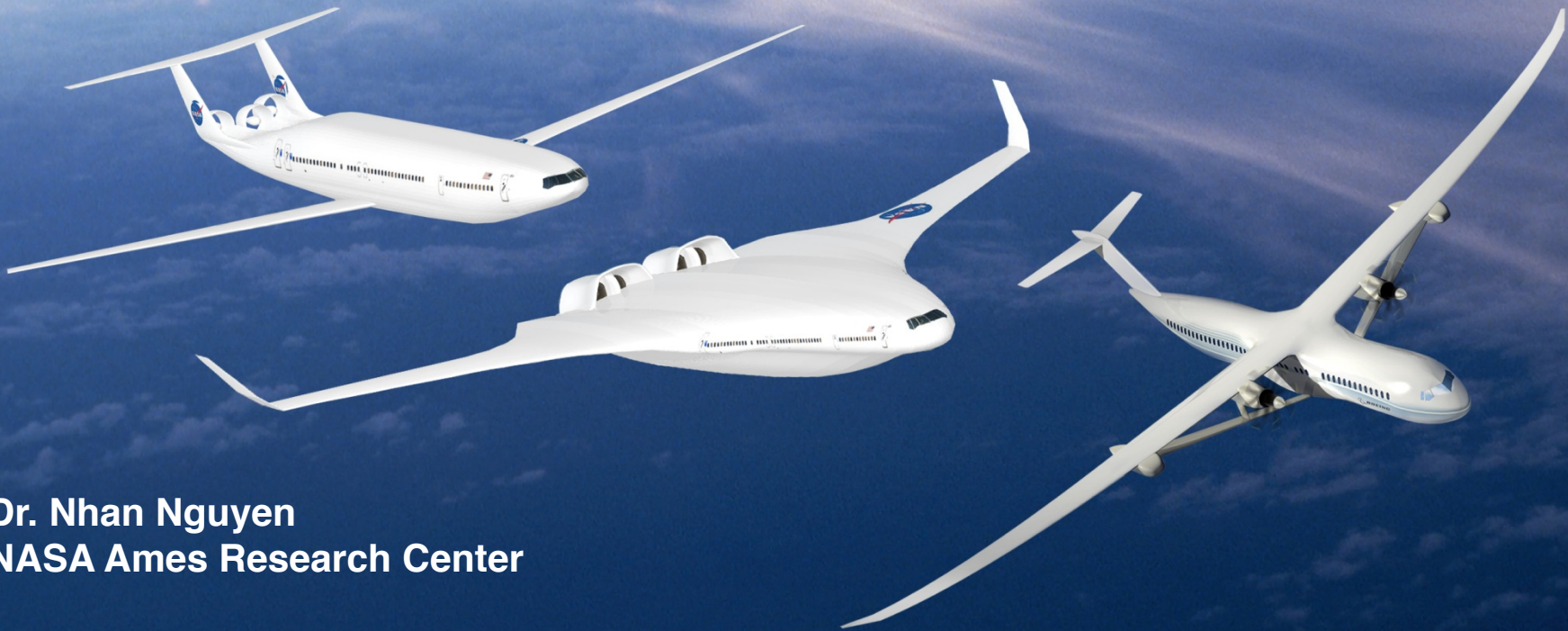
National Aeronautics and Space Administration



Computationally Efficient Transonic and Viscous Potential Flow Aero-Structural Method for Rapid Multidisciplinary Design Optimization of Aeroelastic Wing Shaping Control

Eric Ting
NASA Ames Research Center

Daniel Chaparro
MORi Associates Inc.



Dr. Nhan Nguyen
NASA Ames Research Center

*Advanced Modeling and Simulation (AMS) Seminar Series,
NASA Ames Research Center, June 28, 2017*

www.nasa.gov

Outline

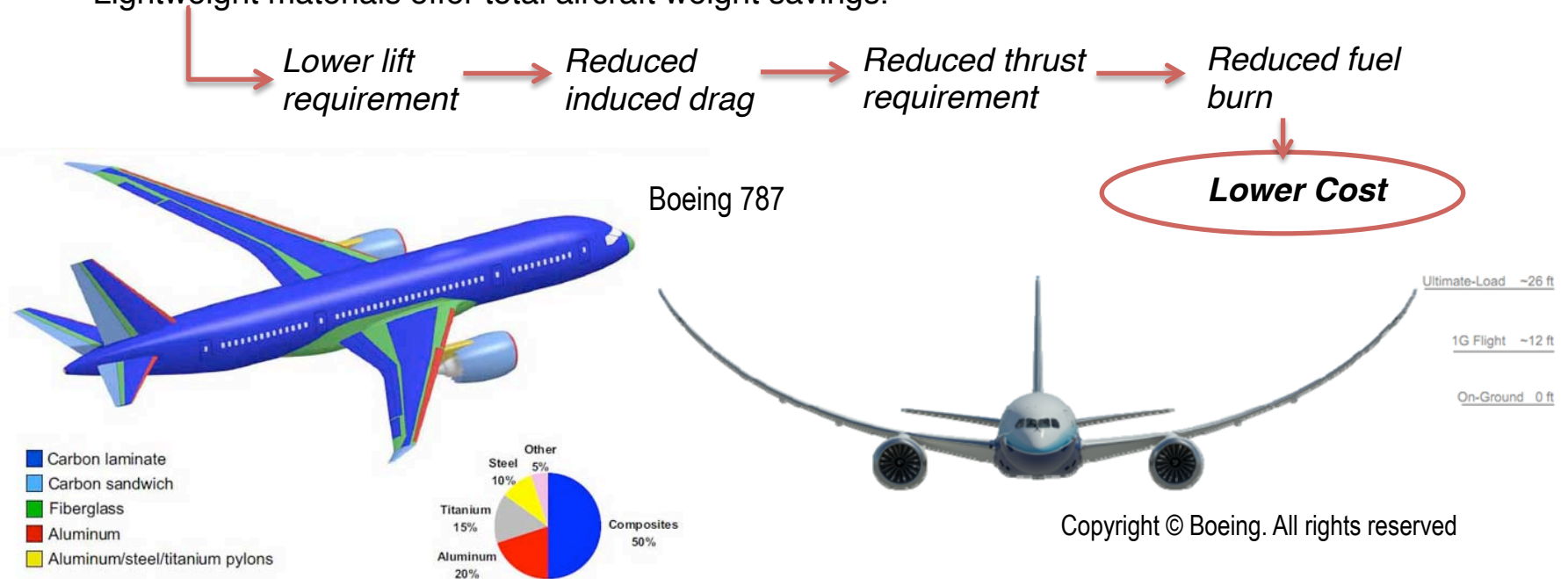


- Introduction
 - Aeroelastic Wing Shaping Control
 - NASA Generic Transport Model (GTM)
 - Variable Camber Continuous Trailing Edge Flap (VCCTEF)
 - Multidisciplinary Design Analysis and Optimization (MDAO/MDO) Framework
- Computationally Efficient Aerodynamic Modeling
 - Coupled Aero-Structural Framework
 - Transonic and Viscous Potential Flow Method
 - Validation
- Structural/Aeroelastic Modeling
 - BEAM3D Finite Element Aeroelasticity
- Flap Optimization
 - Methodology
 - Drag Reduction Results
 - Analysis of Results
- Summary and Future Work

Introduction



- Modern commercial aircraft technology trends is moving towards lightweight, highly flexible, high aspect ratio wing structures.
 - Lightweight materials offer total aircraft weight savings.



- Wing flexibility increases aeroelastic interactions and can adversely impact aircraft performance, structural integrity, stability and control.
- Wing shaping control can be used as a solution to address aerodynamic, structural, and flight control penalties due to wing flexibility.

Aeroelastic Wing Shaping Control Concept



- Wing shaping control is a bio-inspired concept allowing for active tailoring of wing aerodynamics throughout a flight envelope.
 - Aeroelastic wing shaping control can tailor an aeroelastic wing shape to recover optimal aerodynamics at off-design flight conditions.

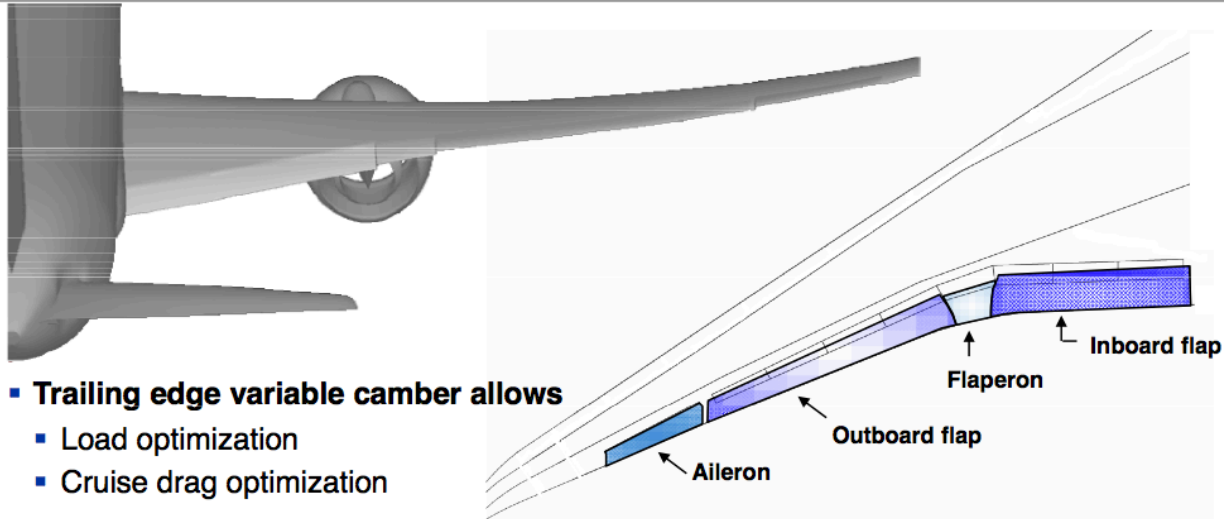


Wing Shaping Control in Modern Transports

- Trailing Edge Variable Camber (TEVC) in Boeing 787

Boeing trailing edge variable camber Committed to 787 in 2005

The next decade in commercial airplane aerodynamics – a Boeing perspective

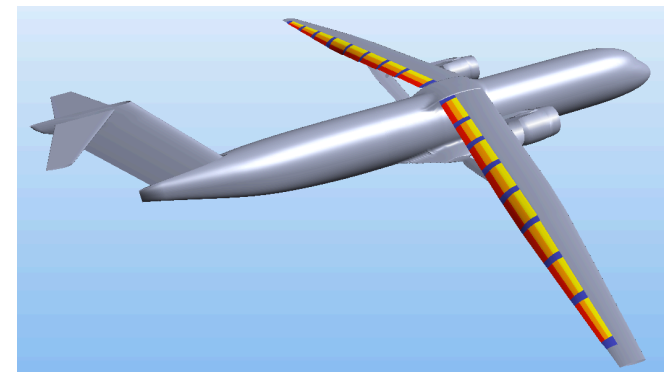
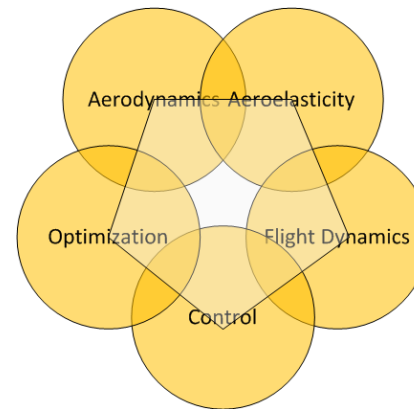


- **Trailing edge variable camber allows**
 - Load optimization
 - Cruise drag optimization
- **In cruise, trailing edge elements are adjusted at regular intervals to minimize drag**
 - Simplified actuation system
 - Small angle variations
 - Up and down movements

Copyright © Boeing. All rights reserved

Performance Adaptive Aeroelastic Wing

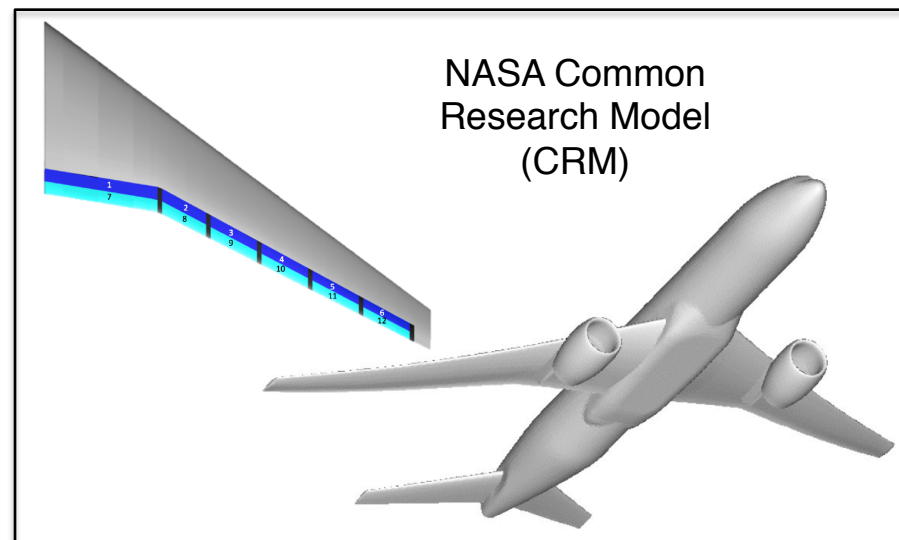
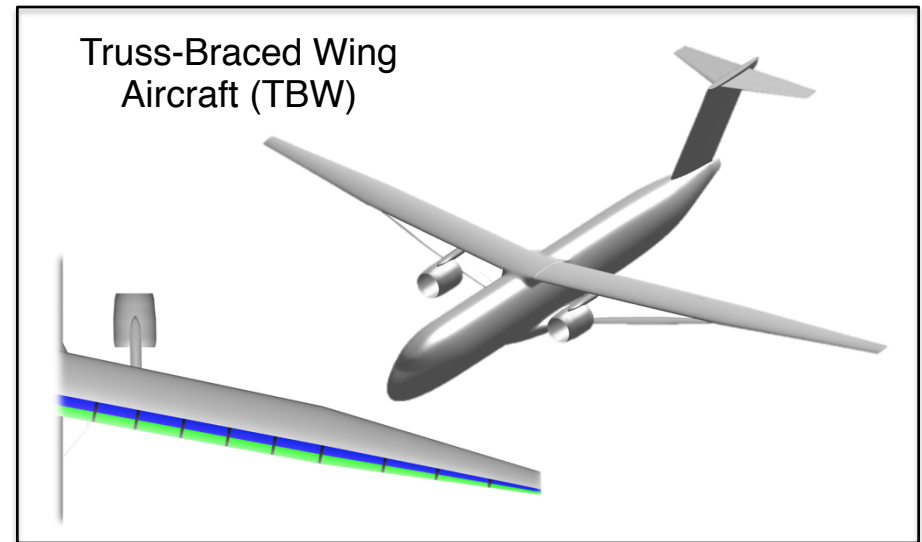
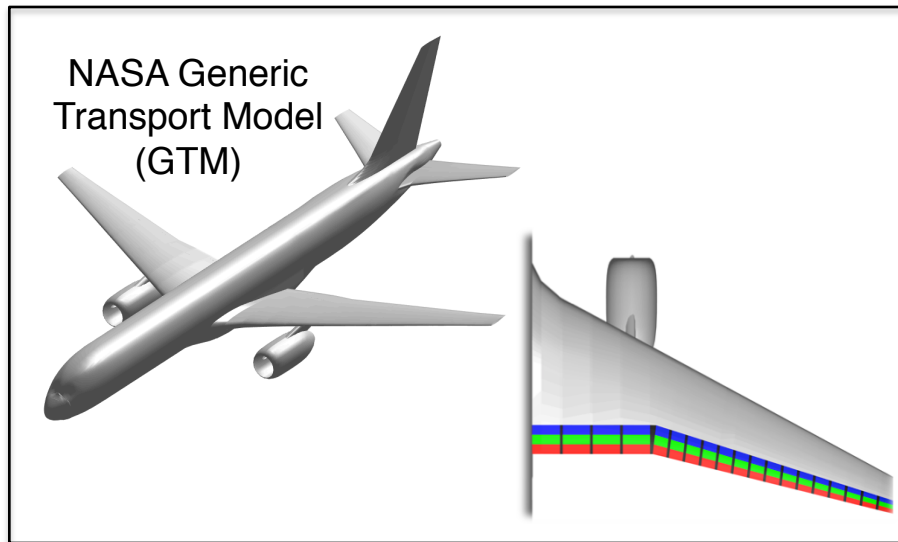
- Performance Adaptive Aeroelastic Wing (PAAW) is a research element under the High Aspect Ratio Flexible Wing technical challenge of NASA ARMD Advanced Air Transport Technology (AATT) project.
- Research objective – Develop wing shaping control technology for flexible wing N+3 transport aircraft for improved aerodynamic efficiency
 - **Multidisciplinary Design, Analysis, and Optimization (MDAO/MDO)** framework development for evaluation of future advanced adaptive wing technology concepts
 - **Variable Camber Continuous Trailing Edge Flap (VCCTEF)** concept investigated as enabling performance adaptive aeroelastic wing technology.



Aircraft Models

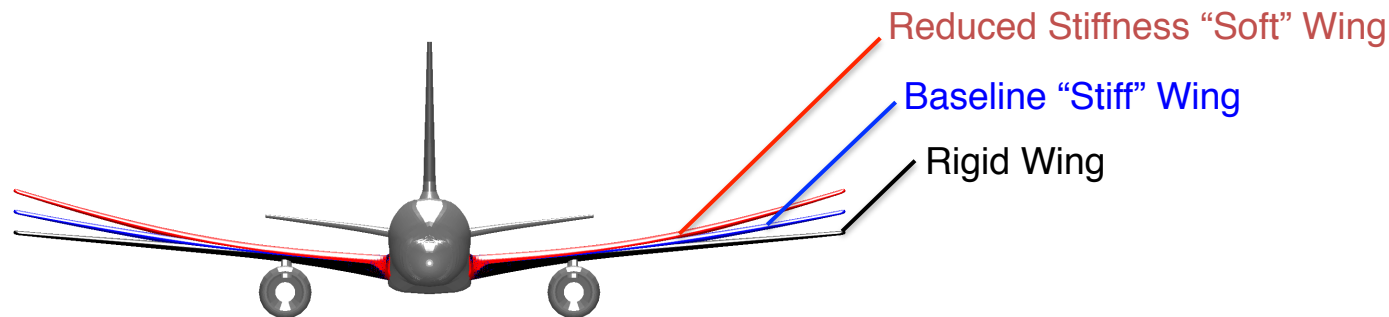


- Different aircraft platforms ranging from current to N+3 configurations utilized for modeling.

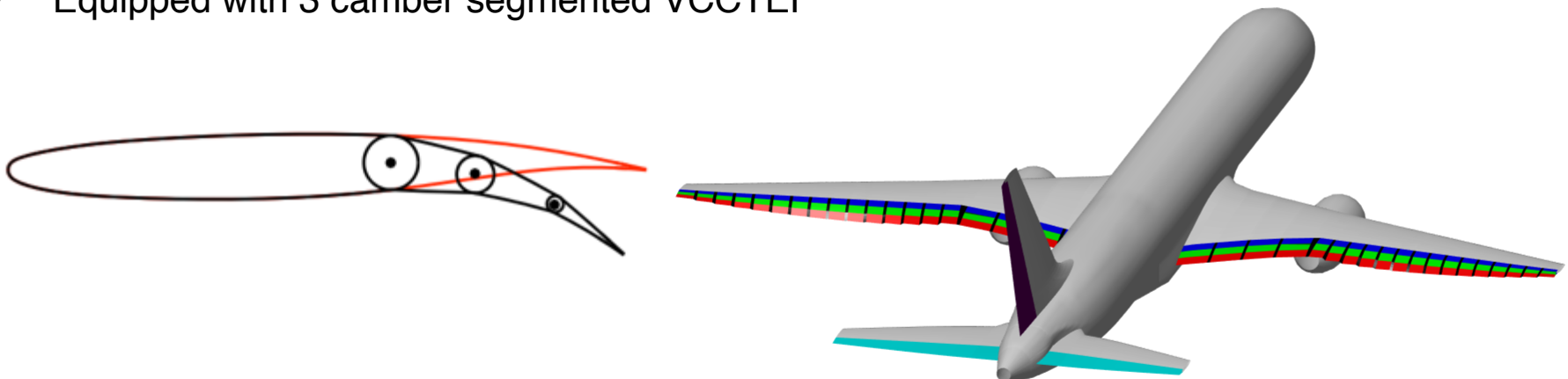


Generic Transport Model (GTM)

- NASA GTM is a notional single aisle, midsize, 200 passenger aircraft representative of a conventional transport configuration.
 - Mid-cruise Mach: 0.797
 - Mid-cruise Altitude: 36,000 ft
 - Cruise $C_L = 0.51$ (Baseline Stiffness), $C_L = 0.497$ (Reduced Stiffness)



- Equipped with 3 camber segmented VCCTEF

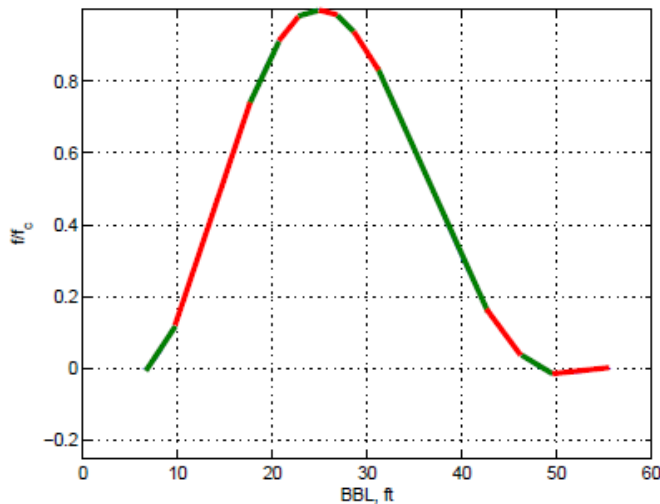


VCCTEF Initial Concept

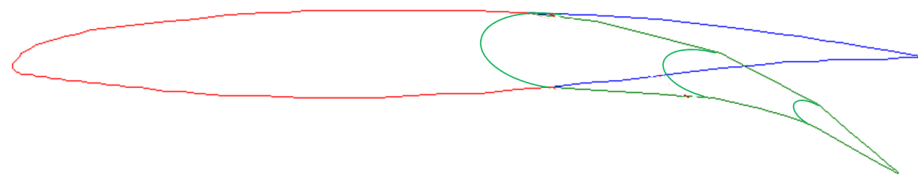
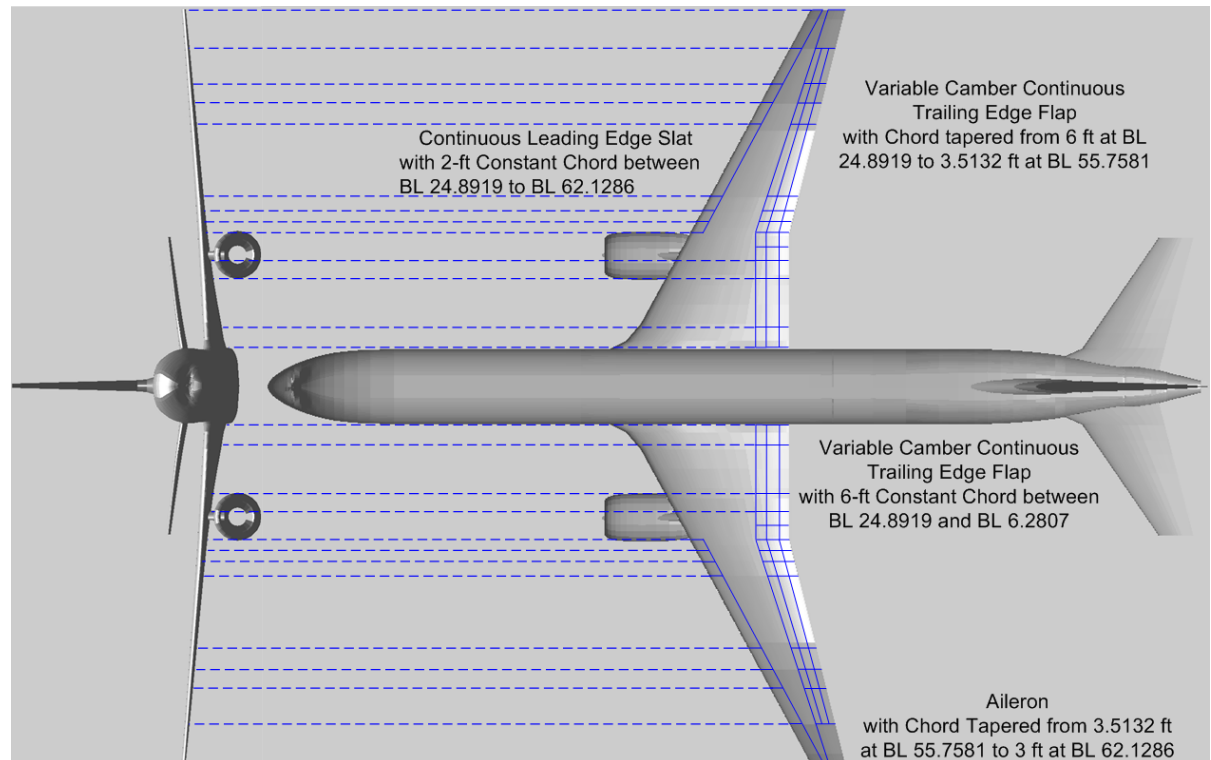


- Initial NASA concept developed in 2010 for GTM

- Elastic wing shapes
- Wing shaping control
- VCCTEF
- Continuous LE slat



Continuous Flap Deflection



Boeing VCCTEF Development



- Boeing Research & Technology (BR&T) concept developed in 2012

FINAL 54 INCH EQUAL CHORD FLAP SECTIONS:

- TWIST SECTIONS WITH 8" SKIN SEPARATOR SECTIONS
- MAIN FLAP - 3 SECTIONS 75" WIDTH – NO TWIST

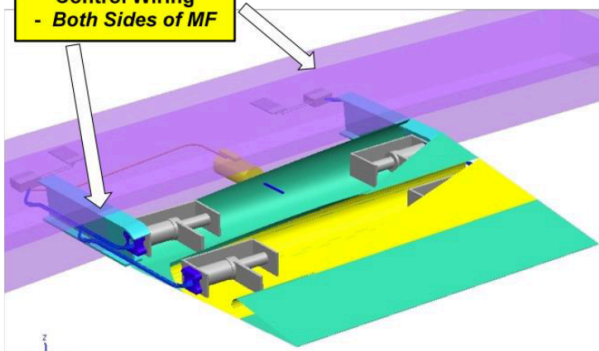
75 Inch Main Flap Actuation Panel Includes –

- Linear Extend Actuator (1-2)
- Shaped Memory Alloy Actuators (4)
- Electro-Mechanical Actuators (2)

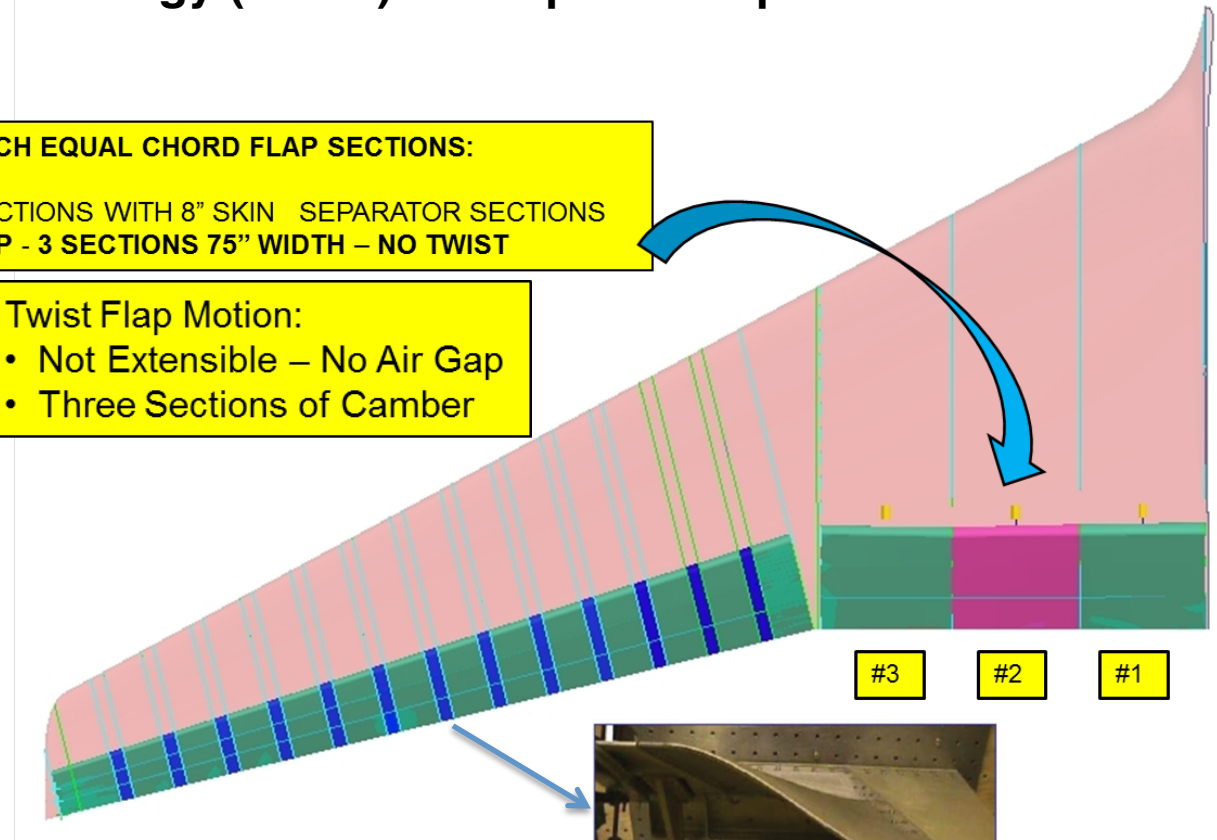
Twist Flap Motion:

- Not Extensible – No Air Gap
- Three Sections of Camber

Electrical Power & Control Wiring
- Both Sides of MF



SMA and EMA Hinge Line Actuation



Conformal Mold Line Material

VCCTEF and Wing Shaping Control Development



FY 2010	Initial concept funded by NASA Innovative Partnership Program (IPP)
FY 2011	NASA Ames (ARC) Intelligent Systems Division (Code TI) in-house investigation
FY 2012	<ul style="list-style-type: none"> Boeing Research and Technology (BR&T) VCCTEF installation layout including actuator selections NASA and BR&T aeroelastic analysis of baseline stiff wing GTM Flight control requirement analysis Multi-objective flight control conceptualization using VCCTEF
FY 2013	<ul style="list-style-type: none"> NASA and BR&T aeroelastic analysis of reduced stiffness wing GTM NASA and BR&T aeroservoelastic state-space modeling NASA ARC Code TI collaboration with Advanced Supercomputing Division (Code TN) for higher order modeling with Euler CFD Wind tunnel test of cruise configuration at University of Washington Aeronautical Laboratory (UWAL)
FY 2014	<ul style="list-style-type: none"> NASA and BR&T aeroelastic flutter suppression NASA and BR&T alternative design trade study of VCCTEF NASA ARC Code TI and Code TN collaboration expanded to include modeling with 2D and 3D RANS OVERFLOW and LAVA CFD. UWAL wind tunnel test of high-lift configuration NASA ARC Code TI aeroelastic analysis of Truss-Braced Wing (TBW)

VCCTEF and Wing Shaping Control Development



FY 2015	<ul style="list-style-type: none">• NASA aeroelastic analysis of TBW with VCCTEF, including drag and load alleviation analysis• NASA collaboration with SSCI for drag minimization with VCCTEF
FY 2016	<ul style="list-style-type: none">• NASA aeroservoelastic ASE flight dynamic modeling and simulation of GTM and TBW with VCCTEF, gust, and multi-objective flight control• NASA viscous RANS CFD analysis of VCCTEF without flexible transition material
FY 2017	<ul style="list-style-type: none">• SSCI and UWAL wind tunnel test of VCCTEF for real-time drag minimization• NASA collaboration between ARC and Langley (LaRC) to develop MDAO optimization of Common Research Model (CRM) for aerodynamic, structural load, and flutter requirements
FY 2018+	<ul style="list-style-type: none">• NASA collaboration with SSCI, UWAL, and BR&T for wind tunnel test of VCCTEF with gust load alleviation• NASA simulation and model of multi-objective flight control of elastic aircraft with VCCTEF technology• NASA integrated MDAO environment for adaptive wing technology evaluation and active wing control• NASA ARC and LaRC collaboration with BR&T for wind tunnel test of higher aspect ratio CRM with wing shaping control

MDAO Framework



MDAO framework includes:

Multi-Fidelity Modeling

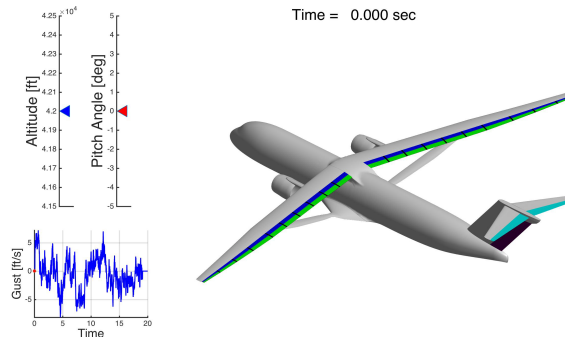
- Multi-fidelity aero modeling (Vorlax, VSPAERO, Cart3D, OVERFLOW, LAVA)
- Aeroelastic FEM (BEAM3D, NASTRAN)
- Coupled aeroelastic FEM with aero codes (Vorlax, VSPAERO, Cart3D, LAVA)
- Flutter analysis

Flight Dynamics

- Dynamics of control actuation
- Dynamic aeroelastic FEM coupled with 6-dof rigid-body flight dynamics

Multi-Disciplinary Optimization

- Aerodynamic optimization for drag reduction (Cart3D, OVERFLOW, Vorlax)
- Multidisciplinary optimization with coupled aeroelasticity (Cart3D, OVERFLOW, Vorlax)



Aeroservoelastic Control

- Aeroservoelastic control (flutter suppression, load alleviation)
- Real-time drag minimization
- Multi-objective flight control for distributed flap system

Control Actuation

- VCCTEF
- Distributed propulsion
- Others (distributed control, active flow control, etc...)

Performance Analysis

- Trajectory optimization to minimize fuel burn
- Mission analysis for energy efficiency

Introduction



- Scope:
 - Develop computationally efficient transonic and viscous flow vortex lattice modeling framework and conduct analysis and VCCTEF optimization of flexible wing GTM transport

MDAO framework includes:

Multi-Fidelity Modeling

- Multi-fidelity aero modeling (Vorlax, VSPAERO, Cart3D, OVERFLOW, LAVA)
- Aeroelastic FEM (BEAM3D, NASTRAN)
- Capabilities to couple aeroelastic FEM with aero codes (Vorlax, VSPAERO, Cart3D, LAVA)
- Flutter analysis

Flight Dynamics

- Dynamics of control actuation
- Dynamic aeroelastic FEM coupled with 6-dof rigid-body flight dynamics

Multi-Disciplinary Optimization

- Aerodynamic optimization for drag reduction (Cart3D, OVERFLOW, Vorlax)
- Multidisciplinary optimization with coupled aeroelasticity (Cart3D, OVERFLOW, Vorlax)

Aeroservoelastic Control

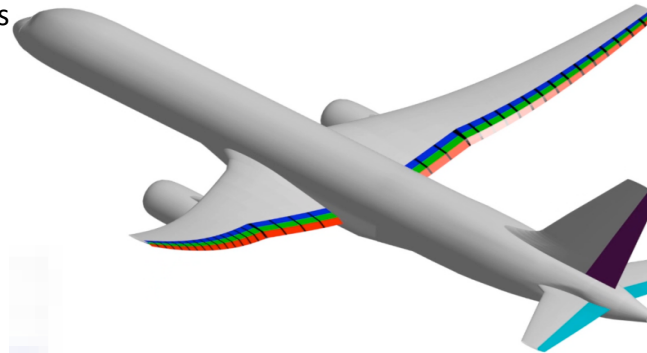
- Aeroservoelastic control (flutter suppression, load alleviation)
- Real-time drag minimization
- Multi-objective flight control for distributed flap system

Control Actuation

- VCCTEF
- Distributed propulsion
- Others (distributed control, active flow control, etc...)

Performance Analysis

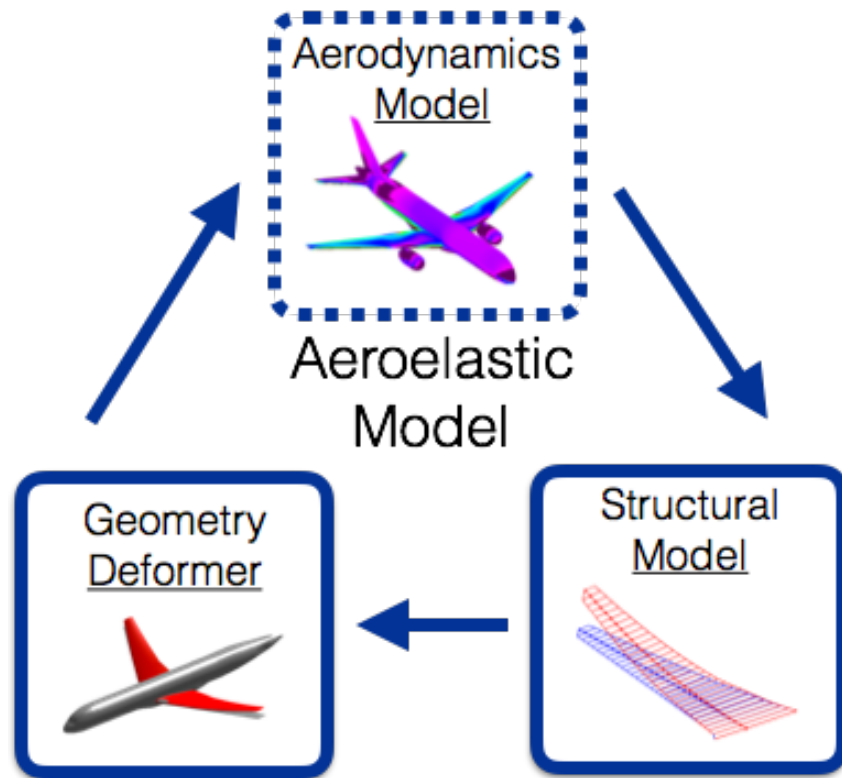
- Trajectory optimization to minimize fuel burn
- Mission analysis for energy efficiency





Computationally Efficient Aerodynamic Modeling

Multi-Fidelity Modeling



Aerodynamic Methods Previously Investigated

- Vortex Lattice Method (Vorlax)
 - Subsonic or fully supersonic potential flow
 - Computationally efficient
 - Mean camber lifting surfaces
 - Inviscid flow
 - Lebofsky et al.
- Euler (Cart3D)
 - Capable of modeling transonic flow
 - More computationally efficient than RANS
 - Flow separation is not captured
 - Inviscid flow
 - Rodriguez et al.
- RANS (LAVA)
 - Capable of modeling viscous boundary layer physics through use of turbulence models
 - Accurate across wide range of Mach and Reynolds numbers
 - Computationally expensive
 - Denison et al.



Aerodynamic Modeling Tools

3D Potential Flow Solver

- Vorlax by Miranda, VSPAERO (In progress)
- Pre/Post Processor: Vorview
- Potential Flow Solver – Inviscid Subsonic or Fully Supersonic Flow

Transonic Small Disturbance Solver (TSD)

- TSFOIL (2D) by Murman, Bailey and Johnson
- Computationally Efficient
- Sequential Mesh Refinement
- Compares Well with Euler Solvers at Moderate Angles of Attack (Chaparro et al)

Integral Boundary Layer Model (IBL)

- Laminar Boundary Layer: Compressible Form of Thwaites' method
- Transition Criteria: Michel's Method
- Turbulent Boundary Layer: Compressible Form of Head's Method
- Compares Well with Xfoil for Subsonic Flow and RANS for Transonic Flow (Fujiwara et al)

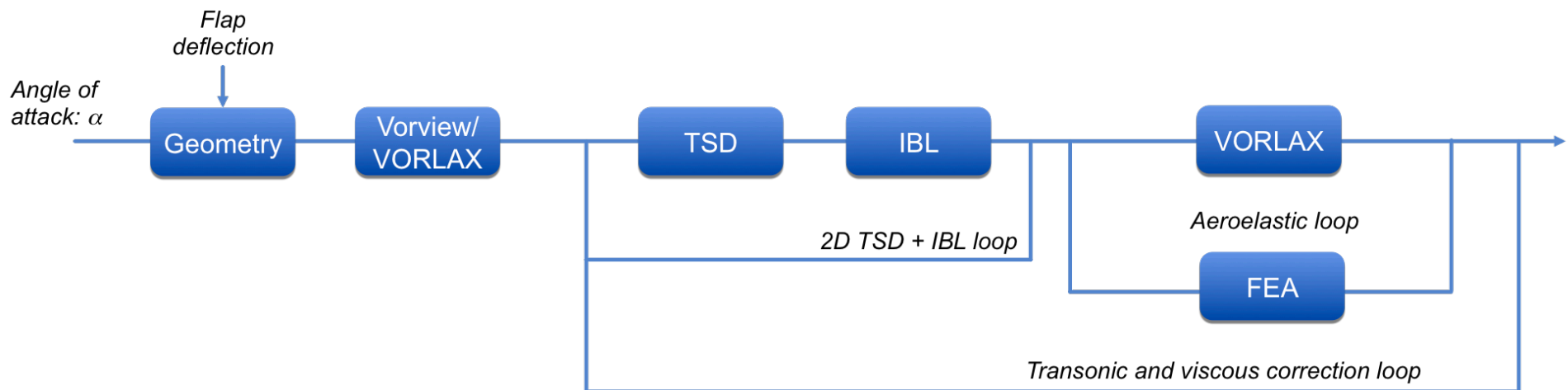
Euler-IBL Model

- MSES by Drela
- Capable of Analyzing Wide Range of Mach and Reynolds Numbers
- Automated Coarsening/Refinement for Robustness and Computational Efficiency



Coupled Aero-Structural Framework

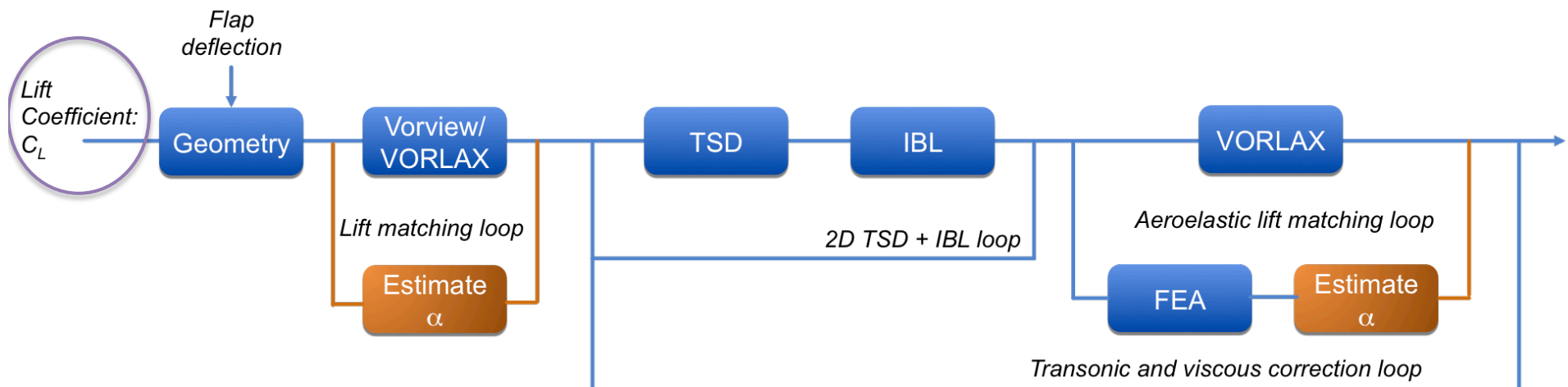
- Geometry deformer deflects the VCCTEF in MATLAB environment and writes input files for the aerodynamic codes
- TSD/IBL loop is placed outside of the aeroelastic loop to improve computational efficiency
- The FEA model is coupled to the VLM model via translation and rotation of the VLM panels





Coupled Aero-Structural Framework

- Geometry deformer deflects the VCCTEF in MATLAB environment and writes input files for the aerodynamic codes
- TSD/IBL loop is placed outside of the aeroelastic loop to improve computational efficiency
- The FEA model is coupled to the VLM model via translation and rotation of the VLM panels

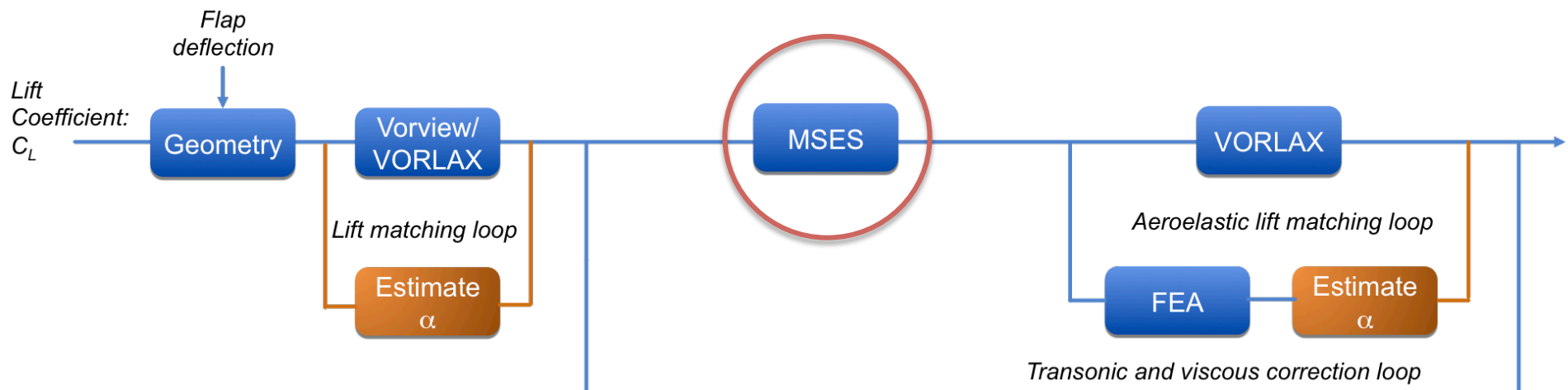


Wall-clock time is comparable if lift coefficient or angle of attack is specified



Coupled Aero-Structural Framework

- Geometry deformer deflects the VCCTEF in MATLAB environment and writes input files for the aerodynamic codes
- TSD/IBL loop is placed outside of the aeroelastic loop to improve computational efficiency
- The FEA model is coupled to the VLM model via translation and rotation of the VLM panels

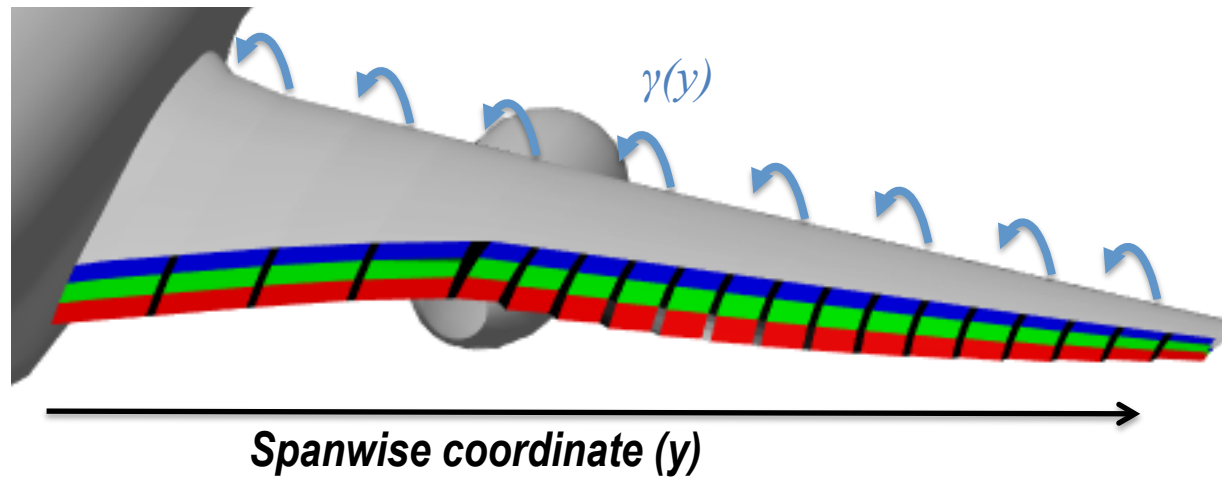


2D TSD/IBL loop is replaced with MSES for comparison

Transonic and Viscous Potential Flow Method



1. The virtual twist angle due to transonic and viscous corrections, $\gamma(y)$, is initialized to zero





Transonic and Viscous Potential Flow Method

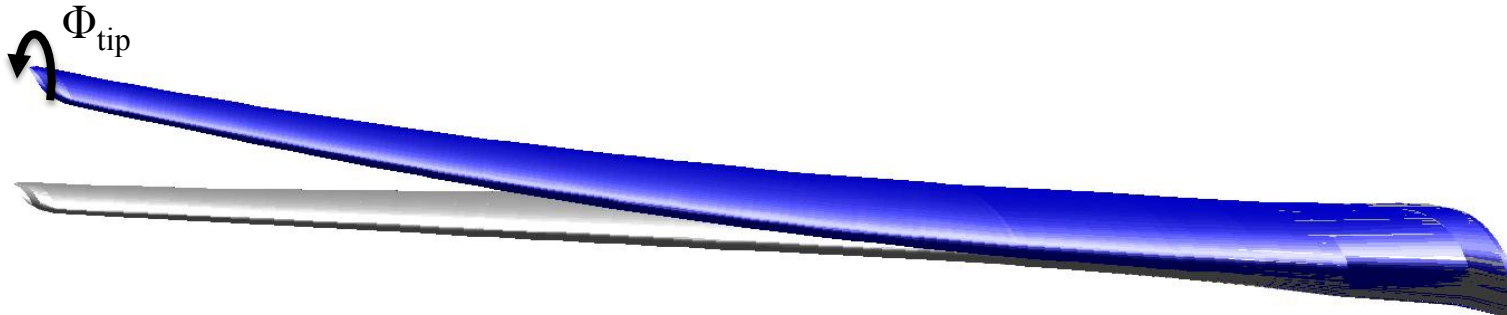
1. The virtual twist angle due to transonic and viscous corrections, $\gamma(y)$, is initialized to zero
2. The VLM model is coupled to the transonic and viscous corrections and the FEA model via the panel incidence angle

$$\underbrace{\tilde{\alpha}_{inc}(y)}_{\text{Effective Incidence Angle}} = \underbrace{\alpha_{inc}(y)}_{\text{Jig-shape Incidence Angle}} + \underbrace{\phi_y(y)}_{\text{Elastic Twist (Pitch Axis)}} + \underbrace{\gamma(y)}_{\text{Virtual Twist Angle}}$$

Transonic and Viscous Potential Flow Method



1. The virtual twist angle due to transonic and viscous corrections, $\gamma(y)$, is initialized to zero
2. The VLM model is coupled to the transonic and viscous corrections and the FEA model via the panel incidence angle
3. The VLM and FEA models iterate until the tip twist converges



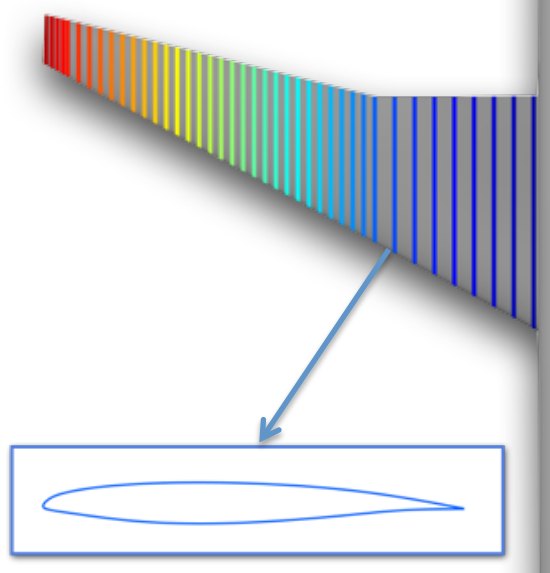
Transonic and Viscous Potential Flow Method

1. The virtual twist angle due to transonic and viscous corrections, $\gamma(y)$, is initialized to zero
2. The VLM model is coupled to the transonic and viscous corrections and the FEA model via the panel incidence angle
3. The VLM and FEA models iterate until the tip twist converges
4. The effective 2D angle of attack is calculated for each airfoil

$$\underbrace{\alpha_{2D}(y)}_{\text{Effective Airfoil Angle of Attack}} = \underbrace{\alpha_o(y)}_{\text{Airfoil Zero Lift Angle of Attack}} + \underbrace{\frac{c_{l_{vlm}}(y)}{c_{l_\alpha}}}_{\substack{\text{Sectional lift coefficient} \\ \text{2D lift slope}}} - \underbrace{\gamma(y)}_{\text{Virtual Twist Angle}}$$

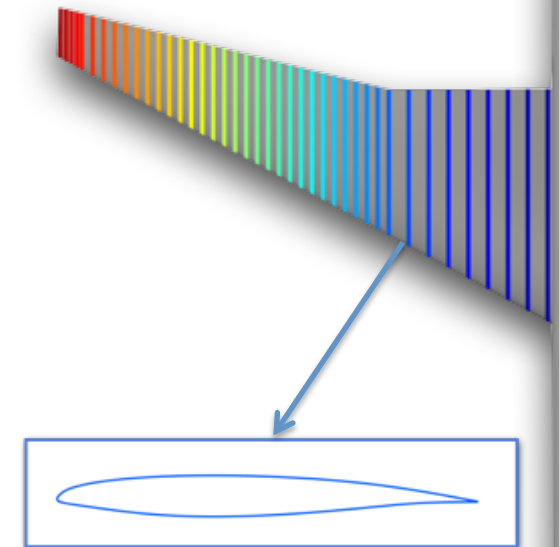
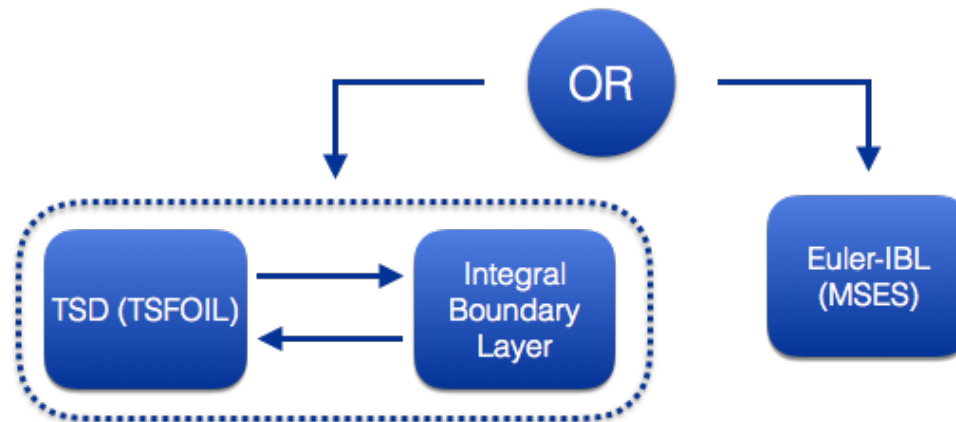
$$c_{l_\alpha} = \frac{2\pi}{\sqrt{1-M_\Lambda^2}}$$

Prandtl-Glauert Transformation



Transonic and Viscous Potential Flow Method

1. The virtual twist angle due to transonic and viscous corrections, $\gamma(y)$, is initialized to zero
2. The VLM model is coupled to the transonic and viscous corrections and the FEA model via the panel incidence angle
3. The VLM and FEA models iterate until the tip twist converges
4. The effective 2D angle of attack is calculated for each airfoil
5. Each airfoil is analyzed by the TSD/IBL or MSES model at the effective angle of attack





Transonic and Viscous Potential Flow Method

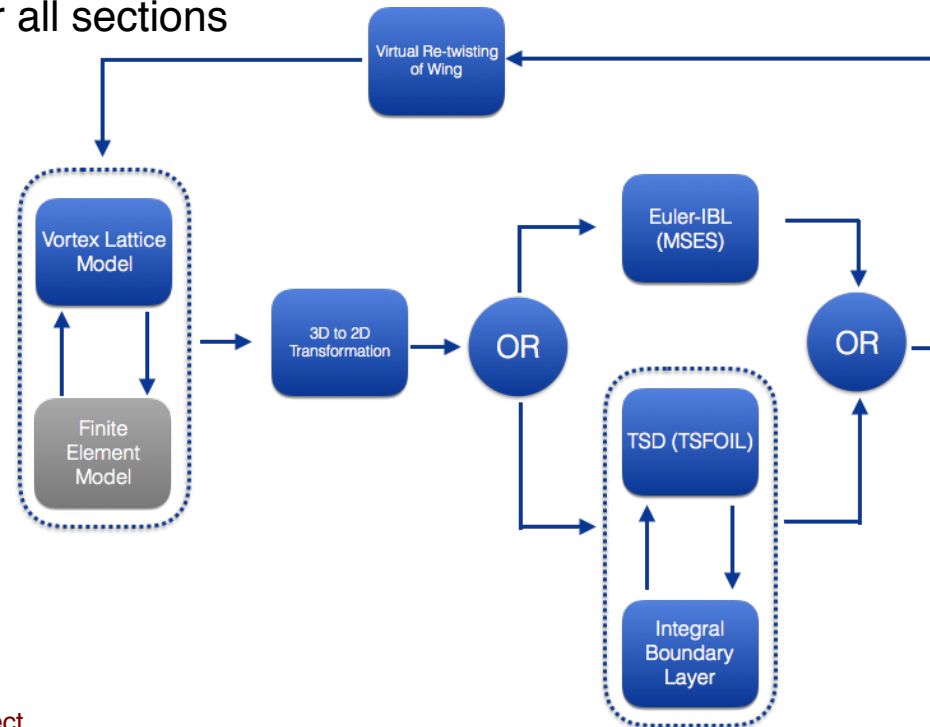
1. The virtual twist angle due to transonic and viscous corrections, $\gamma(y)$, is initialized to zero
2. The VLM model is coupled to the transonic and viscous corrections and the FEA model via the panel incidence angle
3. The VLM and FEA models iterate until the tip twist converges
4. The effective 2D angle of attack is calculated for each airfoil
5. Each airfoil is analyzed by the TSD/IBL or MSES model at the effective angle of attack
6. The virtual twist angle is updated for each section

$$\gamma_{i+1}(y) = \gamma_i(y) + \frac{\text{Airfoil lift coefficient from TSD/IBL or MSES} - \text{Sectional lift coefficient}}{c_{l\alpha}}$$
$$\gamma_{i+1}(y) = \gamma_i(y) + \frac{c_{l_{2D_i}}(y) - c_{l_{vlm_i}}(y)}{c_{l\alpha}}$$



Transonic and Viscous Potential Flow Method

1. The virtual twist angle due to transonic and viscous corrections, $\gamma(y)$, is initialized to zero
2. The VLM model is coupled to the transonic and viscous corrections and the FEA model via the panel incidence angle
3. The VLM and FEA models iterate until the tip twist converges
4. The effective 2D angle of attack is calculated for each airfoil
5. Each airfoil is analyzed by the TSD/IBL or MSES model at the effective angle of attack
6. The virtual twist angle is updated for each section
7. Repeat Steps 2 through 6 until the sectional lift and the 2D lift from the TSD/IBL or MSES model converge for all sections



Transonic and Viscous Potential Flow Method



1. The virtual twist angle due to transonic and viscous corrections, $\gamma(y)$, is initialized to zero
2. The VLM model is coupled to the transonic and viscous corrections and the FEA model via the panel incidence angle
3. The VLM and FEA models iterate until the tip twist converges
4. The effective 2D angle of attack is calculated for each airfoil
5. Each airfoil is analyzed by the TSD/IBL or MSES model at the effective angle of attack
6. The virtual twist angle is updated for each section
7. Repeat Steps 2 through 6 until the sectional lift and the 2D lift from the TSD/IBL or MSES model converge for all sections
8. Wave and friction drag are calculated by the TSD/IBL or MSES model. Lift and induced drag are calculated by the VLM model.



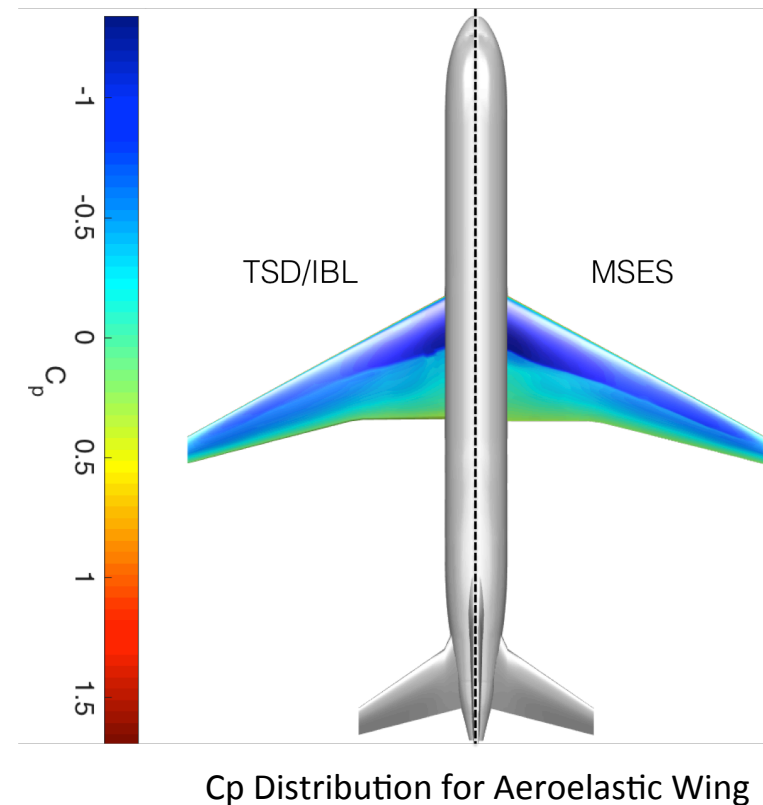
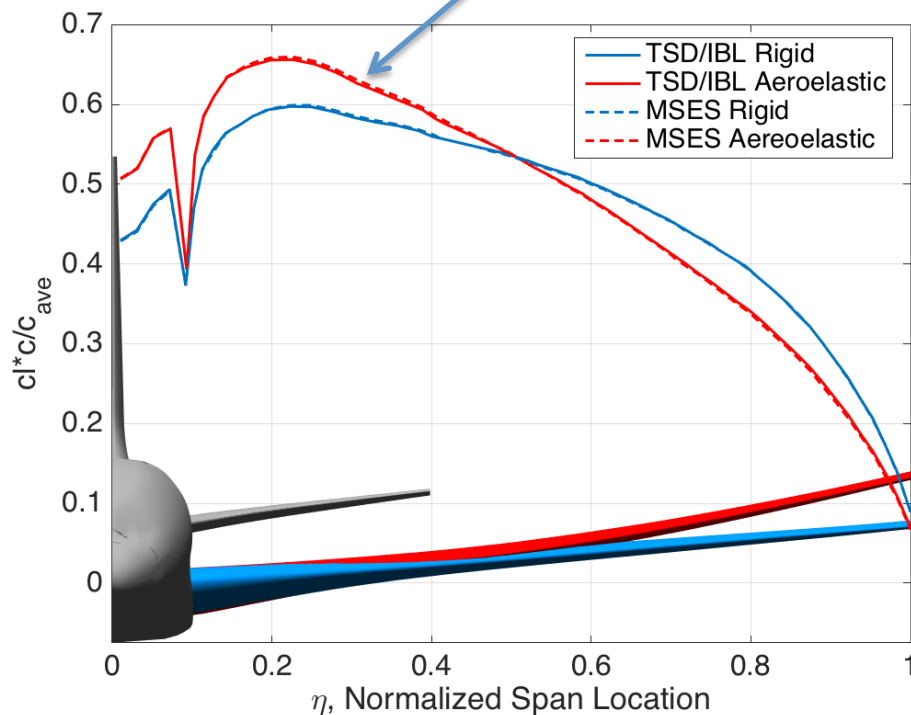
Validation

- TSD/IBL Validation with MSES
- Validation with Euler (Cart3D)
- Validation with RANS (LAVA)

Aeroelastic Clean Wing GTM Comparison with MSES



*Triangular load distribution
due to wing deformation*

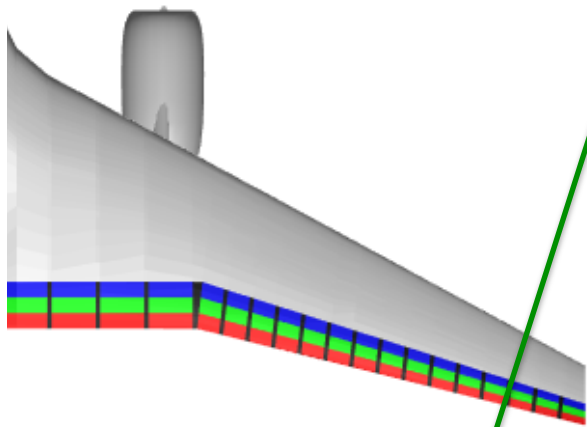


Transonic and viscous flow VLM with TSD/IBL and MSES are in excellent agreement

Rigid Wing GTM with VCCTEF Comparison with MSES

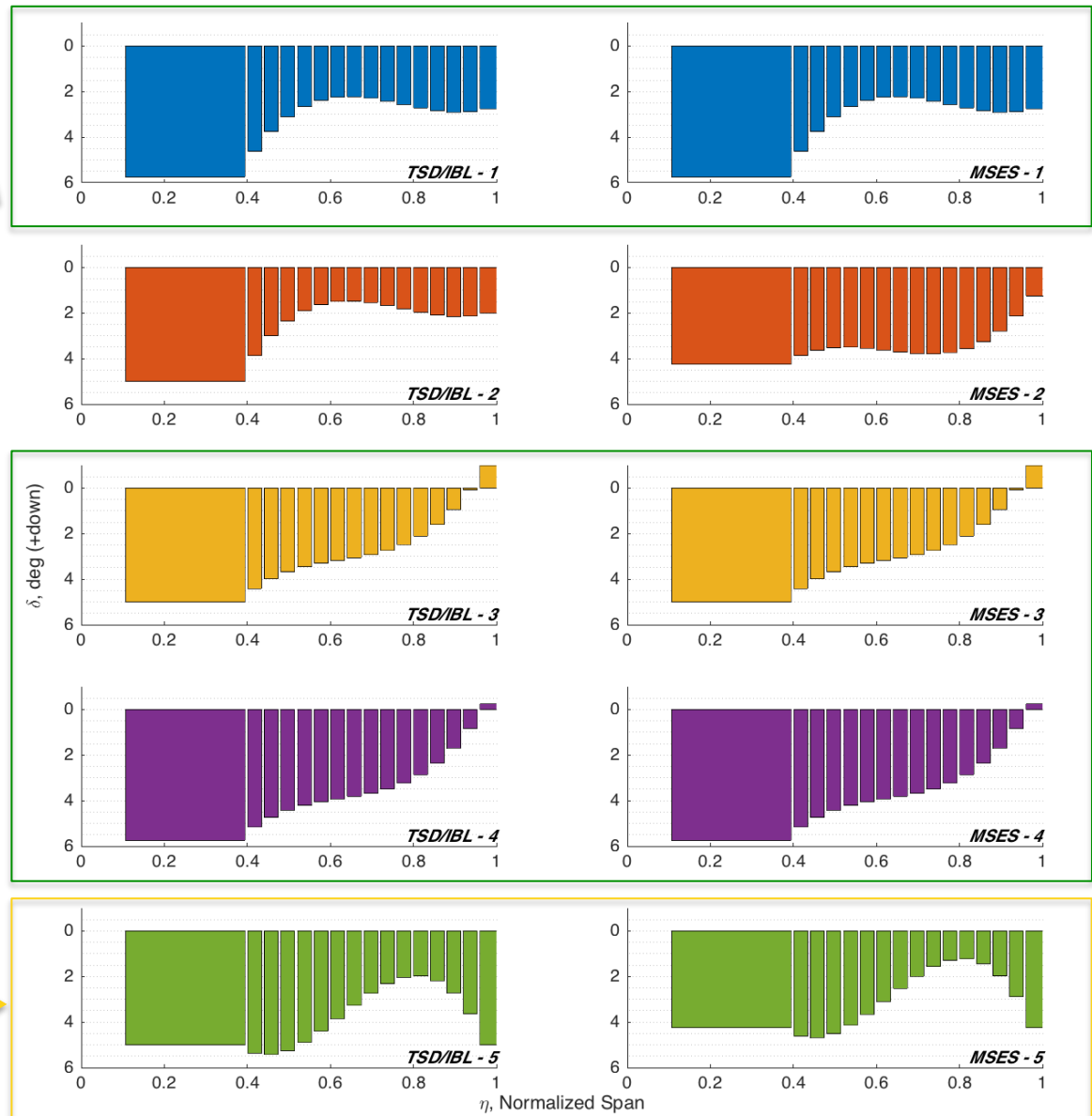


85 Candidate VCCTEF configurations are analyzed by TSD/IBL and MSES frameworks



TSD/IBL and MSES agree on three of the five VCCTEF candidates with lowest drag

TSD/IBL and MSES agree on the shape of the 5th best candidate, but the magnitude is offset by 0.75 degrees

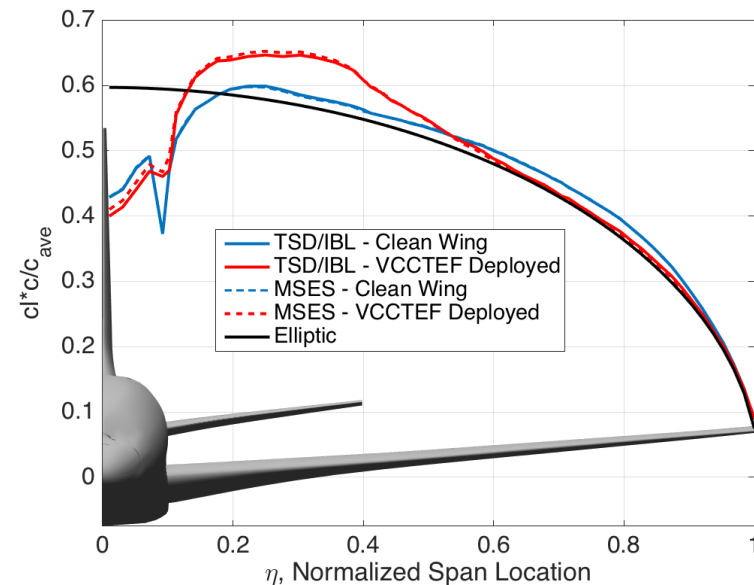


Rigid Wing GTM with VCCTEF Comparison with MSES



- The lift distribution for the minimum drag VCCTEF deflection moves away from elliptic near the root to lower wave drag
 - Lift distribution from the TSD/IBL and MSES models are in good agreement
- Average drag reduction by TSD/IBL agrees with MSES to within 2.3 drag counts

Minimum Drag VCCTEF Deflection



	$\Delta C_{D_{tsd}}$	$\Delta C_{D_{tsd}} (\%)$	$\Delta C_{D_{tsd}} - \Delta C_{D_{mses}}$
TSD/IBL 1	18.2	7.04	3.2
TSD/IBL 2	16.8	6.51	3.7
TSD/IBL 3	16.7	6.47	2.6
TSD/IBL 4	16.7	6.46	2.7
TSD/IBL 5	16.6	6.42	3.6

	$\Delta C_{D_{mses}}$	$\Delta C_{D_{mses}} (\%)$	$\Delta C_{D_{tsd}} - \Delta C_{D_{mses}}$
MSES 1	15.0	5.71	3.2
MSES 2	14.1	5.37	2.2
MSES 3	14.1	5.36	2.6
MSES 4	14.0	5.32	2.7
MSES 5	13.2	5.02	2.7

Rigid Clean Wing GTM Comparison with 3D Euler



- 3D Euler (Cart3D) is compared with transonic flow VLM models

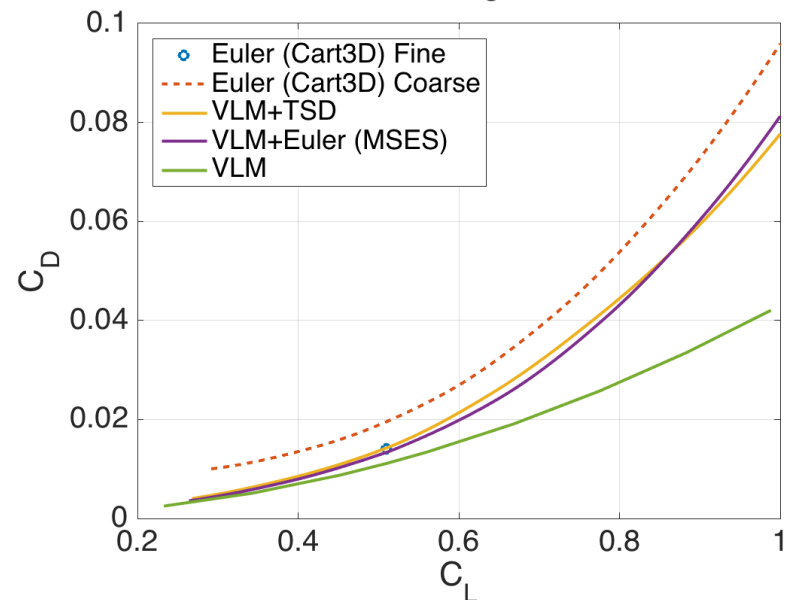
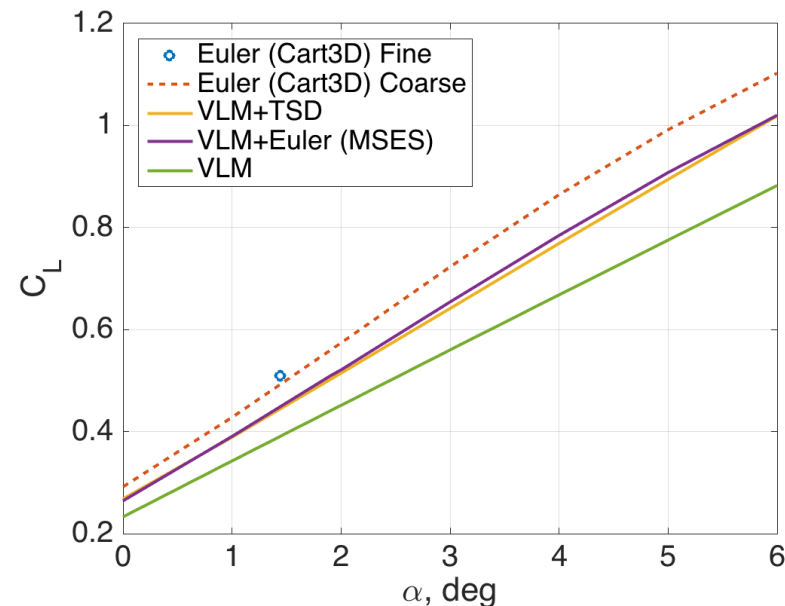
	VLM	VLM+TSD	VLM +MSES	Euler
CL_0	0.233	0.268	0.264	0.292*
CL_α	6.184	7.196	7.295	7.879*
$\frac{L}{D}(cruise)$	45.9	36.3	38.2	36.2**

Percent Difference with Euler

	VLM	VLM+TSD	VLM +MSES
CL_0	20.2%	8.2%	9.6%
CL_α	21.5%	8.7%	7.4%
$\frac{L}{D}(cruise)$	-26.8%	-0.28%	-5.5%

*Coarse Mesh: exploratory studies

**Fine Mesh: higher fidelity drag studies



Rigid Clean Wing GTM Comparison with RANS

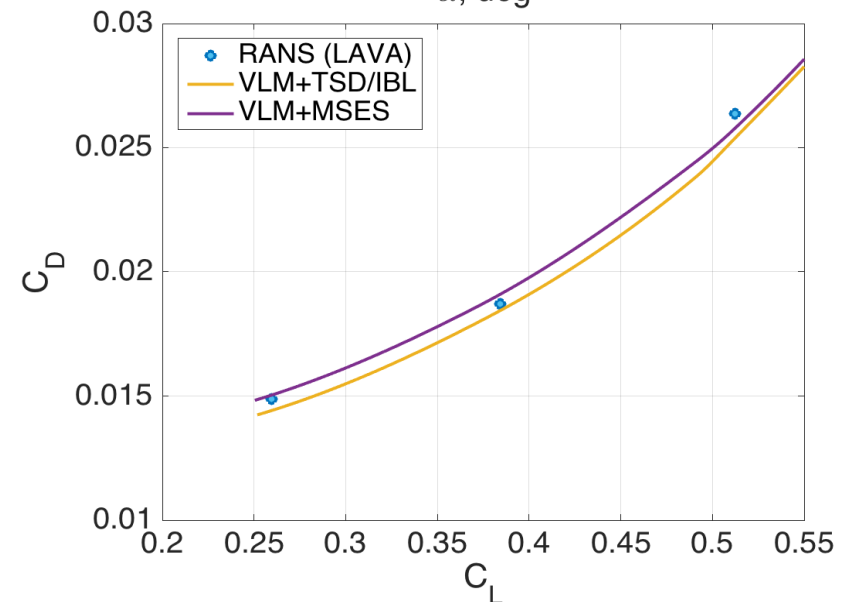
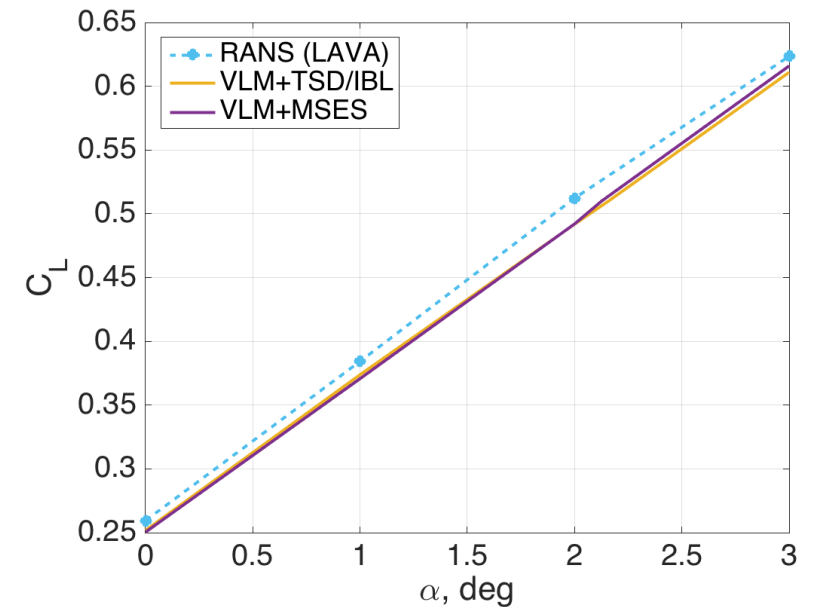


- RANS (LAVA) is compared with transonic and viscous flow VLM models

	VLM+TSD/IBL	VLM+MSES	RANS
CL_0	0.252	0.250	0.259
CL_α	6.852	6.969	6.990
$\frac{L}{D}(cruise)$	20.2	19.9	19.5

Percent Difference with RANS

	VLM+TSD	VLM+MSES
CL_0	2.7%	3.5%
CL_α	2.0%	0.3%
$\frac{L}{D}(cruise)$	-3.6%	-2.1%



Aeroelastic Clean Wing GTM Comparison with RANS

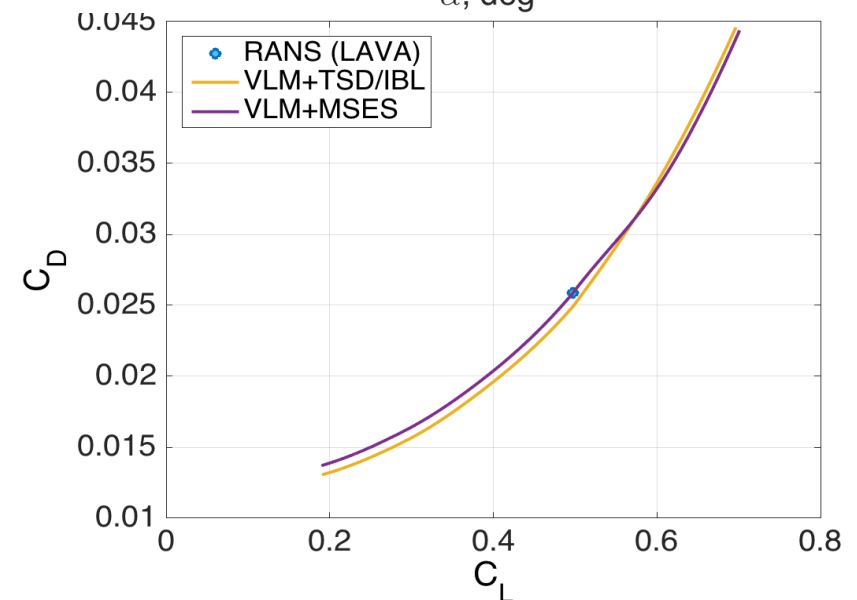
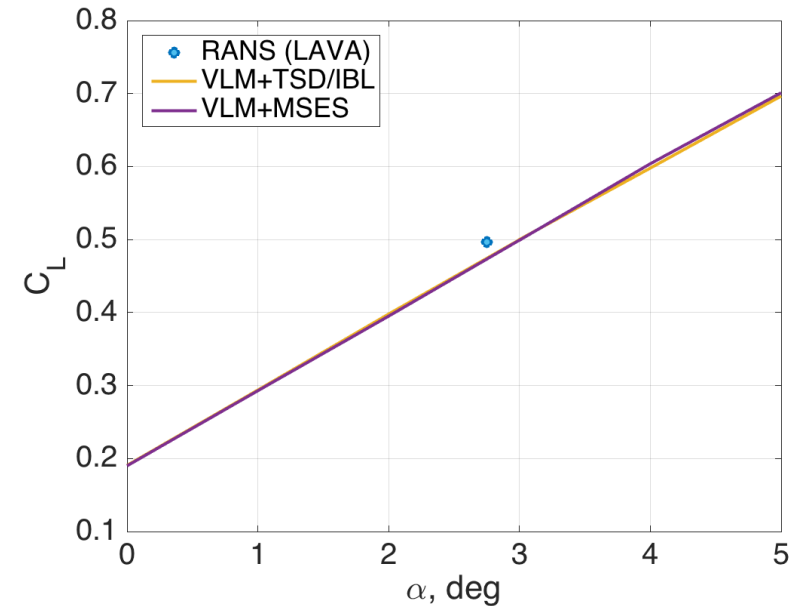


- RANS (LAVA) is compared with transonic and viscous flow VLM models

	VLM+TSD/IBL	VLM+MSES	RANS ³
CL_α	5.805	5.882	N/A
CL_0	0.191	0.190	N/A
$\frac{L}{D}(cruise)$	19.685	19.193	19.219

Percent Difference with RANS

	VLM +TSD/IBL	VLM +MSES
$\frac{L}{D}(cruise)$	-2.4%	0.1%



Aeroelastic Wing GTM with VCCTEF Comparison with RANS



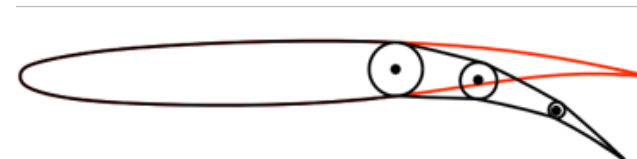
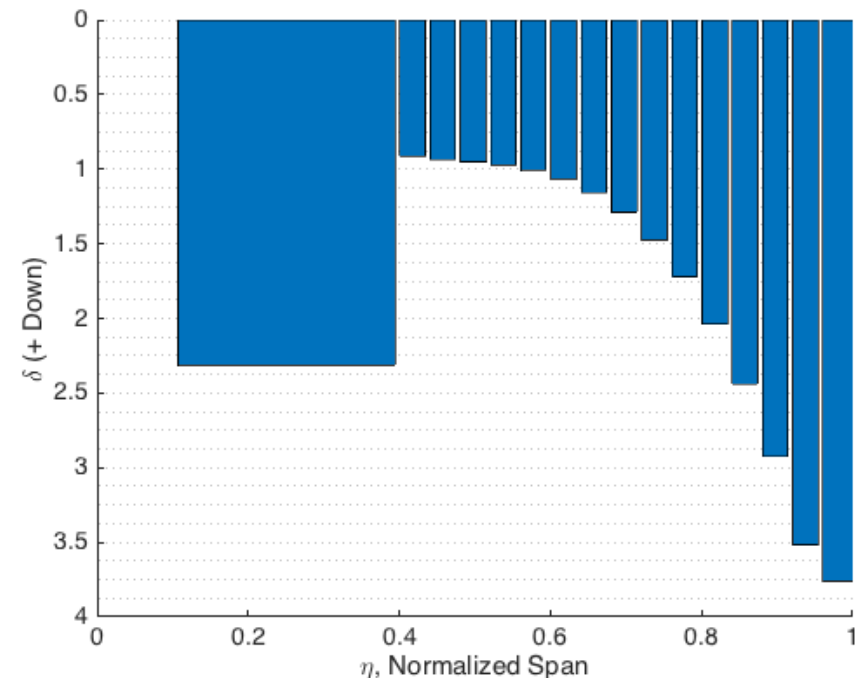
- RANS (LAVA) is compared with transonic and viscous flow VLM at Cruise

	VLM+TSD/IBL	RANS ³
CL	0.497	0.497
CD Clean	248.9	258.6
CD VCCTEF	241.8	248.6
Δ CD	-7.1	-10.0

Percent Difference with RANS

	VLM+TSD/IBL
$\frac{L}{D}(VCCTEF)$	2.8%

VCCTEF Candidate at Cruise



³Denison, M., Housman, J.A., Ting, E., Nguyen, N., "Comparison of Viscous and Inviscid Loads in a Static Aeroelastic Model of the Variable Camber Continuous Trailing Edge Flap Concept in the Transonic Regime", AIAA Aviation 2016 Conference, AIAA paper 2016-3571, 2016.

Advantages and Limitations of the Transonic and Viscous Potential Flow Method



- Limitations
 - TSD is generally valid only for weak shocks
 - Flows with strong shocks can be analyzed by replacing TSD with MSES within the modeling framework
 - Areas of large flow separation
 - IBL solution can become singular
 - Junction flow such as wing/root
 - Strip theory approximation may not be accurate in areas with highly 3D flow
- Advantages
 - Rapid model generation
 - Inputs are mainly the wing wireframe and operating conditions
 - Reasonable agreement with high fidelity CFD tools
 - Lift slope
 - L/D ratio
 - Drag reduction due to VCCTEF
 - Computationally efficient wall-clock time
 - Well-suited for aeroelastic analysis of highly flexible wing aircraft
 - Enables rapid optimization of VCCTEF topology

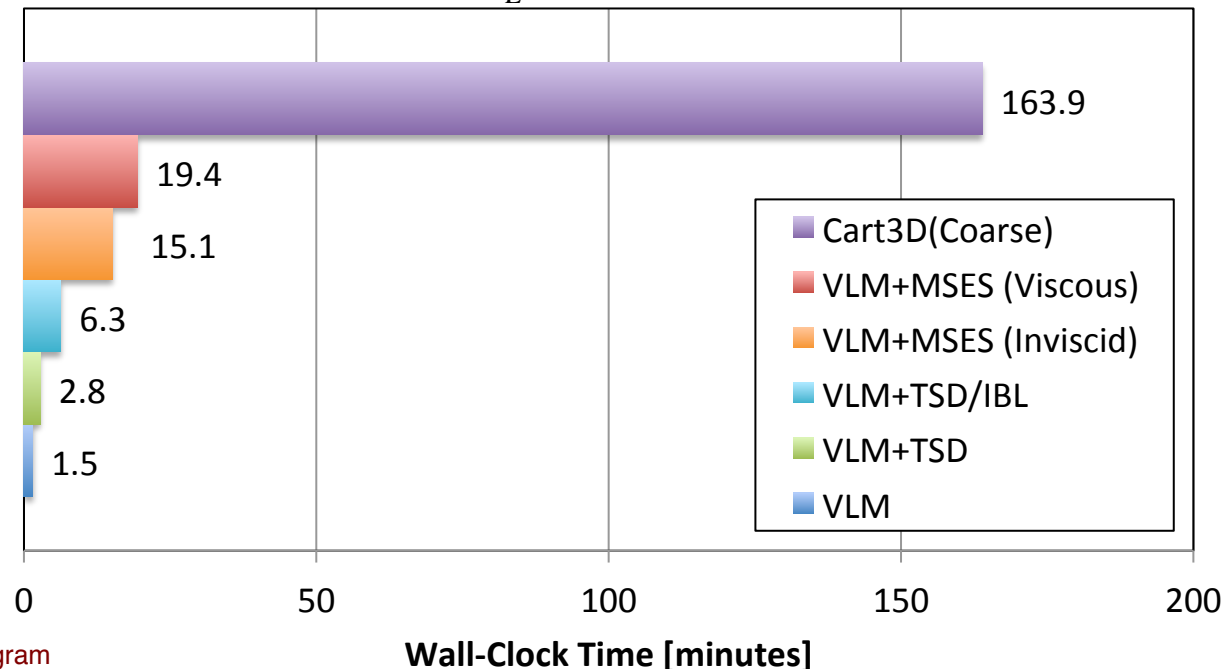


Computational Efficiency

- All calculation are conducted on a Macbook Pro:
 - 16gb Memory, 2.5GHz Intel i7 processor (4 cores)
 - Not practical to run RANS
- VLM +TSD/IBL model is two orders of magnitude faster than Cart3D and captures viscous flow physics
- VLM +TSD/IBL model is ~three times faster than VLM+MSES model with similar modeling fidelity



Wall-clock Comparison of Multiple Aerodynamic Codes for a Single Fixed C_L Aeroelastic Solution



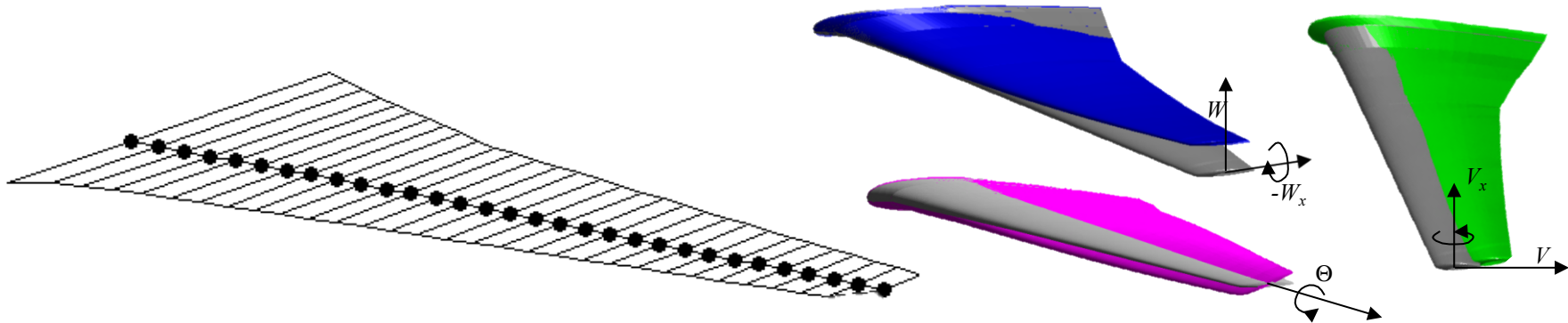


Structural/Aeroelastic Modeling

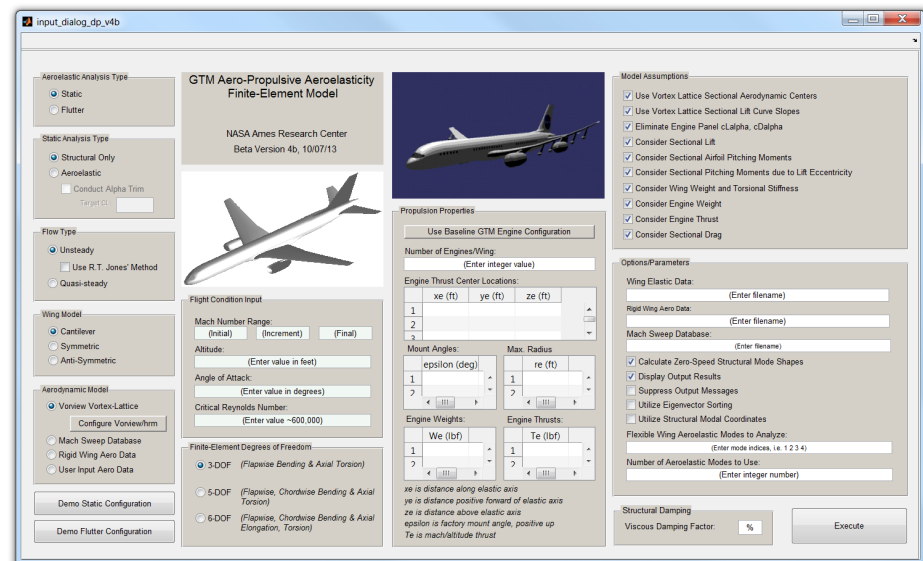
Finite Element Aeroelasticity



- **BEAM3D** is a rigorously developed research program that employs equivalent beam models to construct an aeroelastic finite element model (FEA/FEM) for static and dynamic aeroelastic analysis.

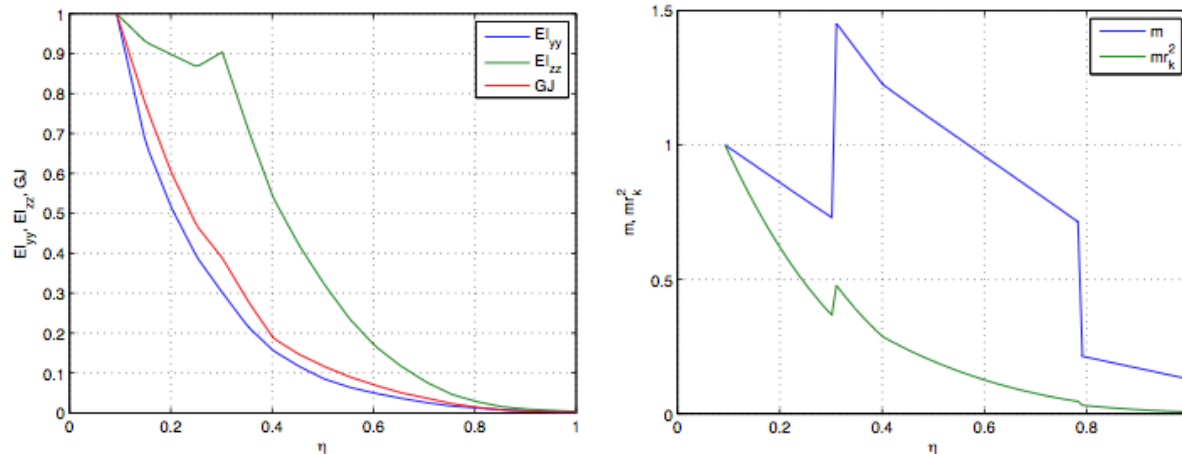


- Key features of BEAM3D:
 - Current development in MATLAB
 - Multi-element beam/frame modeling
 - Modular design with upgradability
 - Capable of dynamic aeroelasticity
 - Nonlinear analysis capability

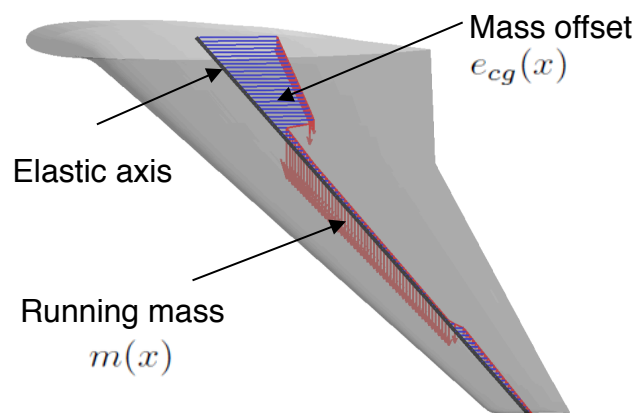


Finite Element Aeroelasticity

- Structural stiffness and mass properties represented by equivalent structure model compared with industry provided estimates.



- User specified fuel ratio models running mass and offset at different flight conditions.

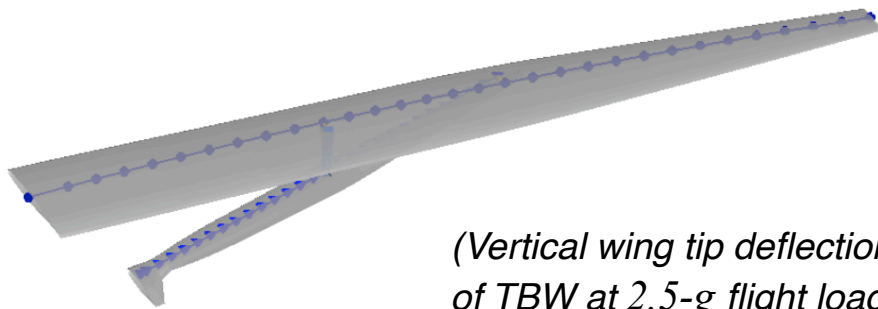


Design	Fuel Condition	Aircraft Weight (lbs)
Baseline	100%	247,500
	80%	232,500
	50%	210,000
	20%	187,500
Reduced Stiffness	100%	242,136
	80%	227,136
	50%	204,636
	20%	182,136

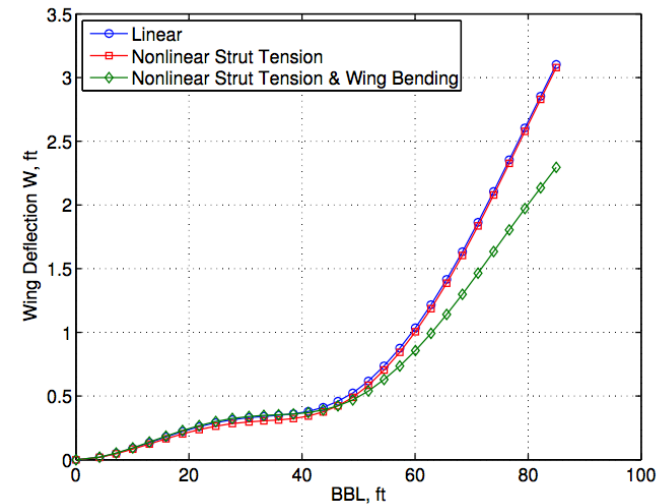
Finite Element Aeroelasticity



- BEAM3D is capable of including nonlinear effects:
- Geometric nonlinear stiffening in tensile-loaded elements
 - Truss Braced Wing multi-element configuration

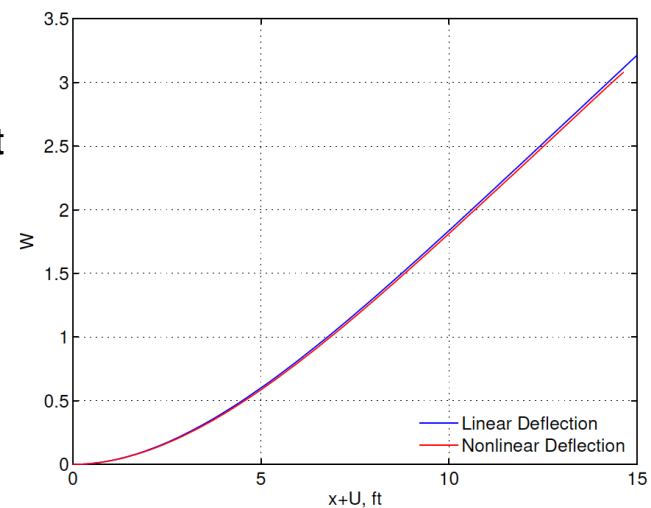


(Vertical wing tip deflection of TBW at 2.5-g flight load)



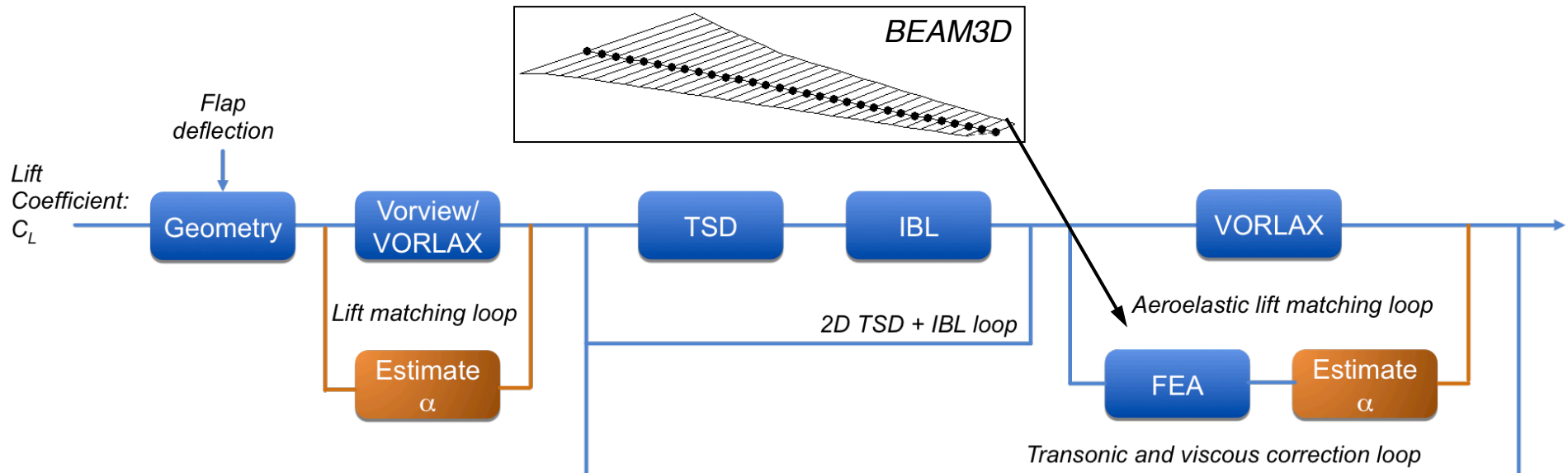
- Nonlinear strain analysis due to large deflection
 - Linear analysis introduces non-physical lengthening.
 - Nonlinear analysis is length preserving and has lower lift and span efficiency.

(Vertical wing tip deflection of an example unswept, aspect ratio 30 wing)



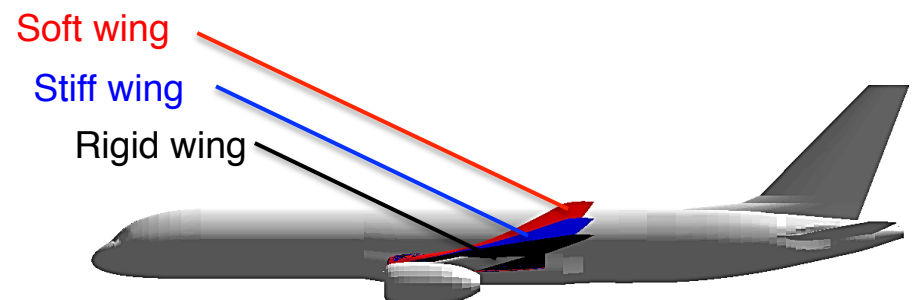
Finite Element Aeroelasticity

- BEAM3D is used to couple FEA to a VLM+TSD/IBL framework via translation and rotation of the VLM panels.



- The reduced stiffness soft wing configuration is selected for flap optimization studies.

	Stiff Wing GTM	Soft Wing GTM
Design \bar{C}_L	0.510	0.497
C_D , count	247.7	243.9
α , deg	2.5480	2.8850
Δz_{tip} , ft	1.9875	3.6065
$\Delta \phi_y$, deg	-1.1641	-2.3508





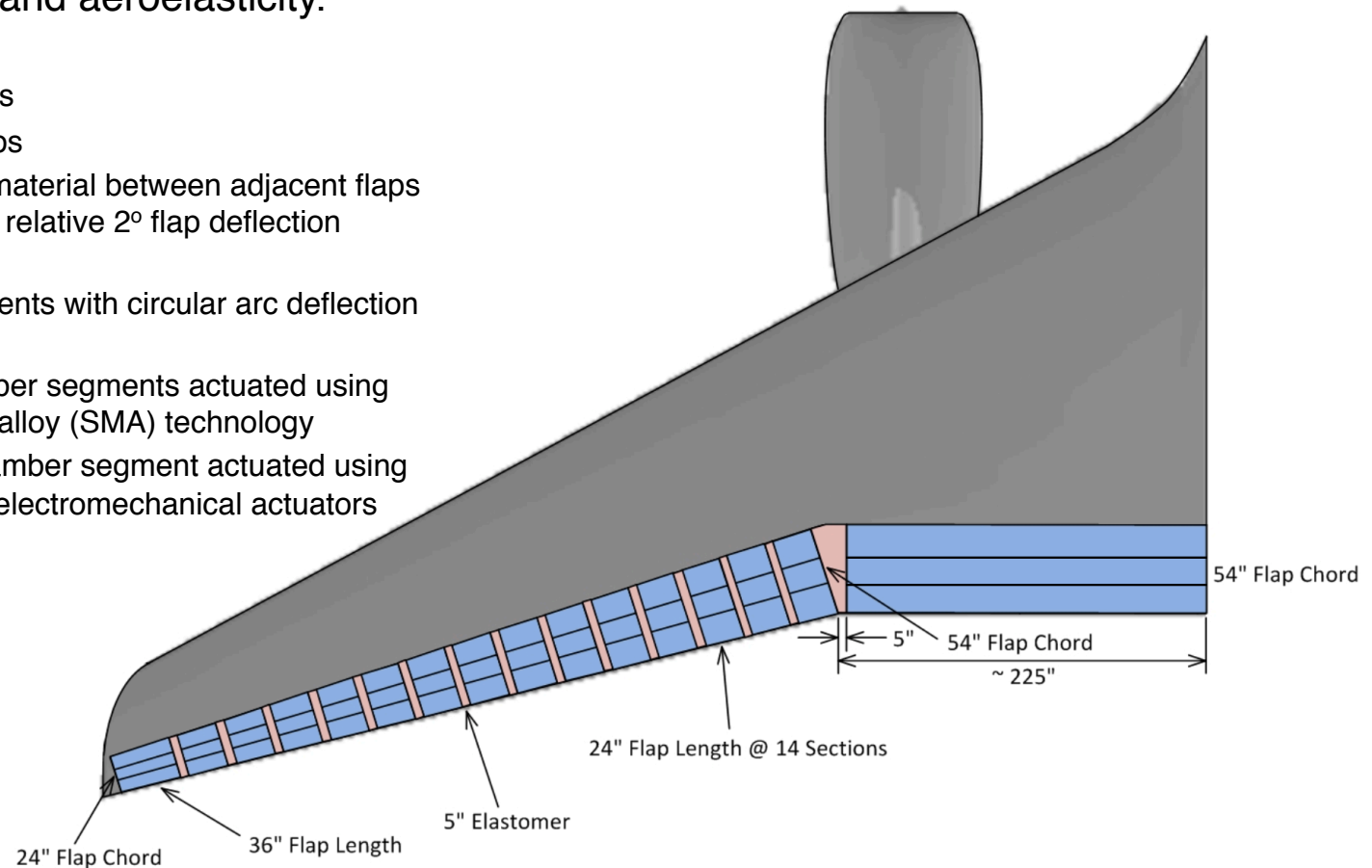
Flap Optimization

Flap Optimization



- Commonly used original layout was selected by NASA and Boeing without optimizing for aerodynamics and aeroelasticity.

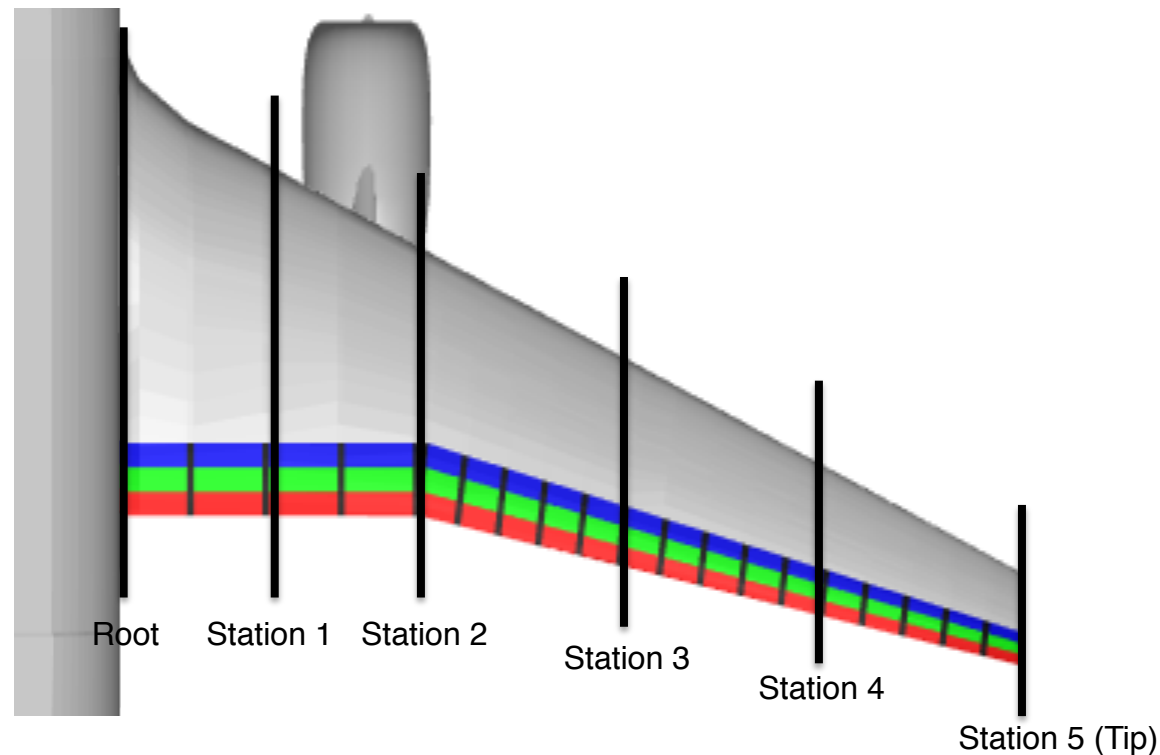
- 1-4 inboard flaps
- 15 outboard flaps
- 5" elastomeric material between adjacent flaps which impose a relative 2° flap deflection constraint.
- 3 camber segments with circular arc deflection profile
- 1st and 2nd camber segments actuated using shape memory alloy (SMA) technology
- 3rd (aft-most) camber segment actuated using traditional, fast electromechanical actuators (EMA).



- Using the rapid aero-structural modeling tool, the VCCTEF configuration can be examined to determine the most efficient number of flaps and deflection profile.

Flexible Jig-shape Retwist

- The original jigshape wing was not designed with reduced stiffness and does not possess an optimal washout at the design lift coefficient.
- To generate a meaningful baseline for VCCTEF studies, drag optimization is run to “redesign” the jigshape for the reduced stiffness design $C_L = 0.497$
- Additional twist at 5 spanwise stations is optimized, and the twist at intermediate spanwise locations are linearly interpolated.

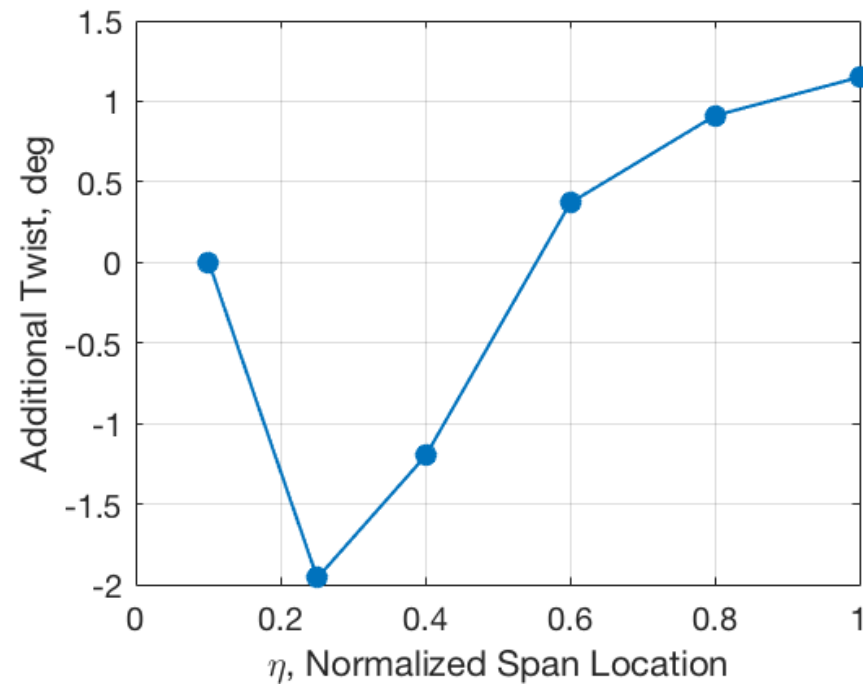




Flexible Jig-shape Retwist

- Optimization results (positive nose-up):

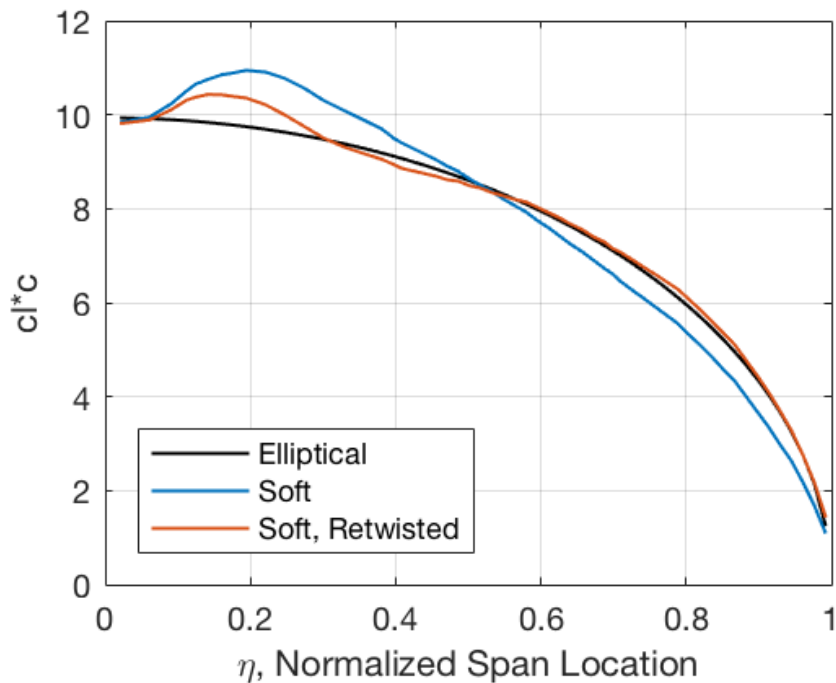
	Root	Station 1	Station 2	Station 3	Station 4	Station 5 (Tip)
Spanwise Location, y, ft	6.2807	15.5890	24.8973	37.3077	49.7182	62.1286
Additional Twist, deg	0	-1.9593	-1.1997	0.3695	0.9108	1.1498





Flexible Jig-shape Retwist

- When applied, the optimized additional twist drives the lift distribution closer to an elliptical lift distribution.



	Soft Wing GTM	Retwisted Soft Wing GTM
α , deg	2.885	3.463
C_D , count	243.9	239.9
z_{tip} , ft	3.6065	4.2316
ϕ_y , deg	2.3508	2.5135

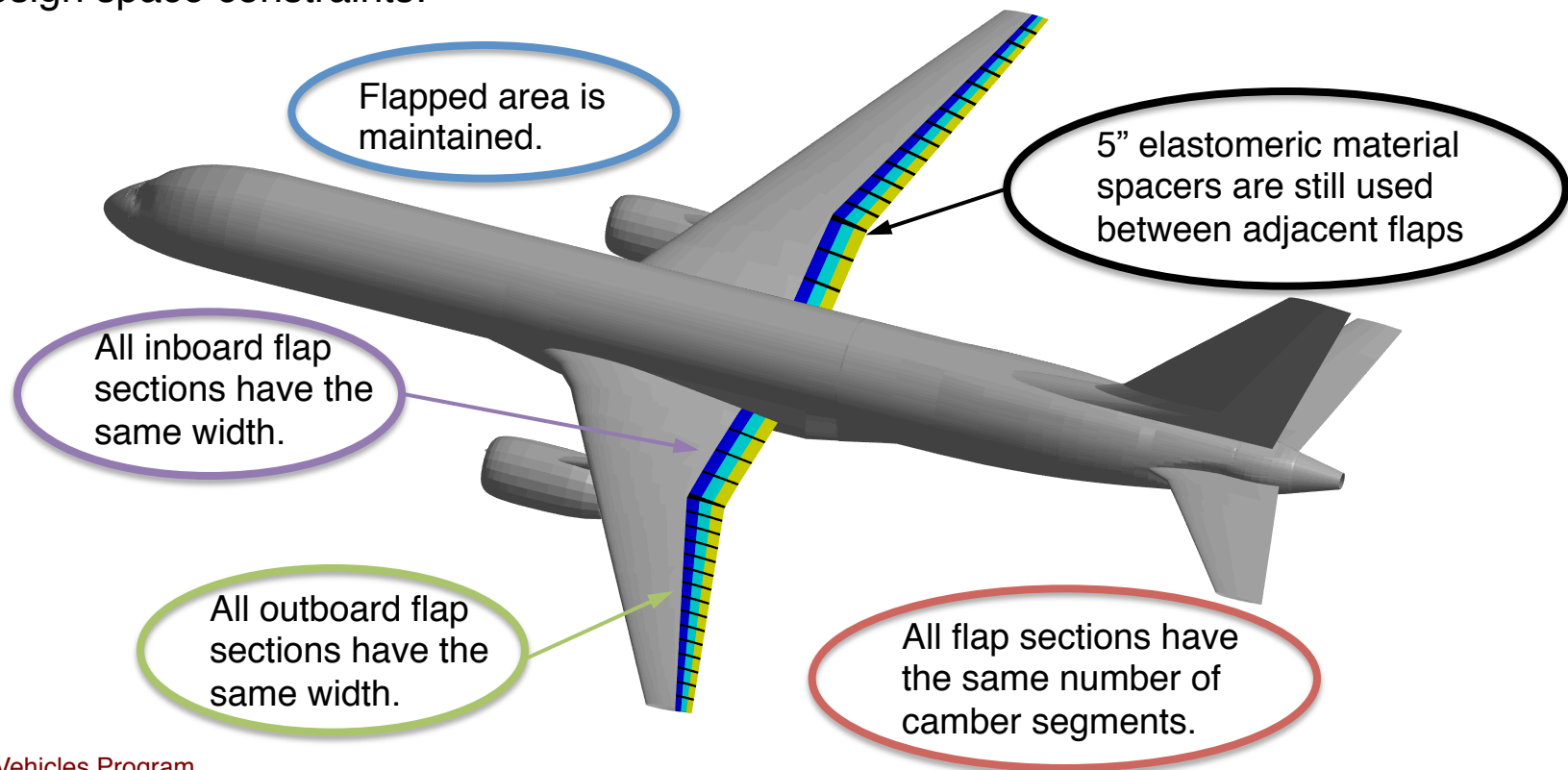
4 drag count reduction

Flap Optimization Methodology

- VCCTEF layout design space can be explored by leveraging the rapid aero-structural modeling capability of VLM+TSD/IBL.
- Different possible layout configurations are designated as:

$$(deflection\ profile)-(n_{camber})-(n_{inboard})-(n_{outboard})$$

- The commonly used VCCTEF layout has a *circular-3-4-15* configuration.
- Design space constraints:





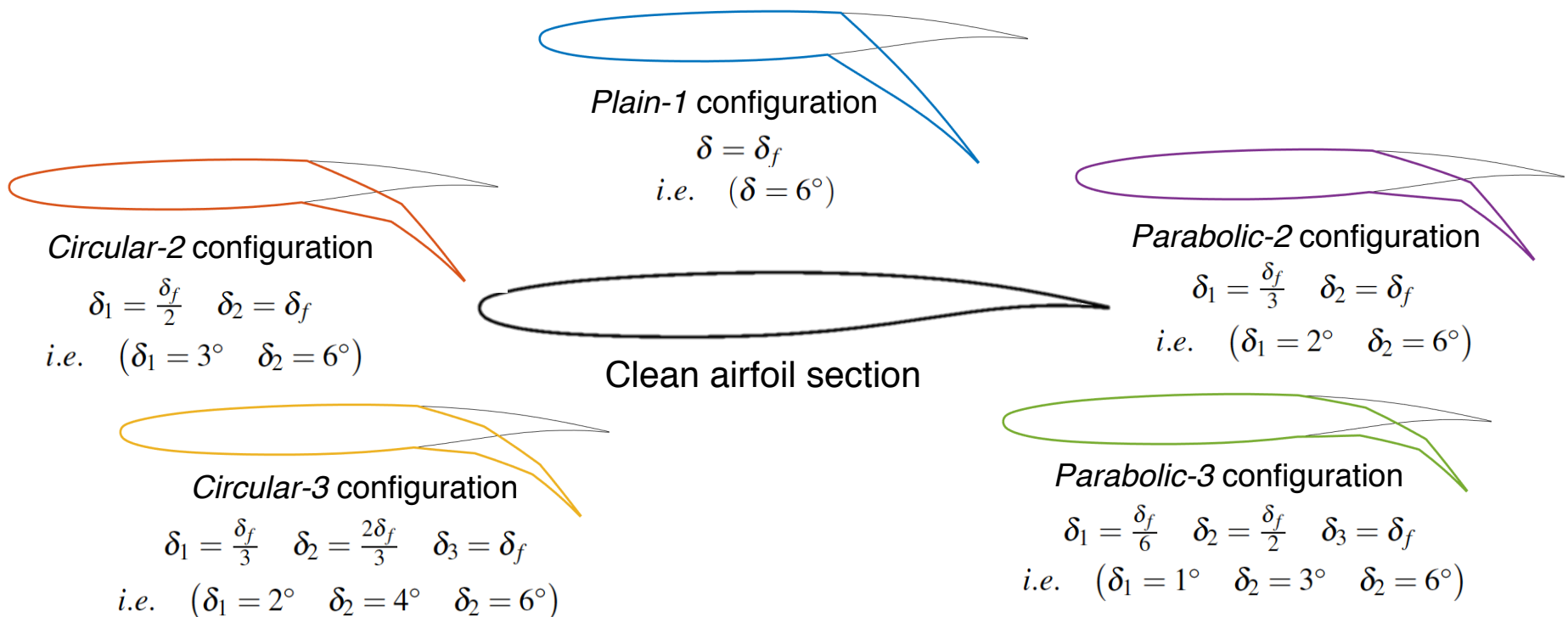
Flap Optimization Methodology

- The VCCTEF is designed to recover optimal wing aerodynamics at off-design flight conditions.
- The flight condition for optimization is selected to be the 80% fuel where the VCCTEF is anticipated to be effective due to higher lift.

Flight Condition	$Mach$	C_L	Altitude (ft)	VCCTEF Optimized?
Design Mid-Cruise	0.797	0.497	36,000	—
80% Fuel Begin Cruise	0.797	0.552	36,000	✓
20% Fuel End Cruise	0.797	0.442	36,000	
+30% Design C_L	0.797	0.646	41,461	
−30% Design C_L	0.797	0.348	28,315	

Flap Optimization Methodology

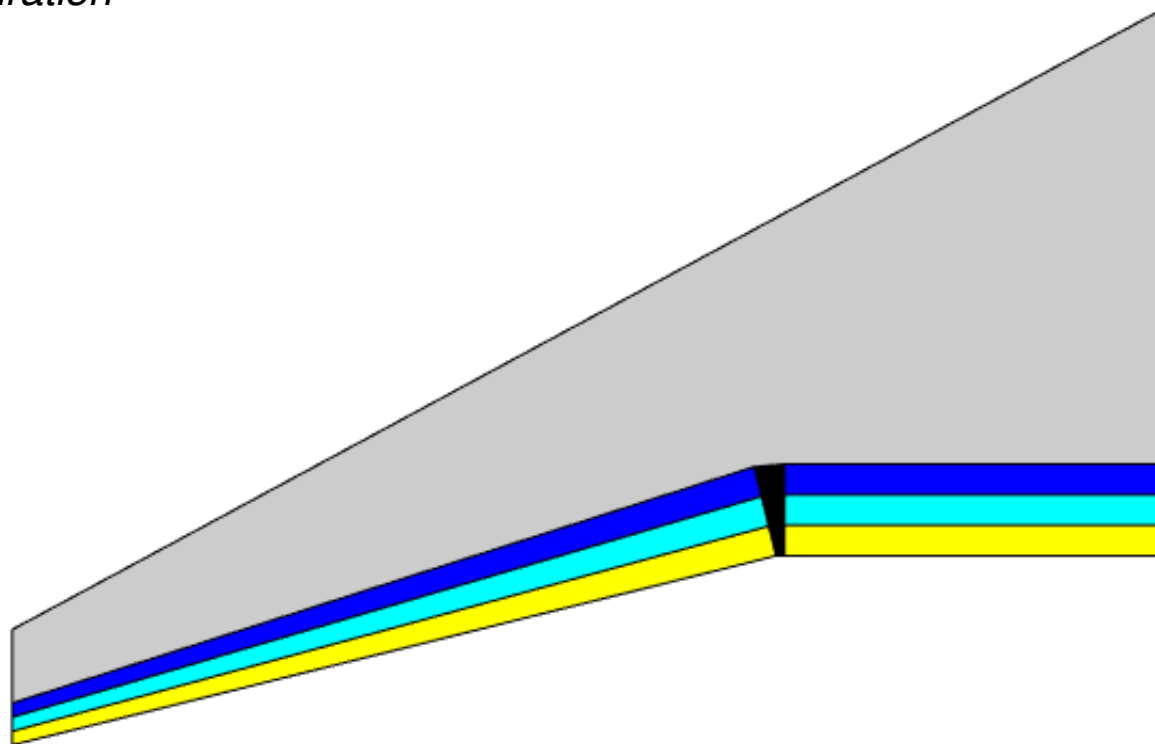
- Drag optimizations are run for different VCCTEF configurations and their maximum drag reductions values are compared.
- Focus is on relative drag reduction and drag reduction trends.
- **5 different camber deflection profiles** are examined:





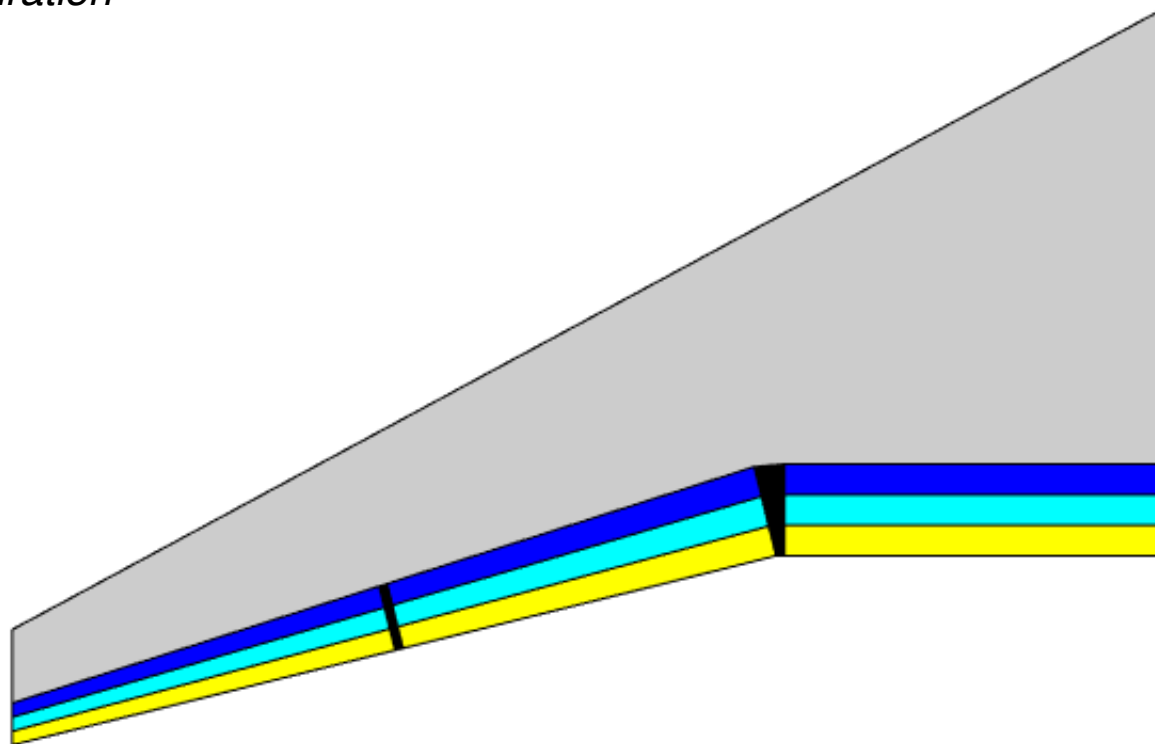
Flap Optimization Methodology

- For each deflection profile, a series of flap section configurations are run.
- A total of **9 flap section configurations** are run for each deflection profile.
- *-1-1 configuration*



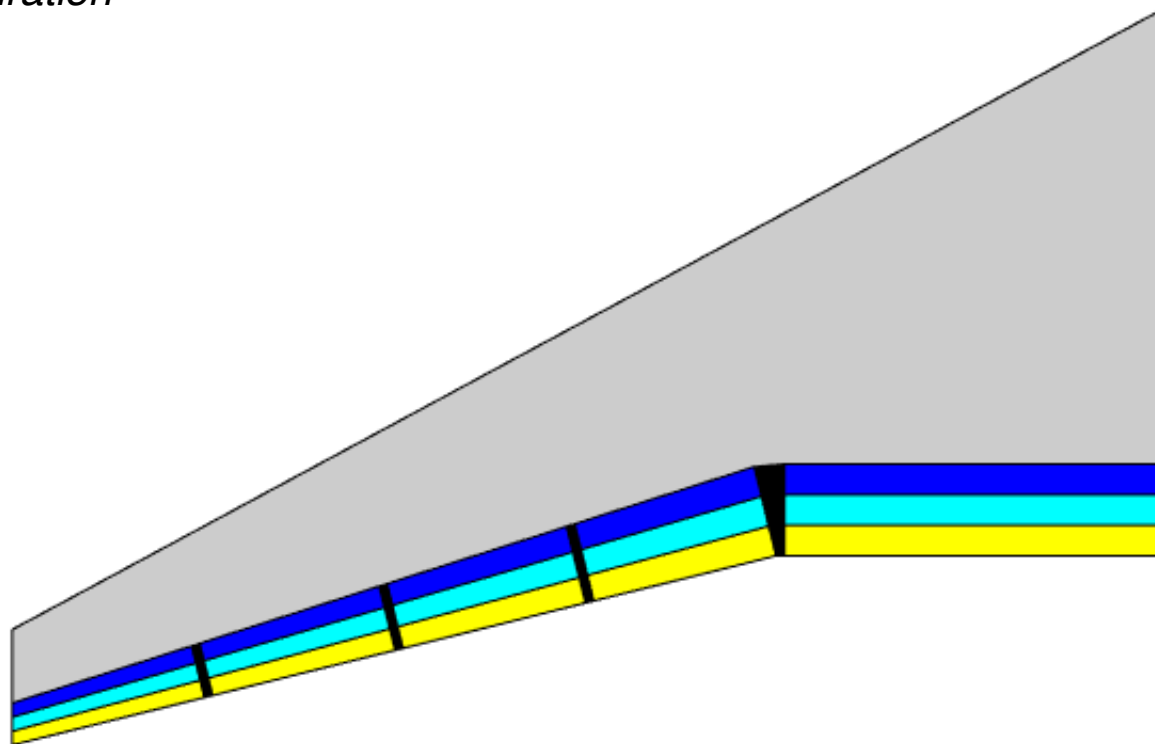
Flap Optimization Methodology

- For each deflection profile, a series of flap section configurations are run.
- A total of **9 flap section configurations** are run for each deflection profile.
- *-1-2 configuration*



Flap Optimization Methodology

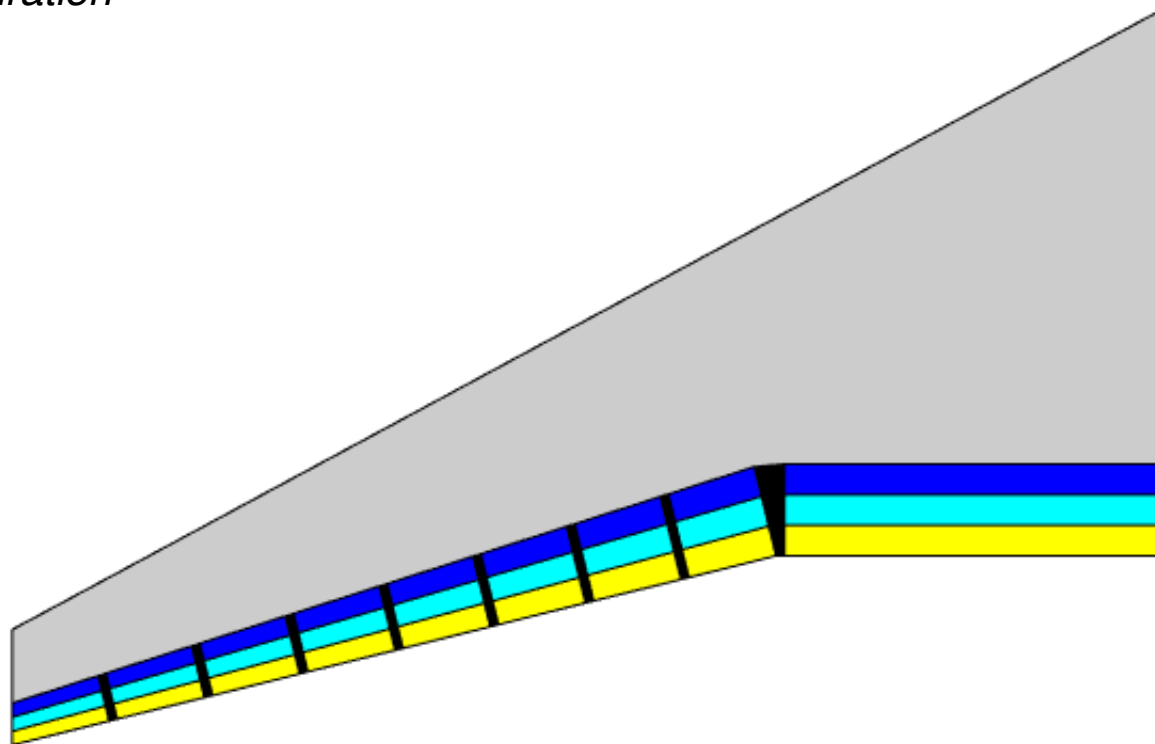
- For each deflection profile, a series of flap section configurations are run.
- A total of **9 flap section configurations** are run for each deflection profile.
- *-1-4 configuration*





Flap Optimization Methodology

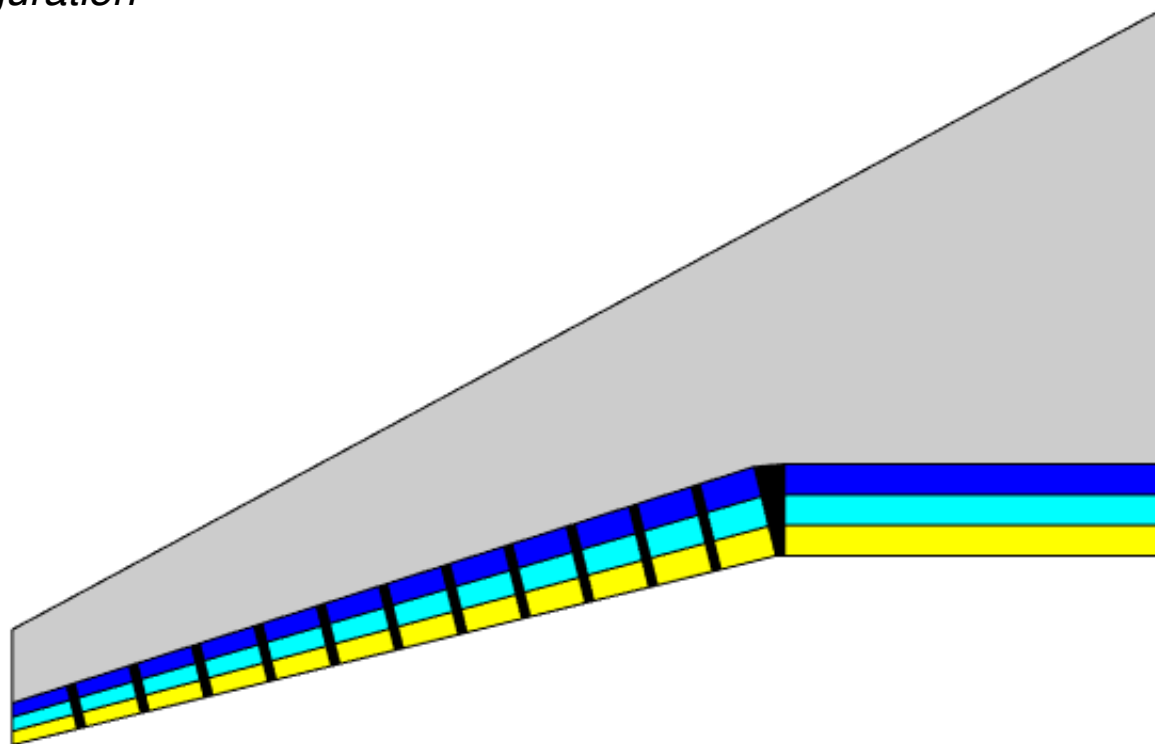
- For each deflection profile, a series of flap section configurations are run.
- A total of **9 flap section configurations** are run for each deflection profile.
- *-1-8 configuration*





Flap Optimization Methodology

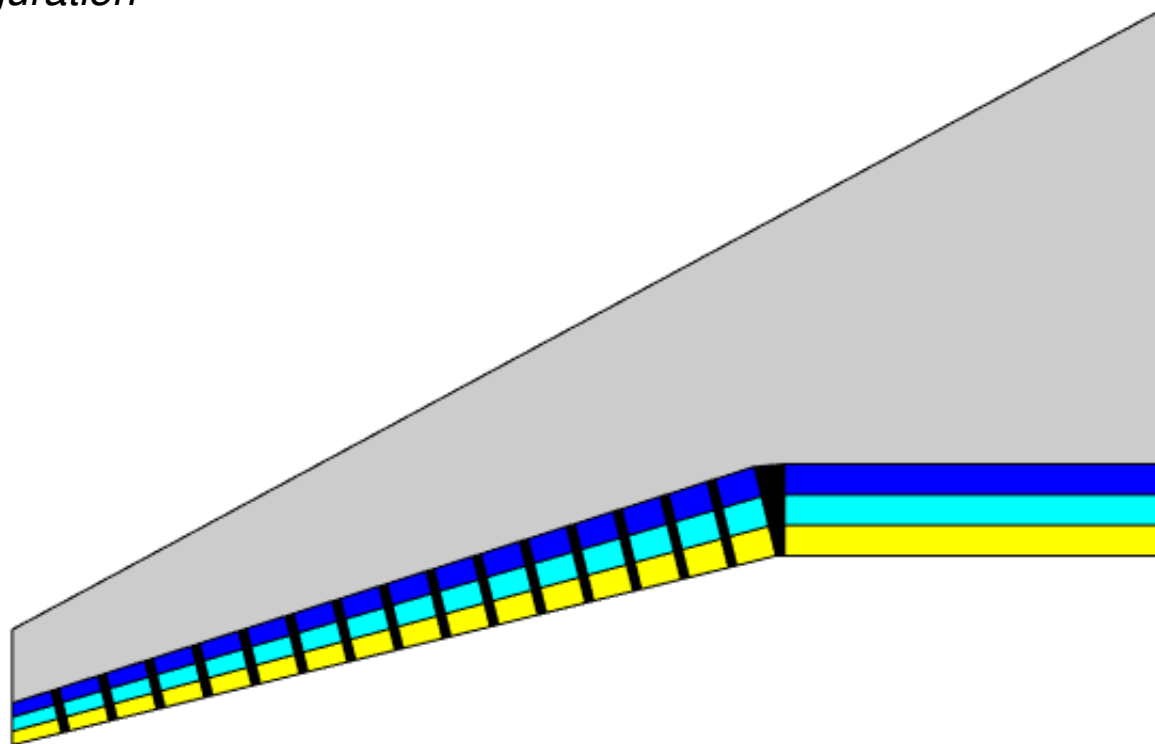
- For each deflection profile, a series of flap section configurations are run.
- A total of **9 flap section configurations** are run for each deflection profile.
- *-1-12 configuration*





Flap Optimization Methodology

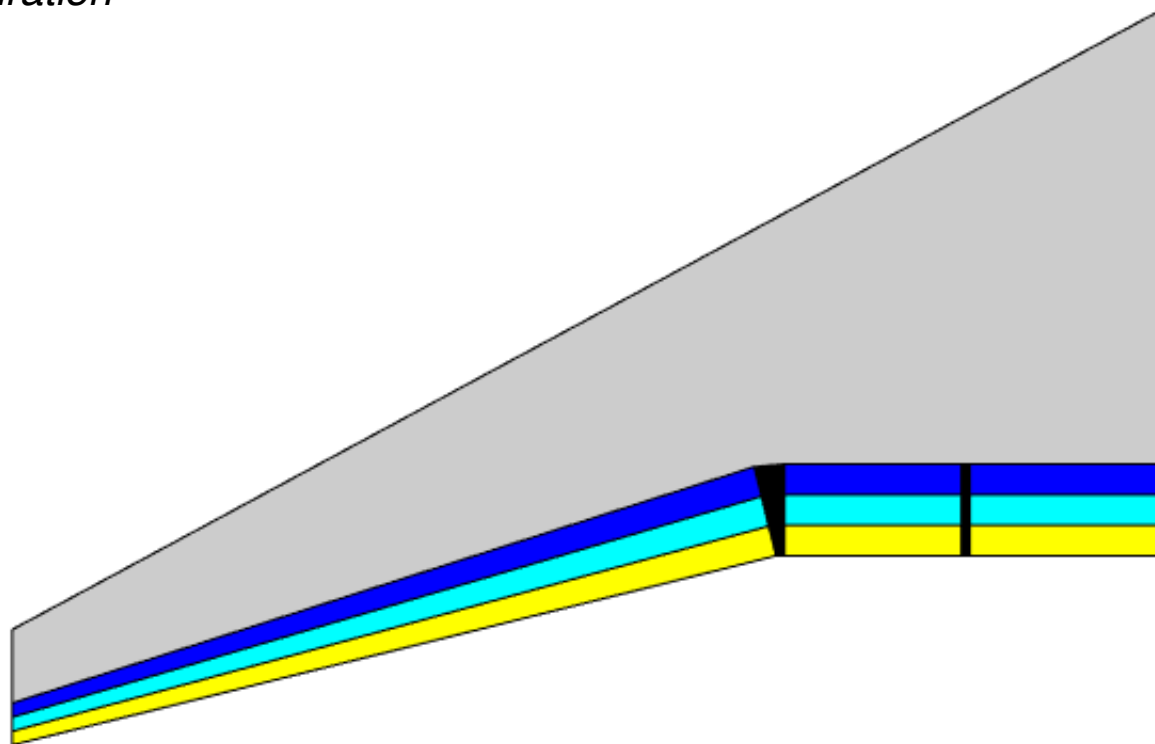
- For each deflection profile, a series of flap section configurations are run.
- A total of **9 flap section configurations** are run for each deflection profile.
- *-1-16 configuration*





Flap Optimization Methodology

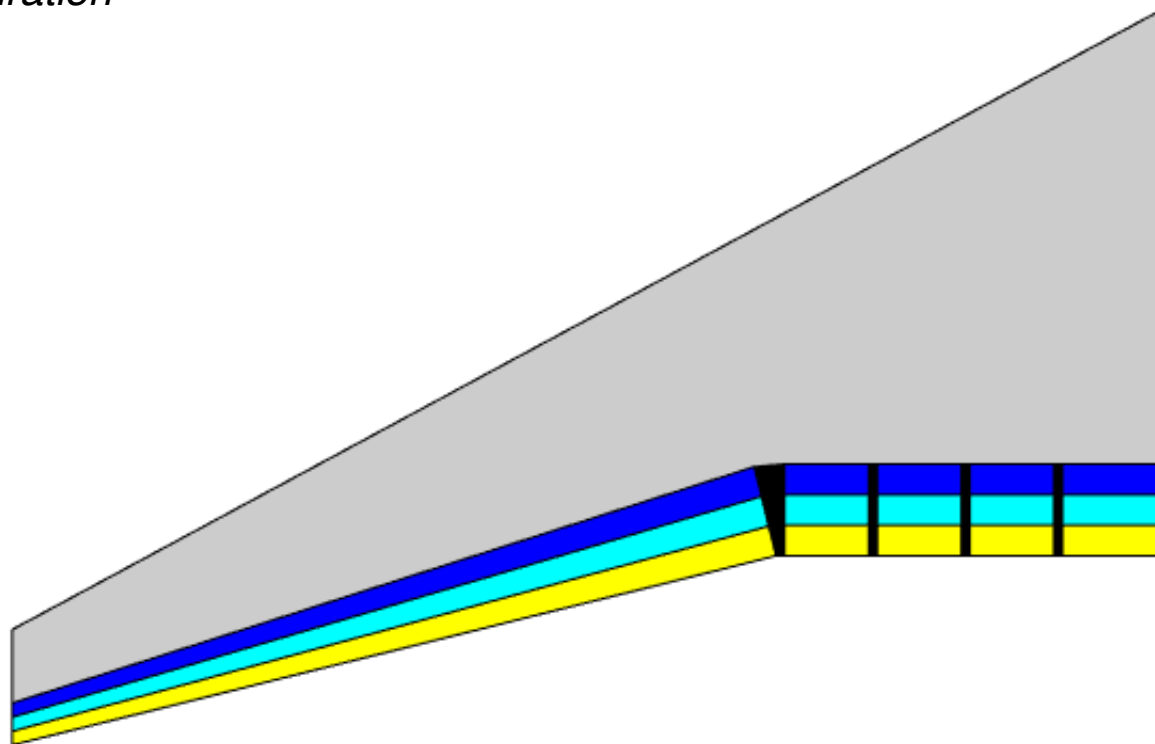
- For each deflection profile, a series of flap section configurations are run.
- A total of **9 flap section configurations** are run for each deflection profile.
- *-2-1 configuration*





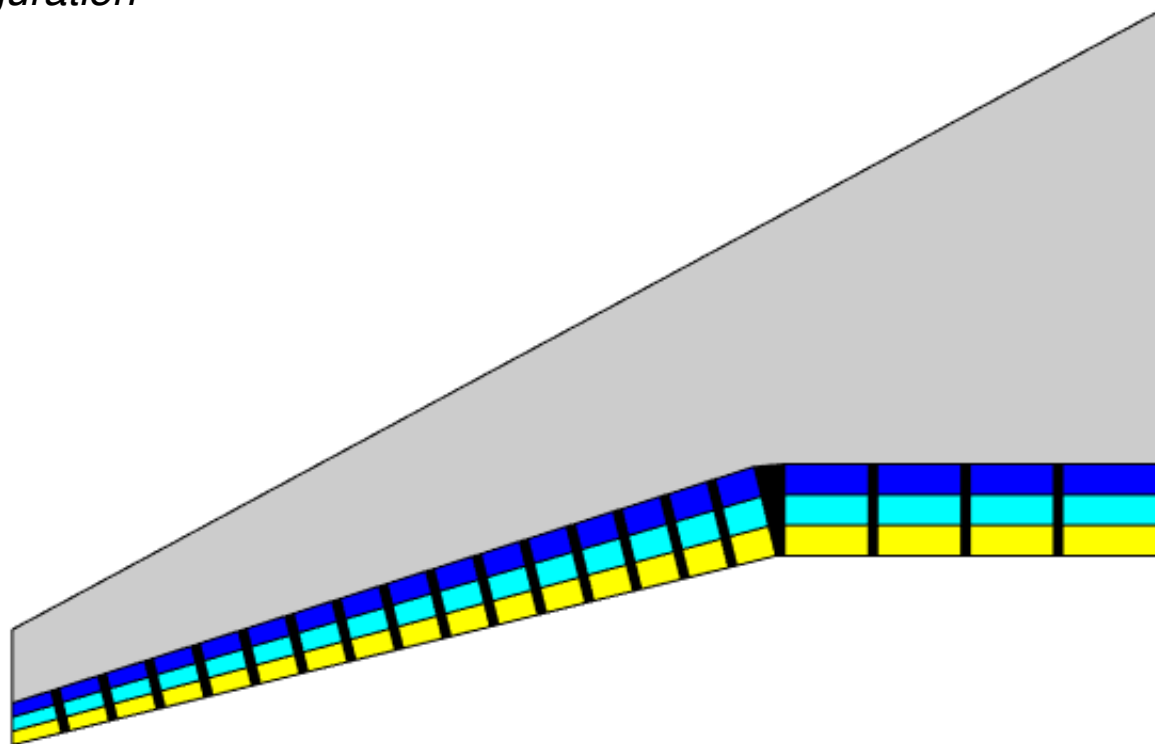
Flap Optimization Methodology

- For each deflection profile, a series of flap section configurations are run.
- A total of **9 flap section configurations** are run for each deflection profile.
- *-4-1 configuration*



Flap Optimization Methodology

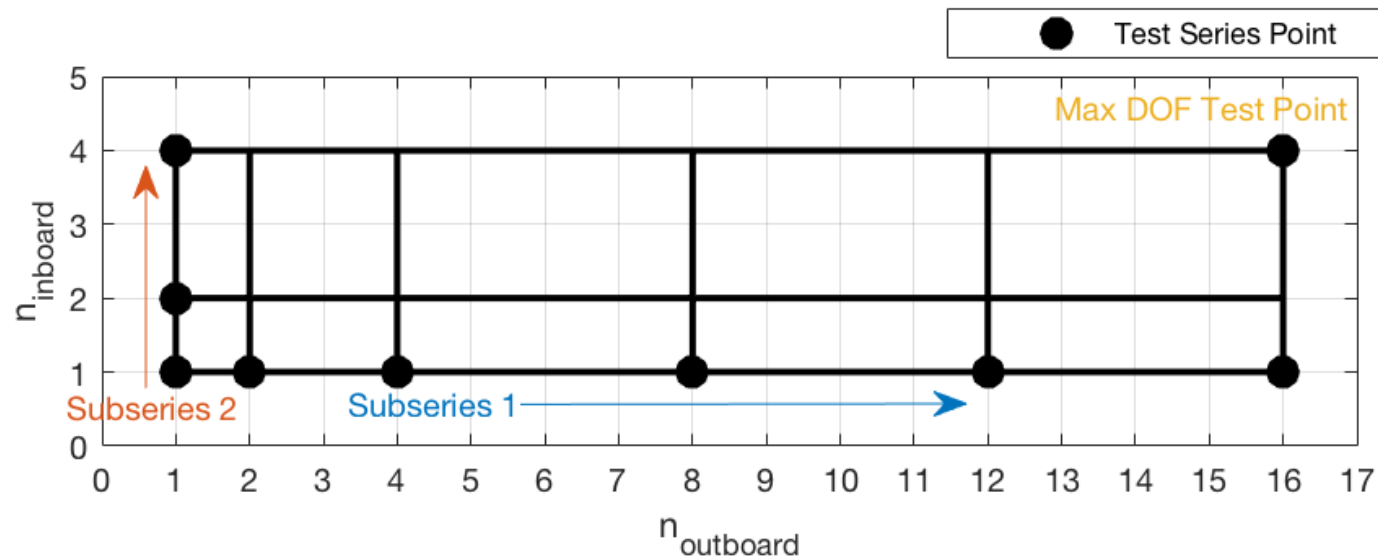
- For each deflection profile, a series of flap section configurations are run.
- A total of **9 flap section configurations** are run for each deflection profile.
- *-4-16 configuration*





Flap Optimization Methodology

- The 9 flap section configurations represent a design space search series where:
 - Subseries 1* – single inboard flap; 1,2,4,6,8,12,16 outboard flaps
 - Subseries 2* – 1,2,4, inboard flaps; single outboard flap
 - Max degrees of freedom (DOF) test point* – 4 inboard flaps; 16 outboard flaps



- A total of (5 deflection profiles) x (9 flap section configurations) = **45 VCCTEF candidate configurations** to be optimized.



Flap Optimization Methodology

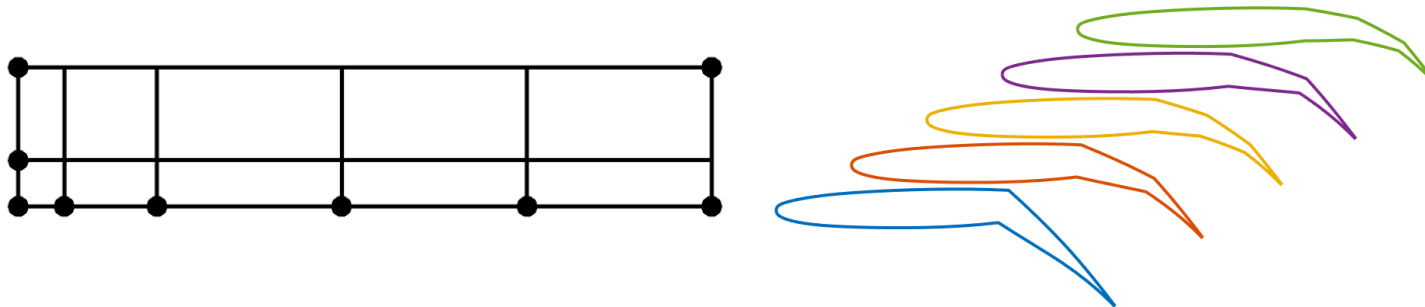
- A relative flap deflection variable is defined:

$$\mathbf{a} = \left[\begin{array}{c} \delta_{f,1} \\ \underbrace{\delta_{f,2} - \delta_{f,1}}_{\text{Relative Setting of Flap 2}} \\ \underbrace{\delta_{f,3} - \delta_{f,2}}_{\text{Relative Setting of Flap 3}} \\ \dots \\ \underbrace{\delta_{f,n_{inboard}+n_{outboard}} - \delta_{f,n_{inboard}+n_{outboard}-1}}_{\text{Relative Setting of Last Flap}} \end{array} \right]$$

- Optimization problem is cast as:

$$\begin{aligned} & \text{minimize } C_D = f(\alpha, \mathbf{a}) \\ & \text{subject to } C_L(\alpha, \mathbf{a}) = \bar{C}_L \\ & \quad -2 \leq a_j \leq 2, \quad j = 2, 3, \dots, n_{inboard} + n_{outboard} \end{aligned}$$

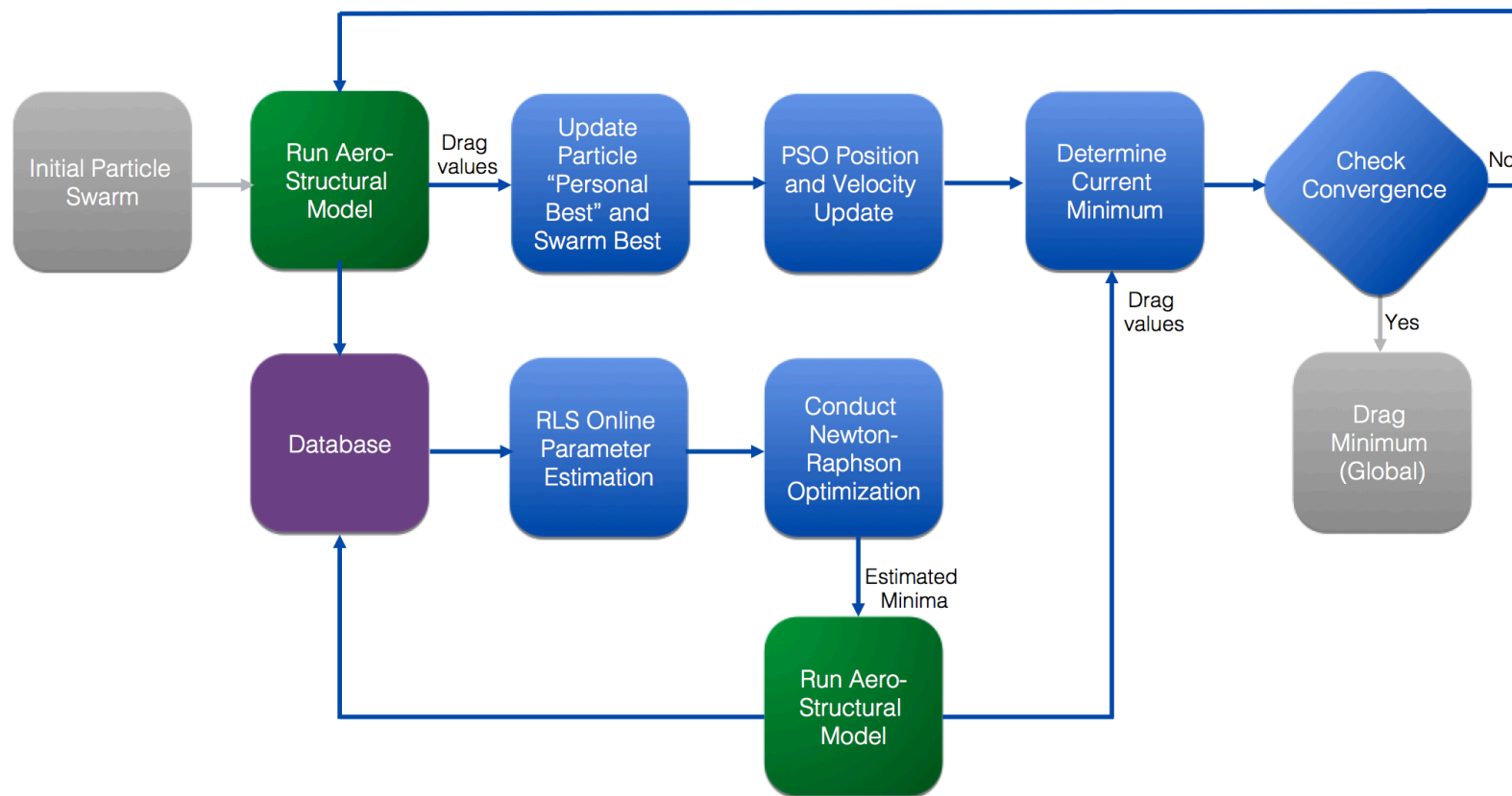
- In-house MATLAB hybrid particle swarm optimization (PSO) and recursive least squares (RLS) or **PSO-RLS** code is utilized to run 45 begin cruise off-design optimization runs.



Flap Optimization Methodology

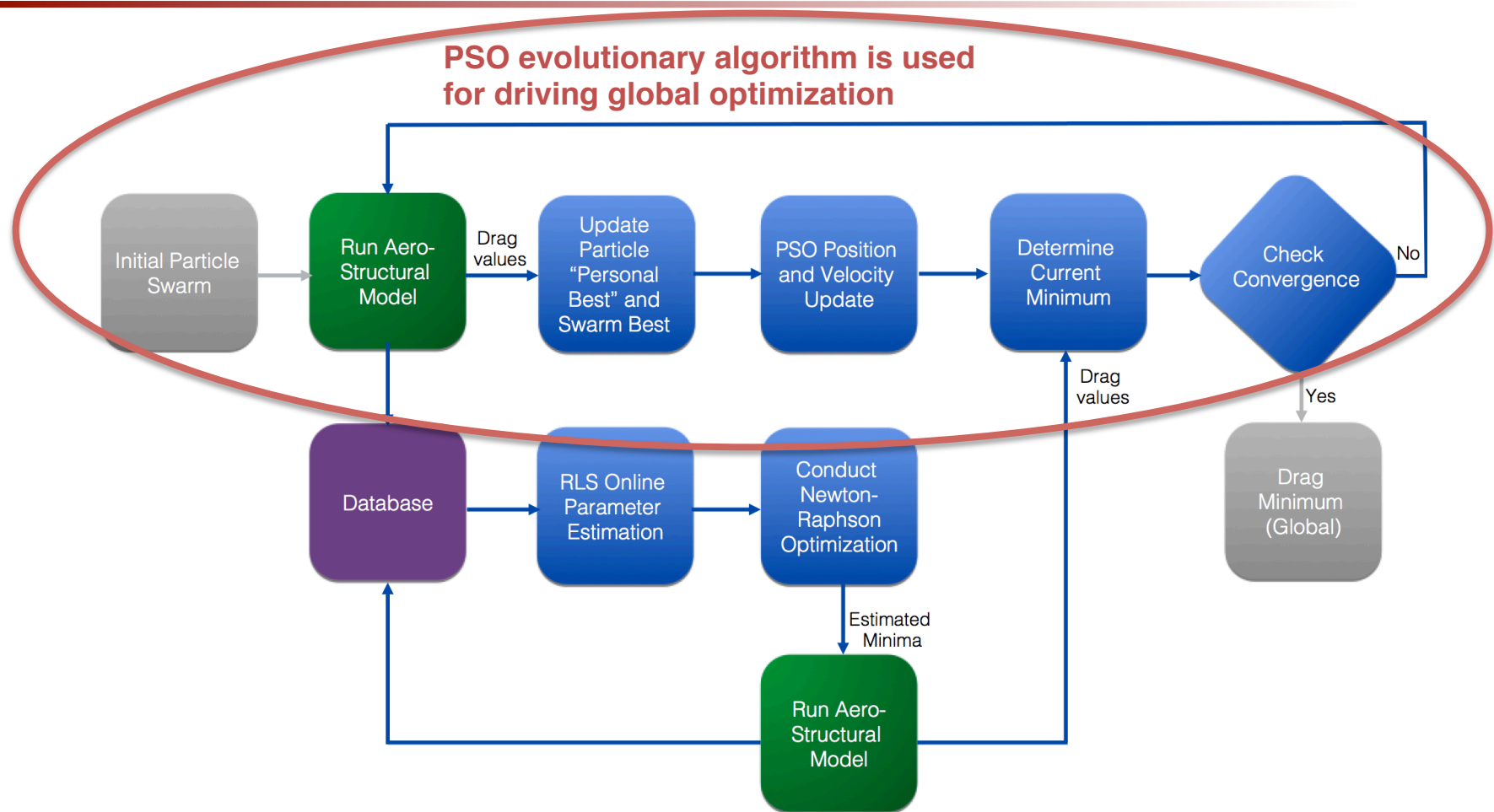


- PSO-RLS framework:



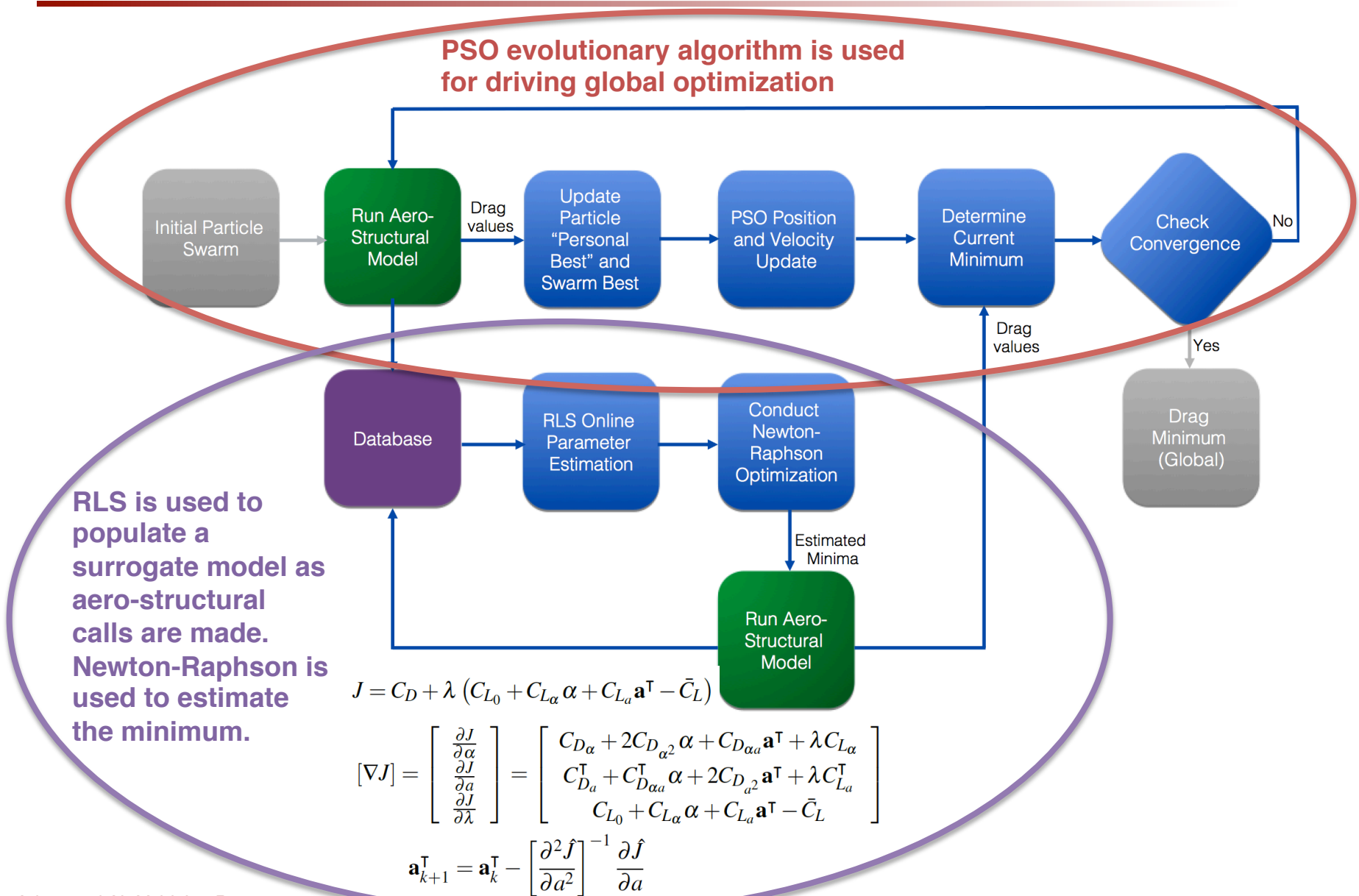


Flap Optimization Methodology



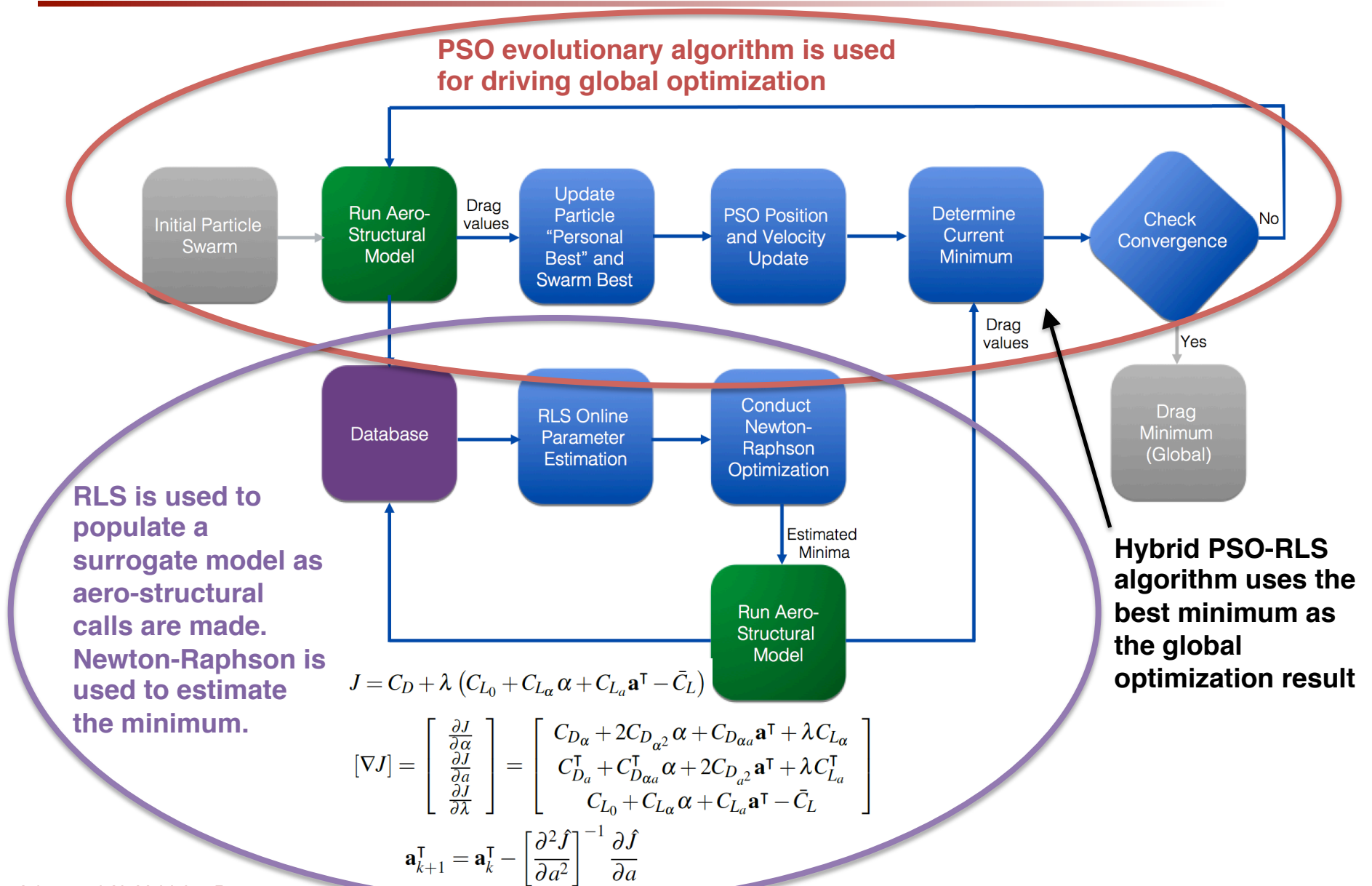


Flap Optimization Methodology





Flap Optimization Methodology

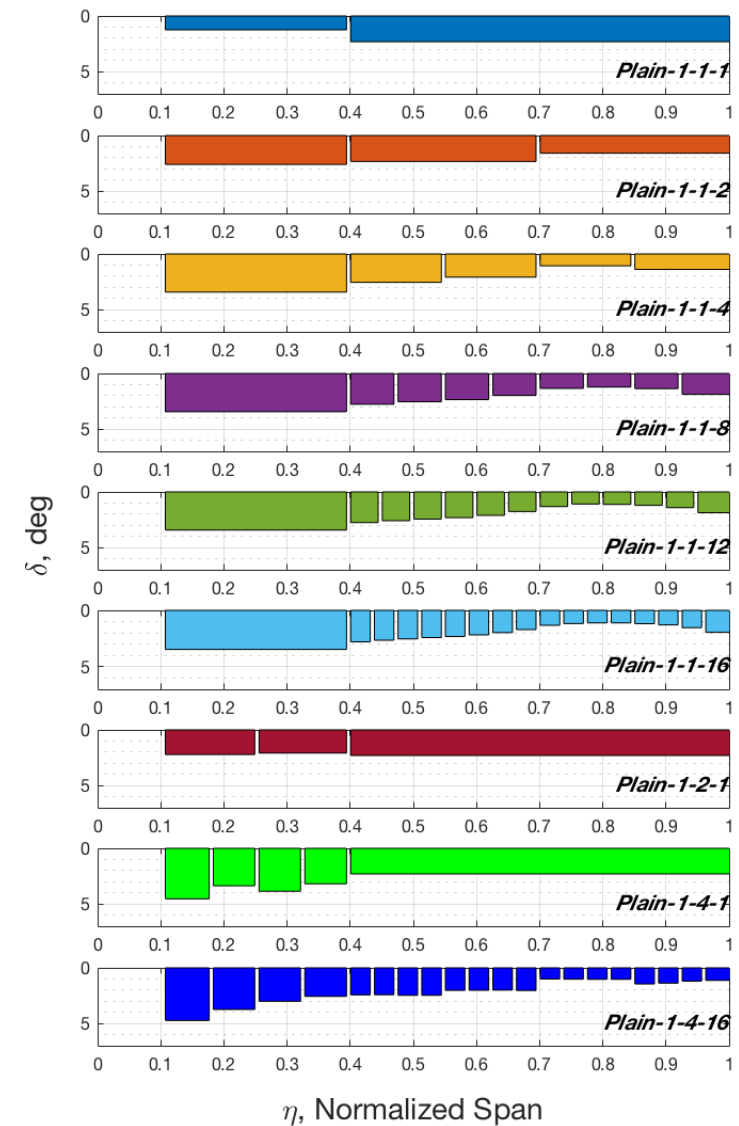


Flap Optimization Results



- *Plain* flap results:

Configuration	Optimized C_D	Clean Wing C_D	ΔC_D
<i>plain-1-1-1</i>	264.7	280.1	15.4
<i>plain-1-1-2</i>	261.4	280.1	18.7
<i>plain-1-1-4</i>	260.9	280.3	19.4
<i>plain-1-1-8</i>	260.6	280.4	19.8
<i>plain-1-1-12</i>	260.7	280.4	19.7
<i>plain-1-1-16</i>	260.7	280.1	19.4
<i>plain-1-2-1</i>	262.5	280.1	17.6
<i>plain-1-4-1</i>	260.4	280.2	19.8
<i>plain-1-4-16</i>	260.3	280.3	20.0

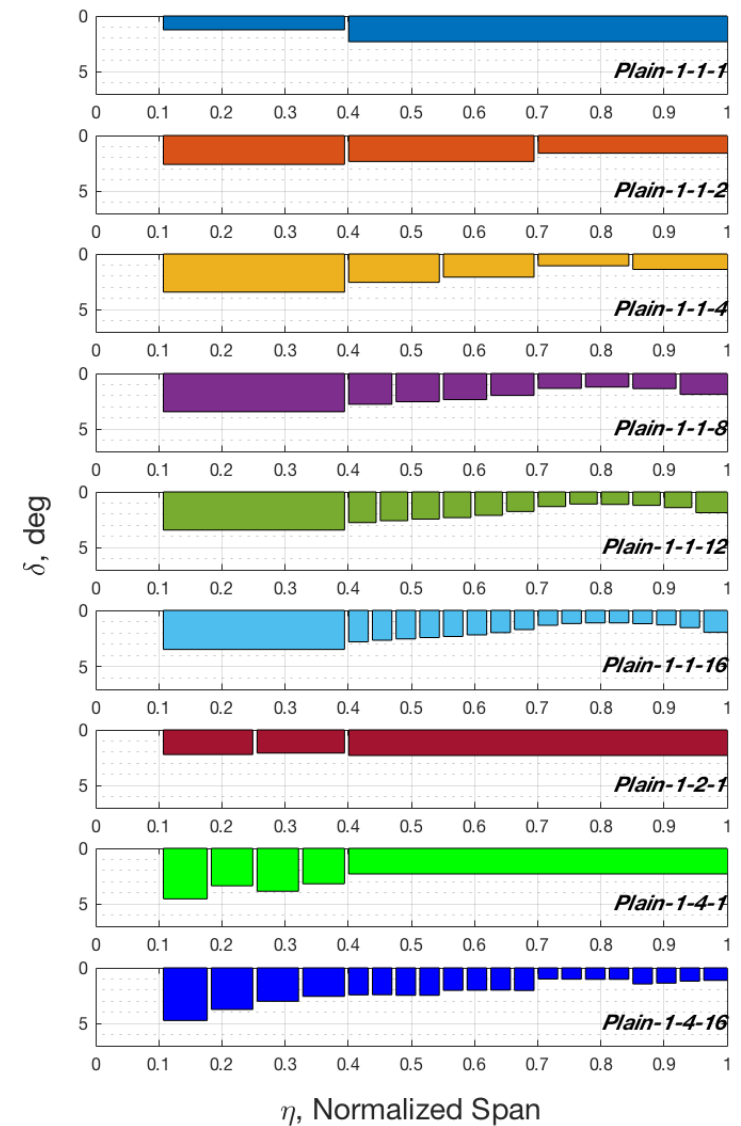




Flap Optimization Results

- *Plain* flap results:
 - *Plain-1-4-16* performs the best with 20.0 drag count reduction.

Configuration	Optimized C_D	Clean Wing C_D	ΔC_D
<i>plain-1-1-1</i>	264.7	280.1	15.4
<i>plain-1-1-2</i>	261.4	280.1	18.7
<i>plain-1-1-4</i>	260.9	280.3	19.4
<i>plain-1-1-8</i>	260.6	280.4	19.8
<i>plain-1-1-12</i>	260.7	280.4	19.7
<i>plain-1-1-16</i>	260.7	280.1	19.4
<i>plain-1-2-1</i>	262.5	280.1	17.6
<i>plain-1-4-1</i>	260.4	280.2	19.8
<i>plain-1-4-16</i>	260.3	280.3	20.0

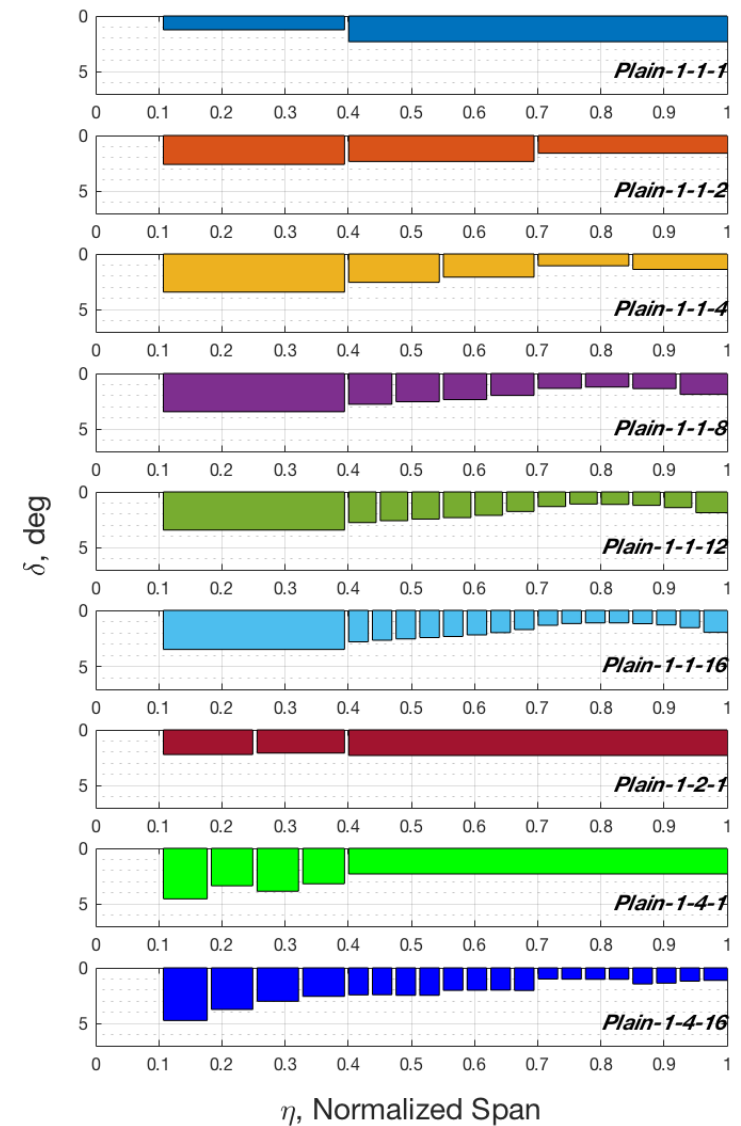




Flap Optimization Results

- *Plain* flap results:
 - *Plain-1-4-16* performs the best with 20.0 drag count reduction.
 - All configurations with 5+ flap sections are within 2% of the maximum (20.0) drag count reduction.

Configuration	Optimized C_D	Clean Wing C_D	ΔC_D
<i>plain-1-1-1</i>	264.7	280.1	15.4
<i>plain-1-1-2</i>	261.4	280.1	18.7
<i>plain-1-1-4</i>	260.9	280.3	19.4
<i>plain-1-1-8</i>	260.6	280.4	19.8
<i>plain-1-1-12</i>	260.7	280.4	19.7
<i>plain-1-1-16</i>	260.7	280.1	19.4
<i>plain-1-2-1</i>	262.5	280.1	17.6
<i>plain-1-4-1</i>	260.4	280.2	19.8
<i>plain-1-4-16</i>	260.3	280.3	20.0

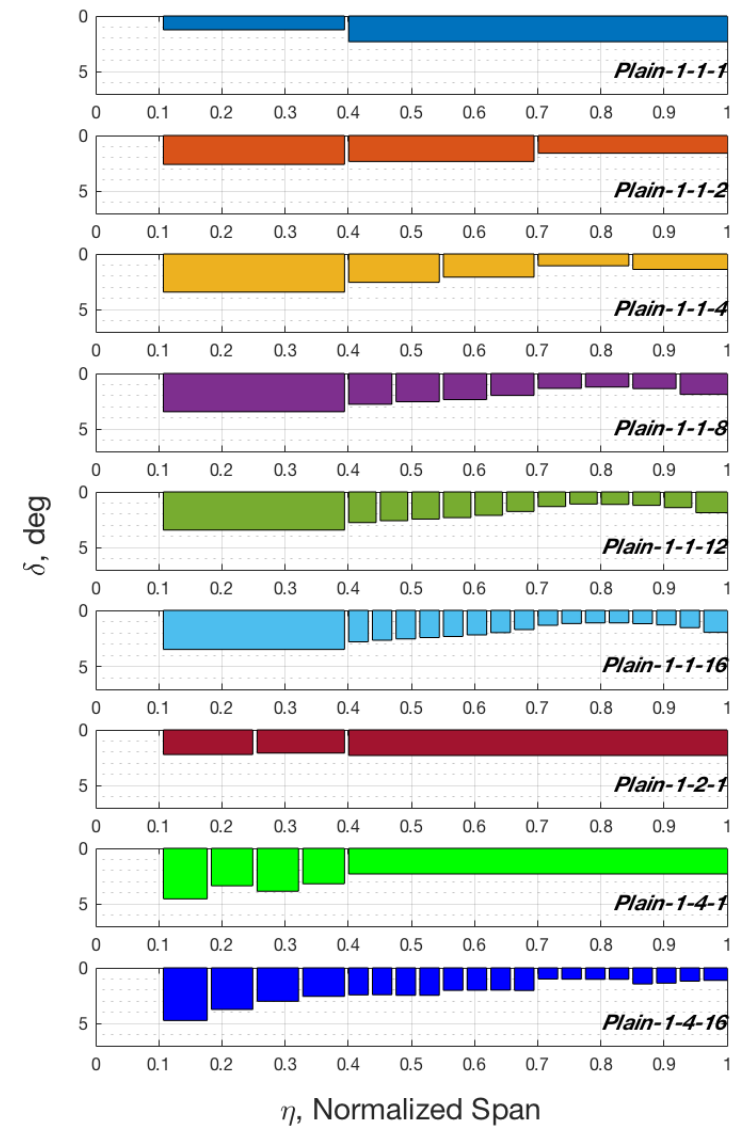


Flap Optimization Results



- *Circular-2* results:

Configuration	Optimized C_D	Clean Wing C_D	ΔC_D
<i>circular-2-1-1</i>	261.6	280.2	18.6
<i>circular-2-1-2</i>	260.8	280.2	19.4
<i>circular-2-1-4</i>	260.6	280.2	19.6
<i>circular-2-1-8</i>	260.5	280.3	19.8
<i>circular-2-1-12</i>	260.6	280.2	19.6
<i>circular-2-1-16</i>	260.4	280.3	19.9
<i>circular-2-2-1</i>	260.9	280.1	19.2
<i>circular-2-4-1</i>	260.6	280.2	19.6
<i>circular-2-4-16</i>	260.3	280.2	19.9

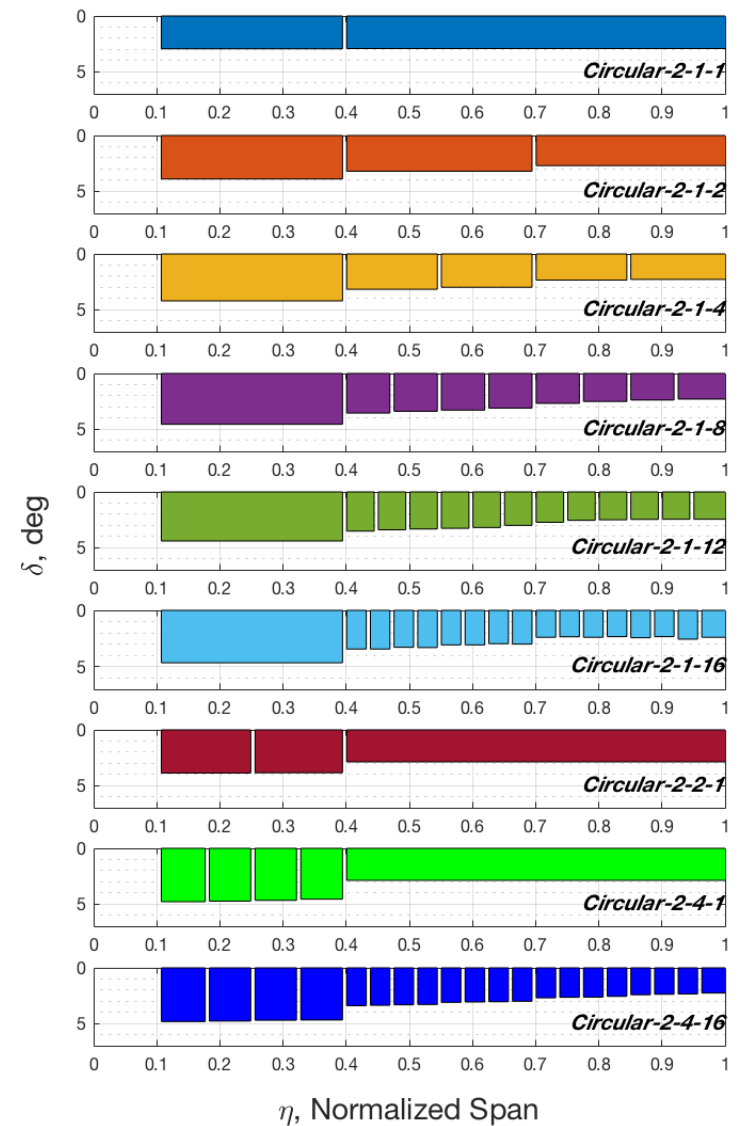


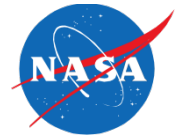


Flap Optimization Results

- *Circular-2* results:
 - *Circular-2-1-16* and *circular-2-4-16* perform the best with 19.9 drag count reduction.

Configuration	Optimized C_D	Clean Wing C_D	ΔC_D
<i>circular-2-1-1</i>	261.6	280.2	18.6
<i>circular-2-1-2</i>	260.8	280.2	19.4
<i>circular-2-1-4</i>	260.6	280.2	19.6
<i>circular-2-1-8</i>	260.5	280.3	19.8
<i>circular-2-1-12</i>	260.6	280.2	19.6
<i>circular-2-1-16</i>	260.4	280.3	19.9
<i>circular-2-2-1</i>	260.9	280.1	19.2
<i>circular-2-4-1</i>	260.6	280.2	19.6
<i>circular-2-4-16</i>	260.3	280.2	19.9

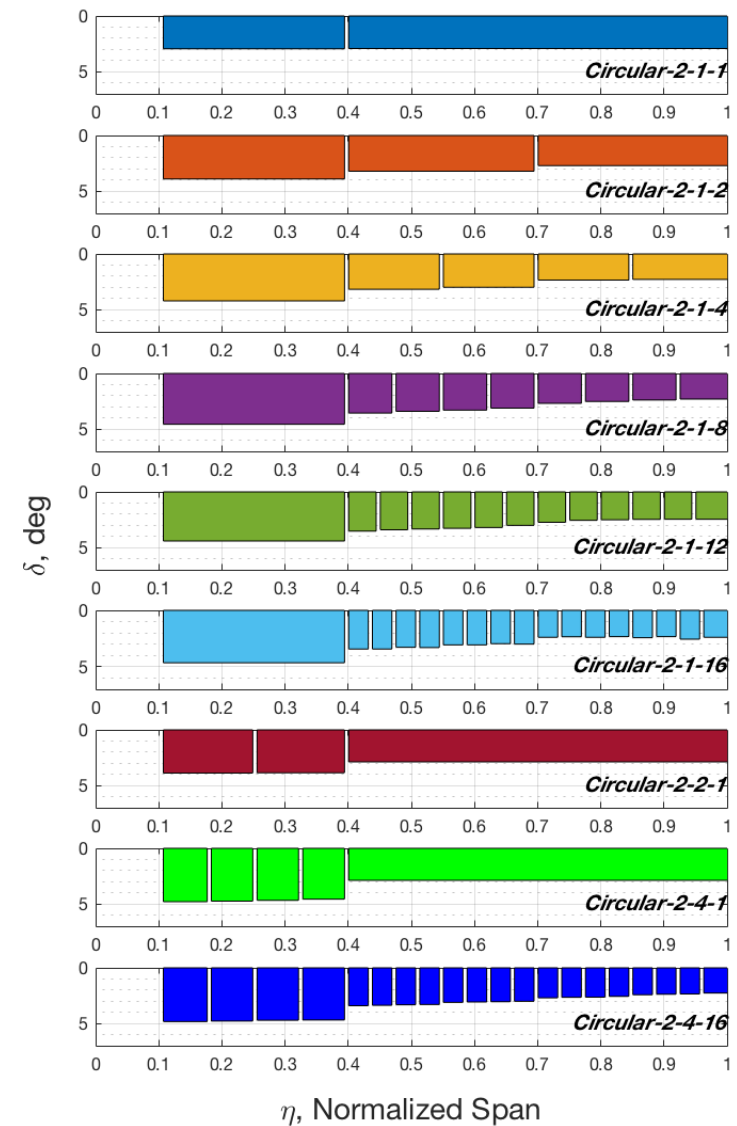




Flap Optimization Results

- *Circular-2* results:
 - *Circular-2-1-16* and *circular-2-4-16* perform the best with 19.9 drag count reduction.
 - All configurations with 5+ flap sections are within 2% of the maximum drag count reduction.

Configuration	Optimized C_D	Clean Wing C_D	ΔC_D
<i>circular-2-1-1</i>	261.6	280.2	18.6
<i>circular-2-1-2</i>	260.8	280.2	19.4
<i>circular-2-1-4</i>	260.6	280.2	19.6
<i>circular-2-1-8</i>	260.5	280.3	19.8
<i>circular-2-1-12</i>	260.6	280.2	19.6
<i>circular-2-1-16</i>	260.4	280.3	19.9
<i>circular-2-2-1</i>	260.9	280.1	19.2
<i>circular-2-4-1</i>	260.6	280.2	19.6
<i>circular-2-4-16</i>	260.3	280.2	19.9

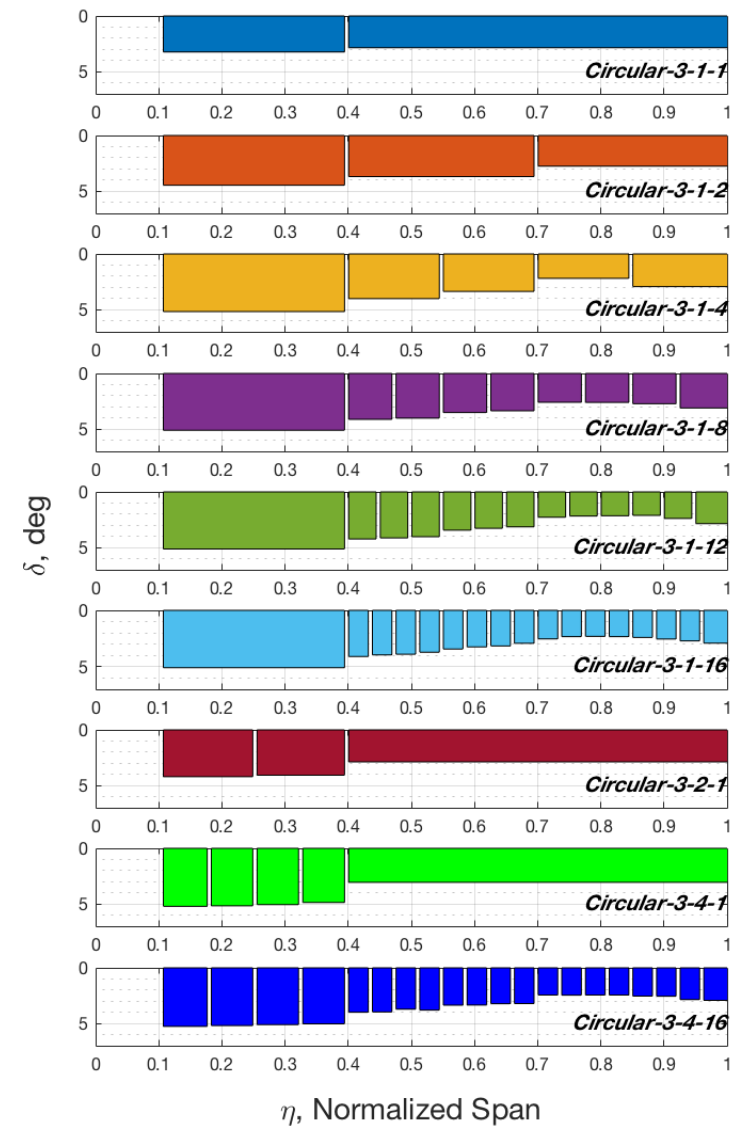


Flap Optimization Results



- Circular-3* results:

Configuration	Optimized C_D	Clean Wing C_D	ΔC_D
<i>circular-3-1-1</i>	260.8	280.2	19.4
<i>circular-3-1-2</i>	259.7	280.2	20.5
<i>circular-3-1-4</i>	258.6	280.2	21.6
<i>circular-3-1-8</i>	258.5	280.2	21.7
<i>circular-3-1-12</i>	258.3	280.3	22.0
<i>circular-3-1-16</i>	258.8	280.2	21.4
<i>circular-3-2-1</i>	259.8	280.2	20.4
<i>circular-3-4-1</i>	259.0	280.3	21.3
<i>circular-3-4-16</i>	258.5	280.3	21.8

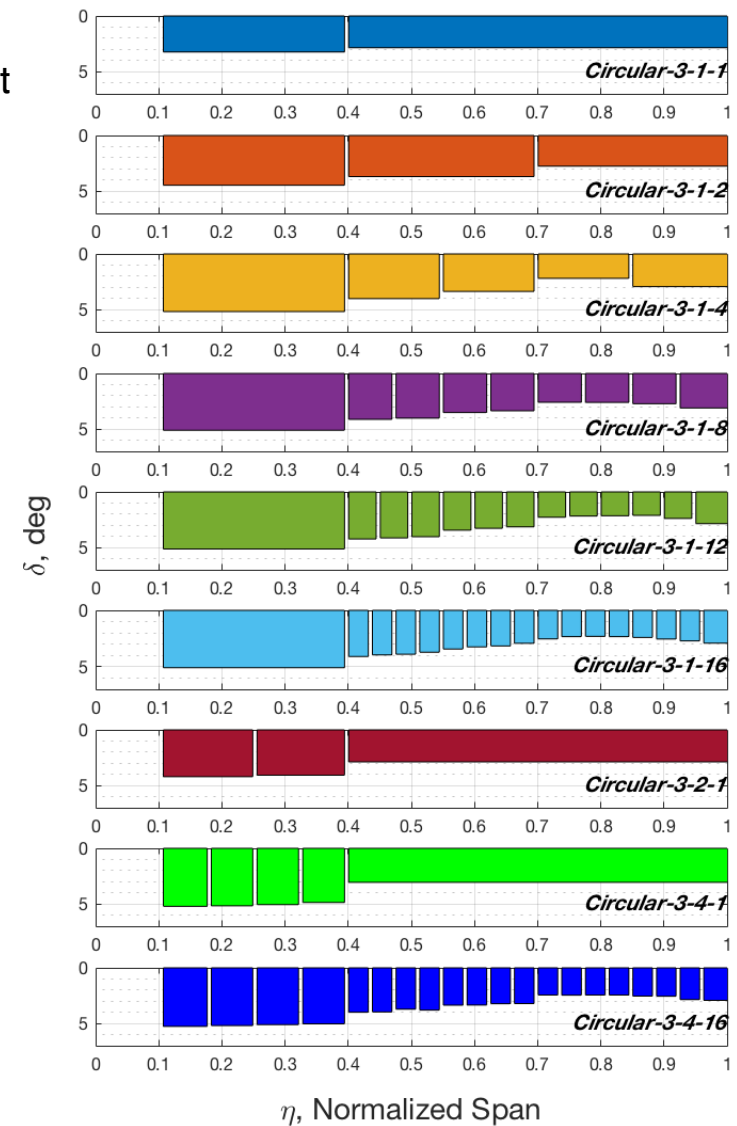




Flap Optimization Results

- *Circular-3* results:
 - *Circular-3-1-12* performs the best with 22.0 drag count reduction.

Configuration	Optimized C_D	Clean Wing C_D	ΔC_D
<i>circular-3-1-1</i>	260.8	280.2	19.4
<i>circular-3-1-2</i>	259.7	280.2	20.5
<i>circular-3-1-4</i>	258.6	280.2	21.6
<i>circular-3-1-8</i>	258.5	280.2	21.7
<i>circular-3-1-12</i>	258.3	280.3	22.0
<i>circular-3-1-16</i>	258.8	280.2	21.4
<i>circular-3-2-1</i>	259.8	280.2	20.4
<i>circular-3-4-1</i>	259.0	280.3	21.3
<i>circular-3-4-16</i>	258.5	280.3	21.8

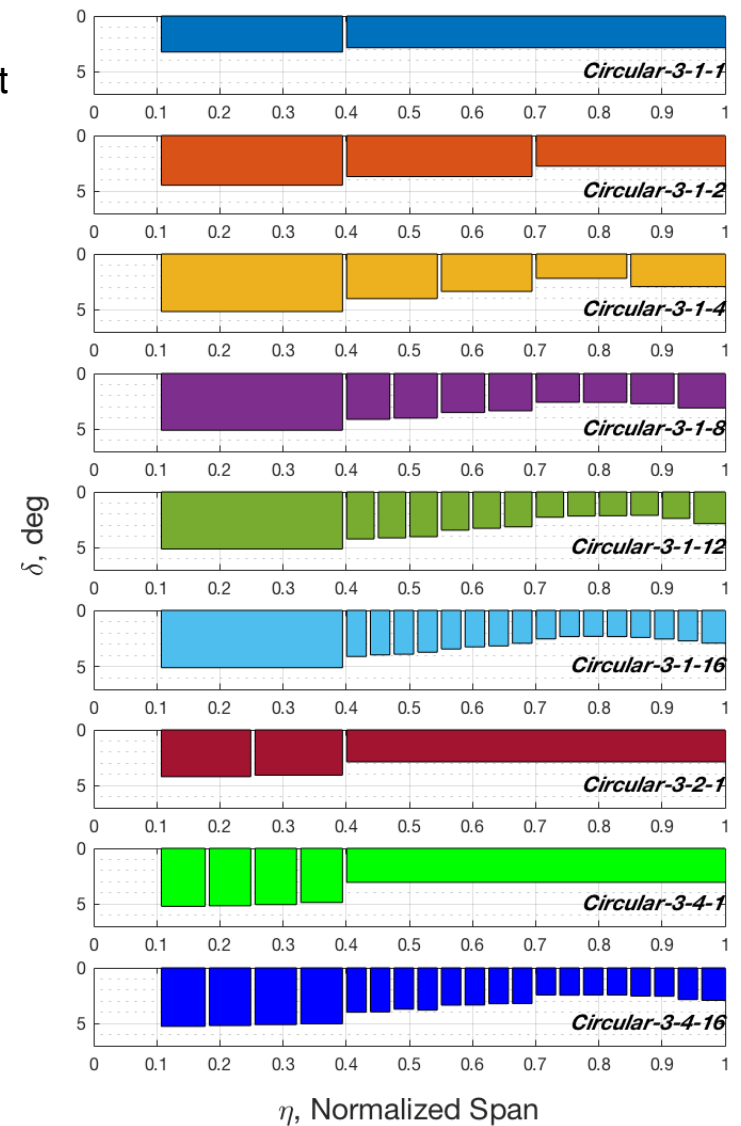




Flap Optimization Results

- *Circular-3* results:
 - *Circular-3-1-12* performs the best with 22.0 drag count reduction.
 - *Circular-3-1-4*, *circular-3-1-8*, and *circular-3-4-16* are within 2% of the maximum drag count reduction.

Configuration	Optimized C_D	Clean Wing C_D	ΔC_D
<i>circular-3-1-1</i>	260.8	280.2	19.4
<i>circular-3-1-2</i>	259.7	280.2	20.5
<i>circular-3-1-4</i>	258.6	280.2	21.6
<i>circular-3-1-8</i>	258.5	280.2	21.7
<i>circular-3-1-12</i>	258.3	280.3	22.0
<i>circular-3-1-16</i>	258.8	280.2	21.4
<i>circular-3-2-1</i>	259.8	280.2	20.4
<i>circular-3-4-1</i>	259.0	280.3	21.3
<i>circular-3-4-16</i>	258.5	280.3	21.8

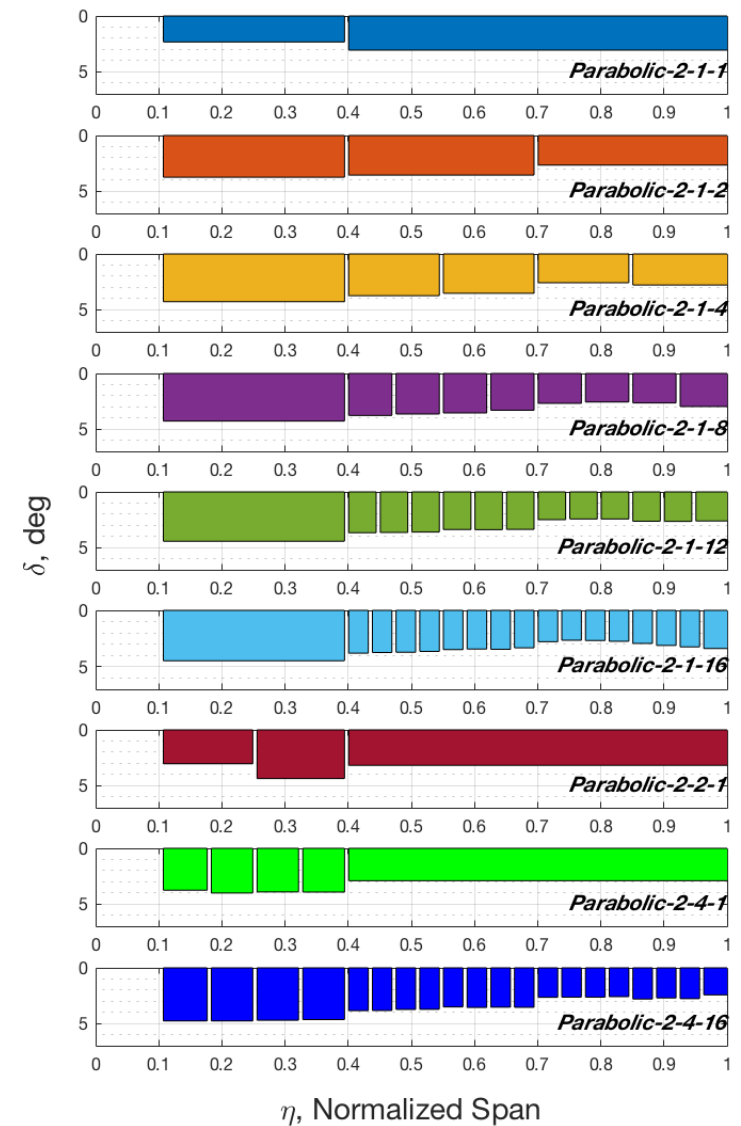




Flap Optimization Results

- *Parabolic-2* results:

Configuration	Optimized C_D	Clean Wing C_D	ΔC_D
<i>parabolic-2-1-1</i>	262.8	280.1	17.3
<i>parabolic-2-1-2</i>	261.1	280.1	19.0
<i>parabolic-2-1-4</i>	260.7	280.2	19.5
<i>parabolic-2-1-8</i>	260.4	280.1	19.7
<i>parabolic-2-1-12</i>	260.2	280.3	20.1
<i>parabolic-2-1-16</i>	260.0	280.3	20.3
<i>parabolic-2-2-1</i>	261.0	280.2	19.2
<i>parabolic-2-4-1</i>	260.9	280.2	19.3
<i>parabolic-2-4-16</i>	259.6	280.2	20.6

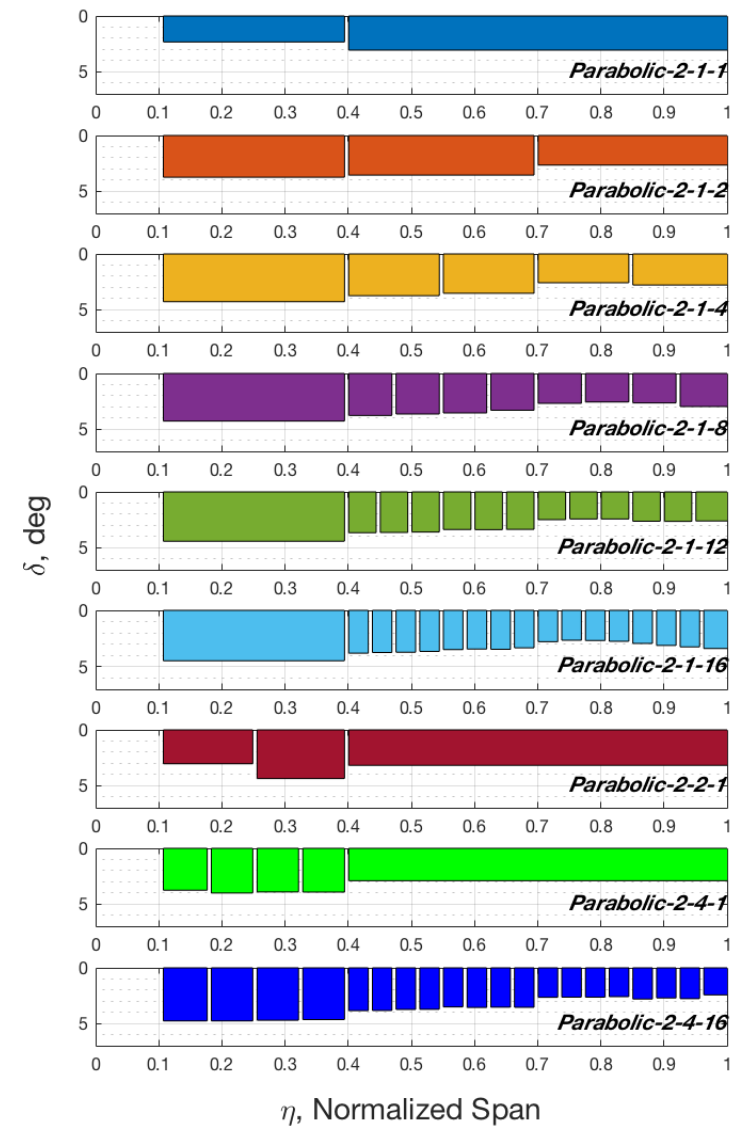




Flap Optimization Results

- *Parabolic-2* results:
 - *Parabolic-2-4-16* performs the best with 20.6 drag count reduction.

Configuration	Optimized C_D	Clean Wing C_D	ΔC_D
<i>parabolic-2-1-1</i>	262.8	280.1	17.3
<i>parabolic-2-1-2</i>	261.1	280.1	19.0
<i>parabolic-2-1-4</i>	260.7	280.2	19.5
<i>parabolic-2-1-8</i>	260.4	280.1	19.7
<i>parabolic-2-1-12</i>	260.2	280.3	20.1
<i>parabolic-2-1-16</i>	260.0	280.3	20.3
<i>parabolic-2-2-1</i>	261.0	280.2	19.2
<i>parabolic-2-4-1</i>	260.9	280.2	19.3
<i>parabolic-2-4-16</i>	259.6	280.2	20.6

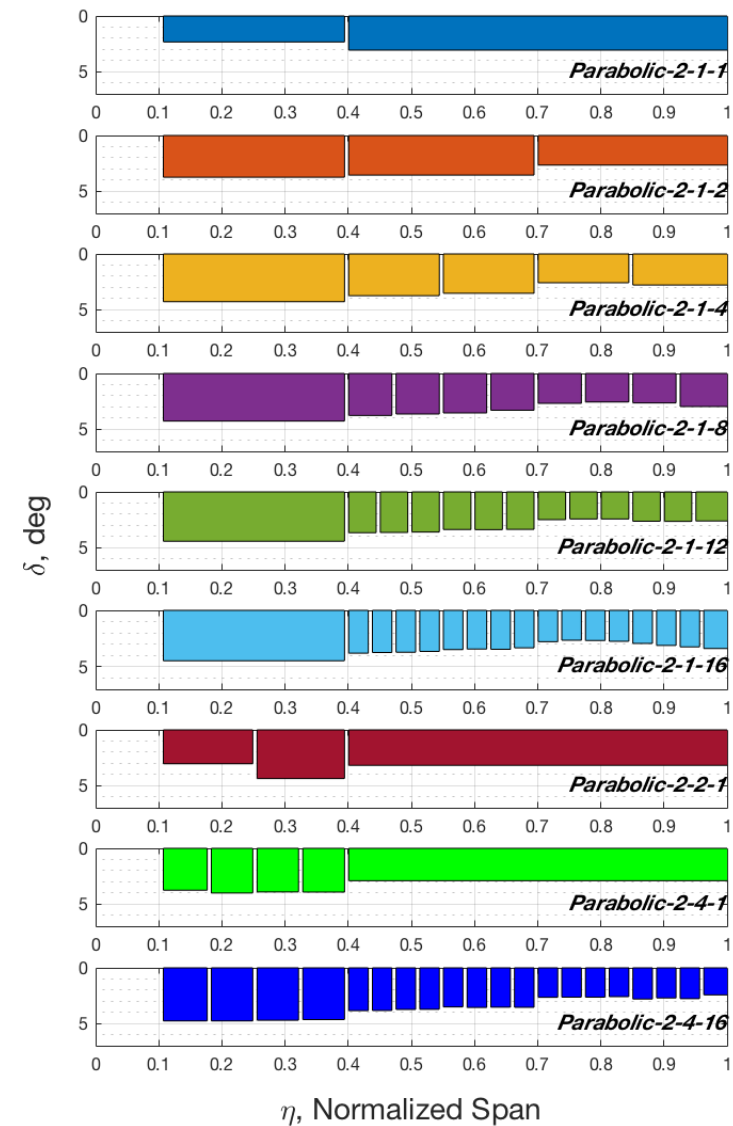




Flap Optimization Results

- *Parabolic-2* results:
 - *Parabolic-2-4-16* performs the best with 20.6 drag count reduction.
 - *Parabolic-2-1-16* is within 2% of the maximum drag count reduction.

Configuration	Optimized C_D	Clean Wing C_D	ΔC_D
<i>parabolic-2-1-1</i>	262.8	280.1	17.3
<i>parabolic-2-1-2</i>	261.1	280.1	19.0
<i>parabolic-2-1-4</i>	260.7	280.2	19.5
<i>parabolic-2-1-8</i>	260.4	280.1	19.7
<i>parabolic-2-1-12</i>	260.2	280.3	20.1
<i>parabolic-2-1-16</i>	260.0	280.3	20.3
<i>parabolic-2-2-1</i>	261.0	280.2	19.2
<i>parabolic-2-4-1</i>	260.9	280.2	19.3
<i>parabolic-2-4-16</i>	259.6	280.2	20.6

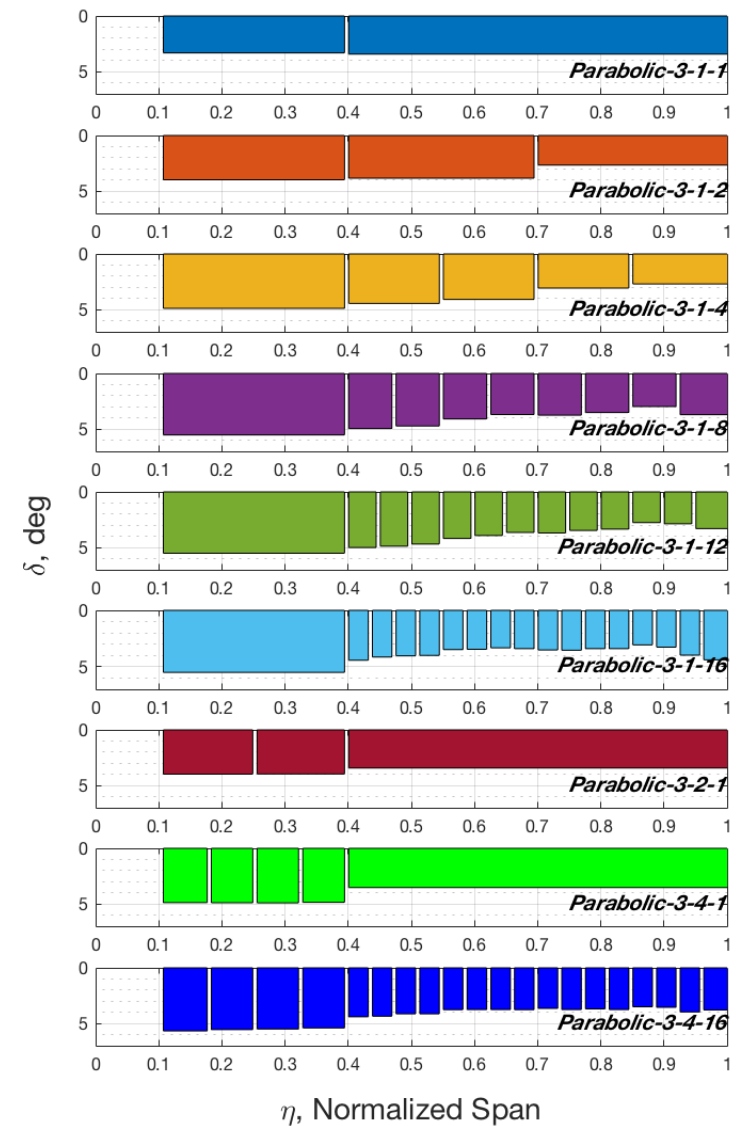


Flap Optimization Results



- *Parabolic-3* results:

Configuration	Optimized C_D	Clean Wing C_D	ΔC_D
<i>parabolic-3-1-1</i>	260.5	280.2	19.7
<i>parabolic-3-1-2</i>	258.7	280.4	21.7
<i>parabolic-3-1-4</i>	257.2	280.4	22.3
<i>parabolic-3-1-8</i>	256.3	280.5	24.2
<i>parabolic-3-1-12</i>	255.6	280.5	24.9
<i>parabolic-3-1-16</i>	256.0	280.5	24.5
<i>parabolic-3-2-1</i>	260.0	280.2	21.2
<i>parabolic-3-4-1</i>	256.9	280.3	23.4
<i>parabolic-3-4-16</i>	255.5	280.6	25.1

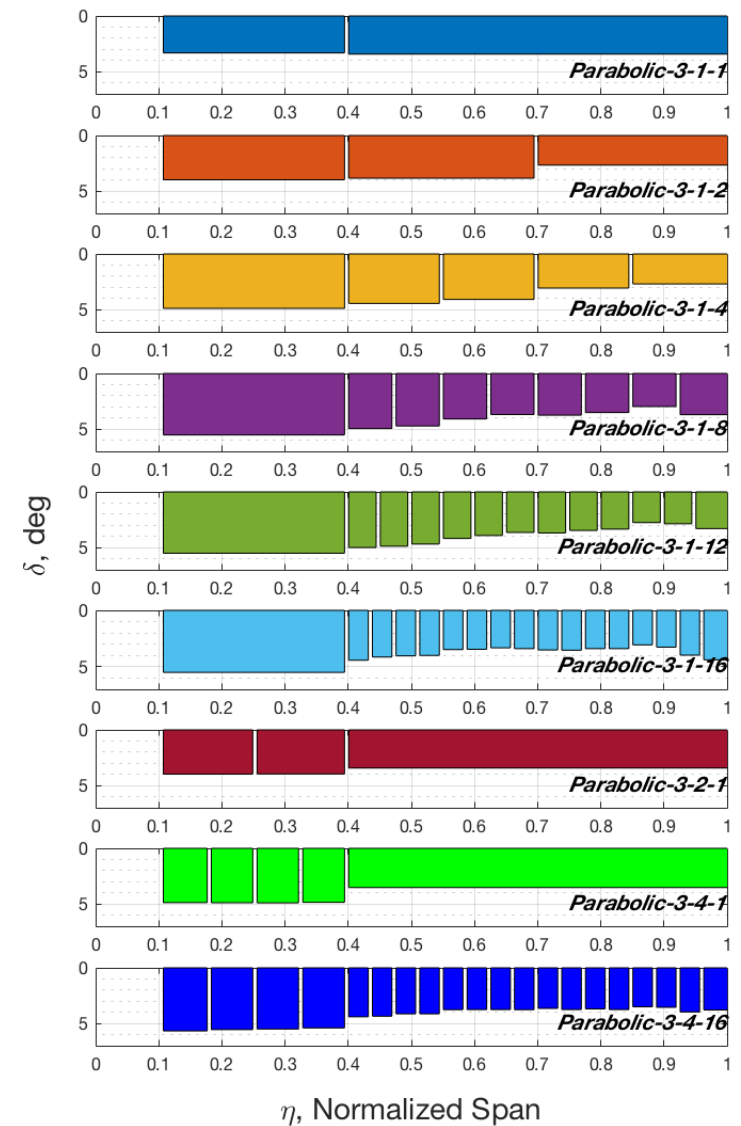




Flap Optimization Results

- *Parabolic-3* results:
 - *Parabolic-3-4-16* performs the best with 20.6 drag count reduction.

Configuration	Optimized C_D	Clean Wing C_D	ΔC_D
<i>parabolic-3-1-1</i>	260.5	280.2	19.7
<i>parabolic-3-1-2</i>	258.7	280.4	21.7
<i>parabolic-3-1-4</i>	257.2	280.4	22.3
<i>parabolic-3-1-8</i>	256.3	280.5	24.2
<i>parabolic-3-1-12</i>	255.6	280.5	24.9
<i>parabolic-3-1-16</i>	256.0	280.5	24.5
<i>parabolic-3-2-1</i>	260.0	280.2	21.2
<i>parabolic-3-4-1</i>	256.9	280.3	23.4
<i>parabolic-3-4-16</i>	255.5	280.6	25.1

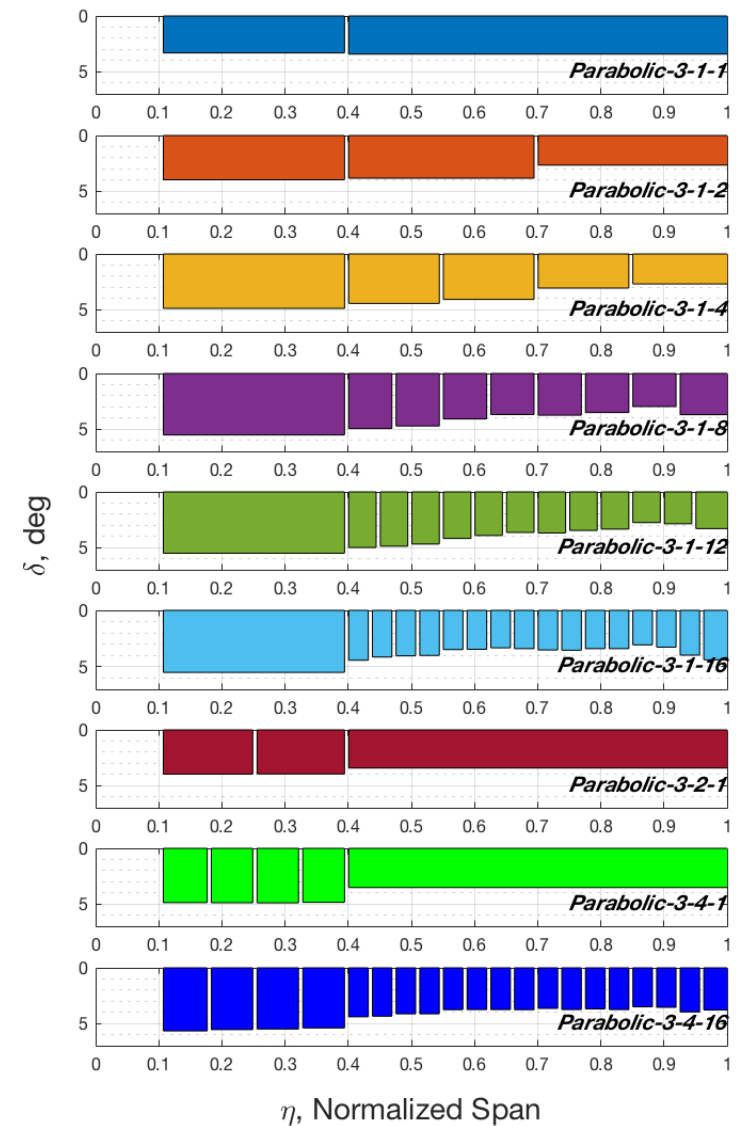




Flap Optimization Results

- *Parabolic-3* results:
 - *Parabolic-3-4-16* performs the best with 20.6 drag count reduction.
 - *Parabolic-3-1-12* is within 2% of the maximum drag count reduction.

Configuration	Optimized C_D	Clean Wing C_D	ΔC_D
<i>parabolic-3-1-1</i>	260.5	280.2	19.7
<i>parabolic-3-1-2</i>	258.7	280.4	21.7
<i>parabolic-3-1-4</i>	257.2	280.4	22.3
<i>parabolic-3-1-8</i>	256.3	280.5	24.2
<i>parabolic-3-1-12</i>	255.6	280.5	24.9
<i>parabolic-3-1-16</i>	256.0	280.5	24.5
<i>parabolic-3-2-1</i>	260.0	280.2	21.2
<i>parabolic-3-4-1</i>	256.9	280.3	23.4
<i>parabolic-3-4-16</i>	255.5	280.6	25.1





Flap Optimization Analysis

- Top 12 best drag reduction configurations:

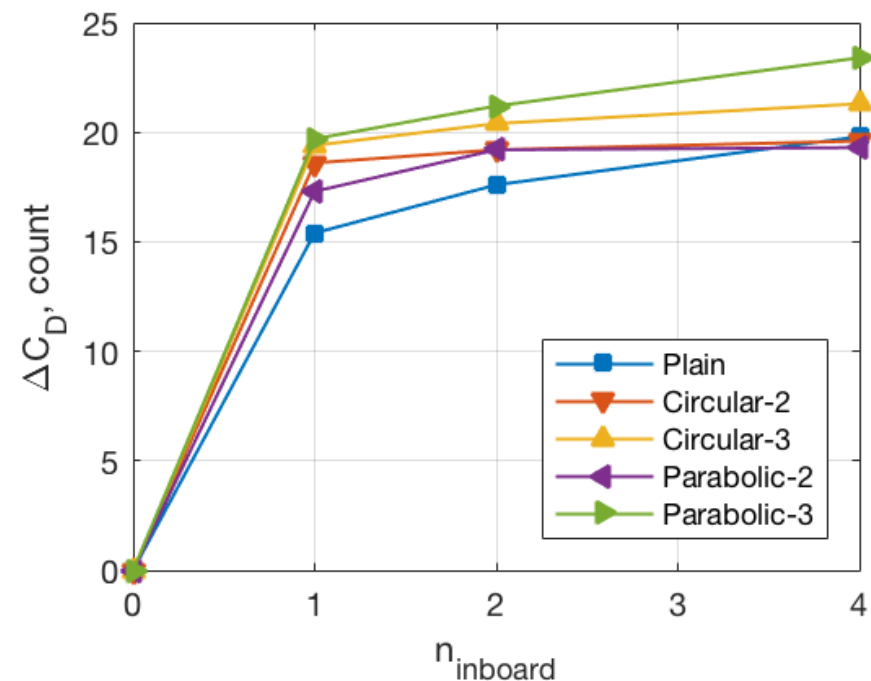
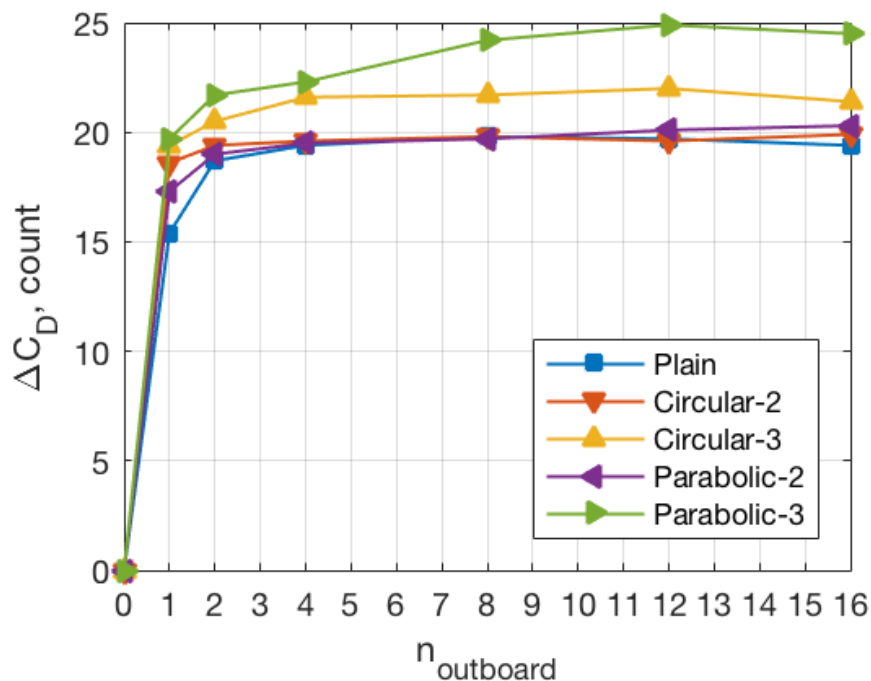
Rank	Configuration	ΔC_D	% Drag Reduction
1	<i>parabolic-3-4-16</i>	25.1	8.95
2	<i>parabolic-3-1-12</i>	24.9	8.88
3	<i>parabolic-3-1-16</i>	24.5	8.73
4	<i>parabolic-3-1-8</i>	24.2	8.63
5	<i>parabolic-3-4-1</i>	23.4	8.35
6	<i>parabolic-3-1-4</i>	22.3	7.95
7	<i>circular-3-1-12</i>	22.0	7.85
8	<i>circular-3-4-16</i>	21.8	7.78
9	<i>parabolic-3-1-2</i>	21.7	7.74
10	<i>circular-3-1-8</i>	21.7	7.74
11	<i>circular-3-1-4</i>	21.6	7.71
12	<i>circular-3-1-16</i>	21.4	7.63

- Top drag reduction performance is with the *parabolic-3* with top 6 performers achieving 7.95–8.95% drag reduction.
- Circular-3* achieves next best performance with 7.85% drag reduction.
- Parabolic-2* achieves a maximum of 7.35% drag reduction.
- Plain* and *Circular-2* achieve a maximum of 7.14% and 7.10% drag reduction, respectively.

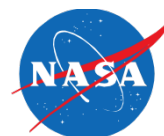


Flap Optimization Analysis

- To estimate the most efficient number of VCCTEF sections, flap result trends are observed.
- Max drag reduction is plotted against the number of outboard flaps with a single inboard flap (subseries 1) and the number of inboard flaps with a single outboard flap (subseries 2).

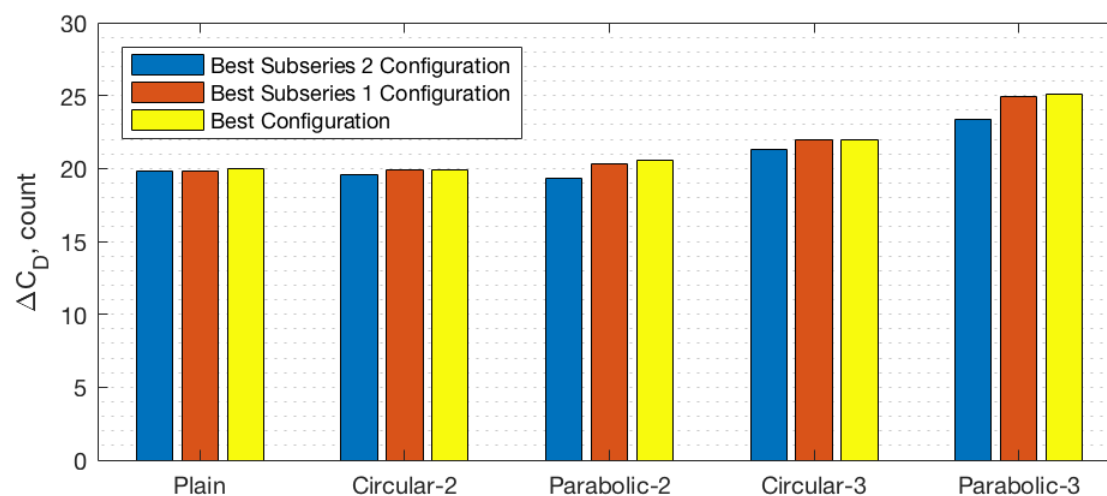


- When using only a single or dual camber flap configuration, the drag reduction does not improve much past using 4 outboard flaps.
- The *parabolic-3* configuration experiences drag reduction up to about when 12 outboard flaps are employed.

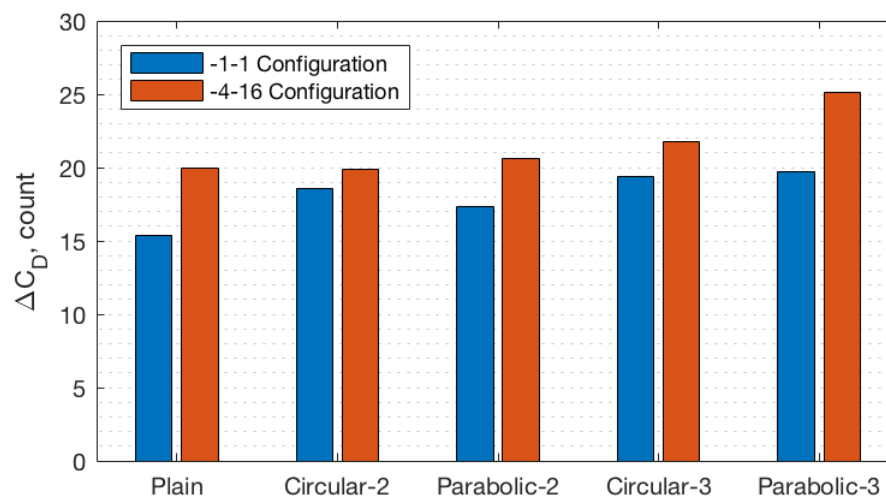


Flap Optimization Analysis

- In general, it seems adequate to use a single inboard flap with more outboard flaps.



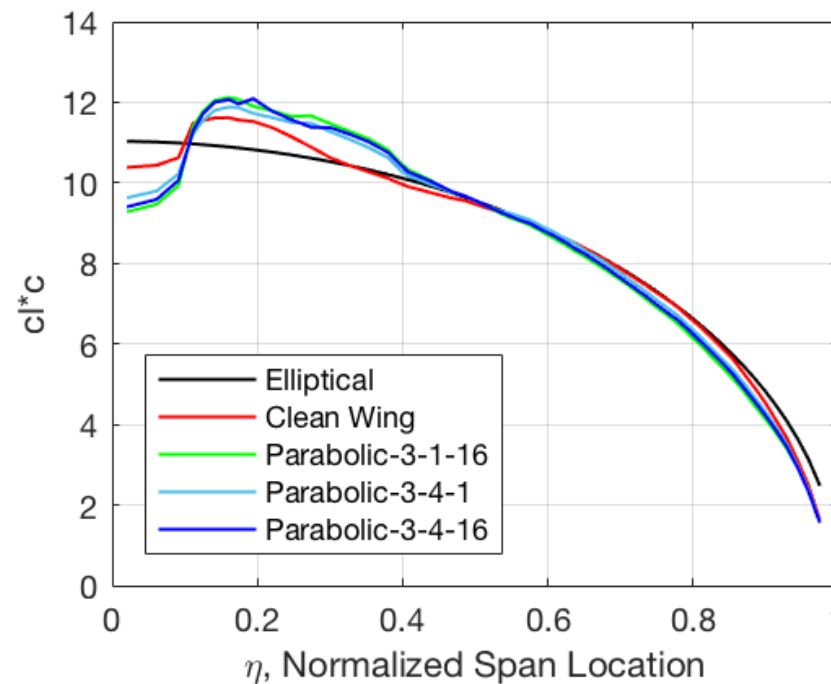
- Drag reduction is tightly coupled with deflection profile.





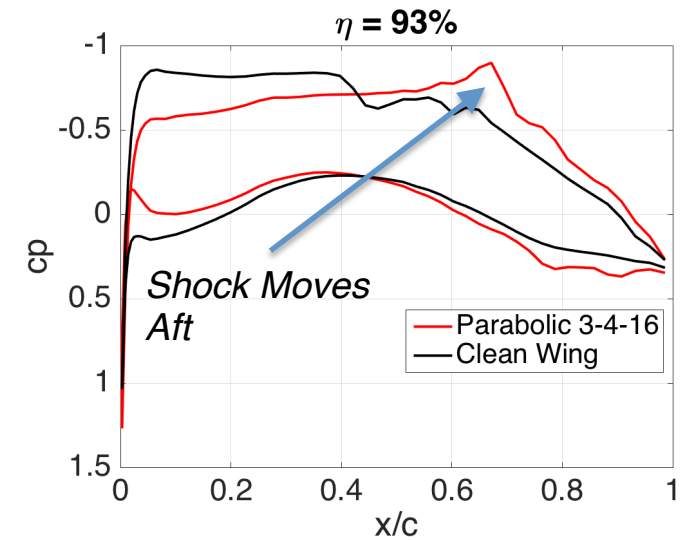
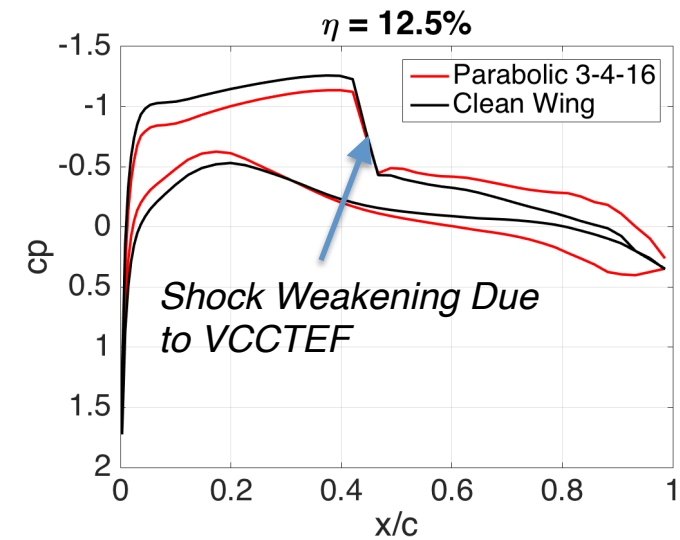
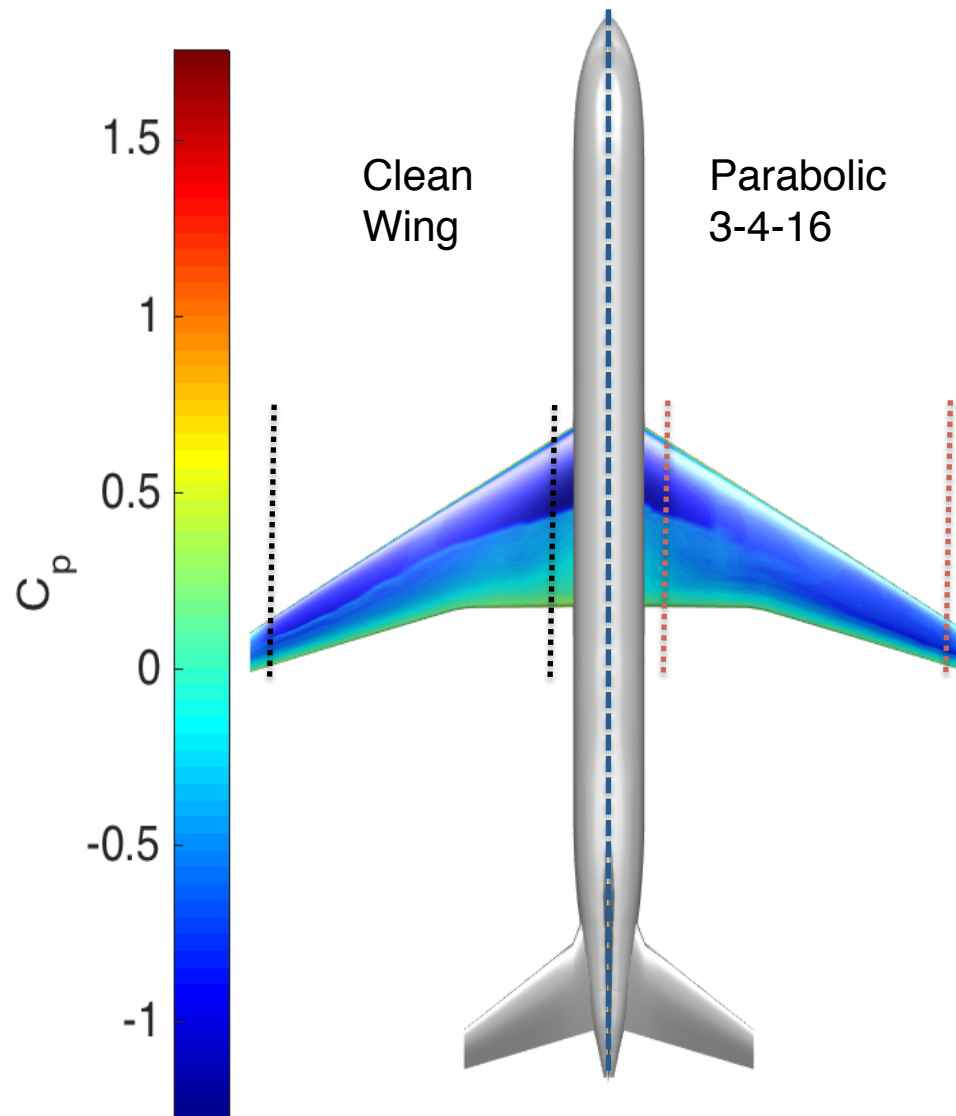
Flap Optimization Analysis

- Aerodynamic analysis is conducted in order to gain insight into optimization results.
- The lift distributions of the optimized *parabolic-3-1-16*, *parabolic-3-4-1*, and *parabolic-3-4-16* are shown:



Results show that the optimized flap deflections push the lift away from an elliptical distribution.

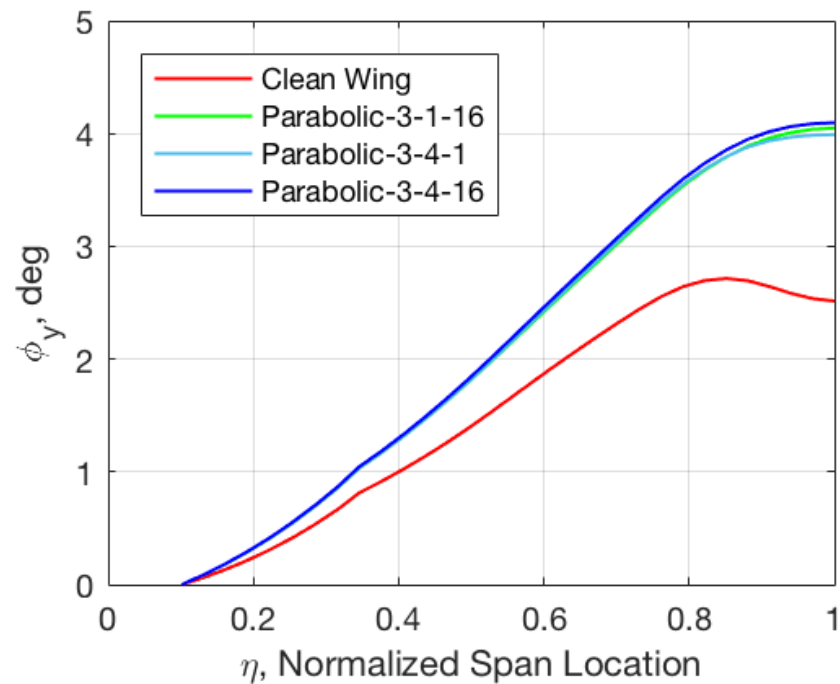
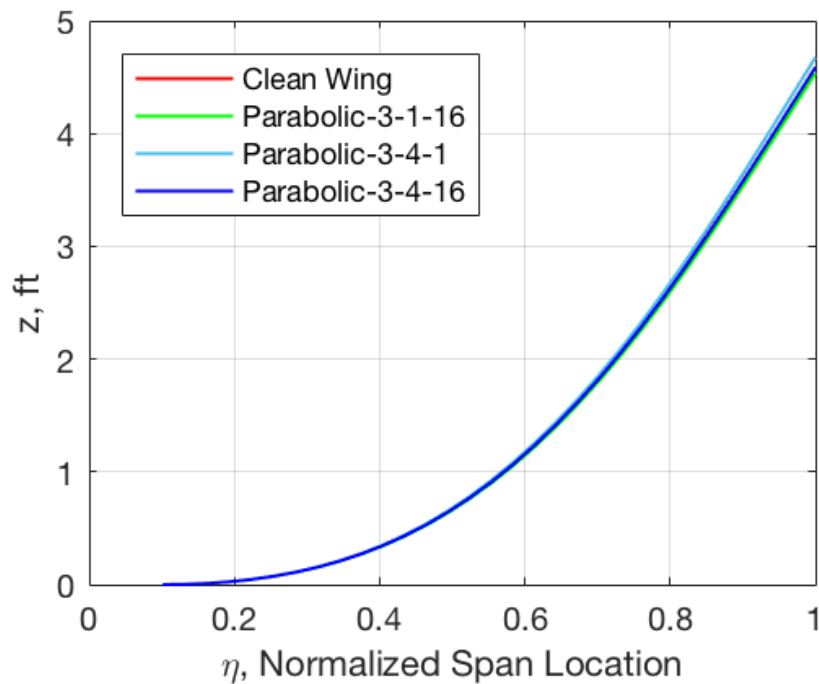
Flap Optimization Analysis





Flap Optimization Analysis

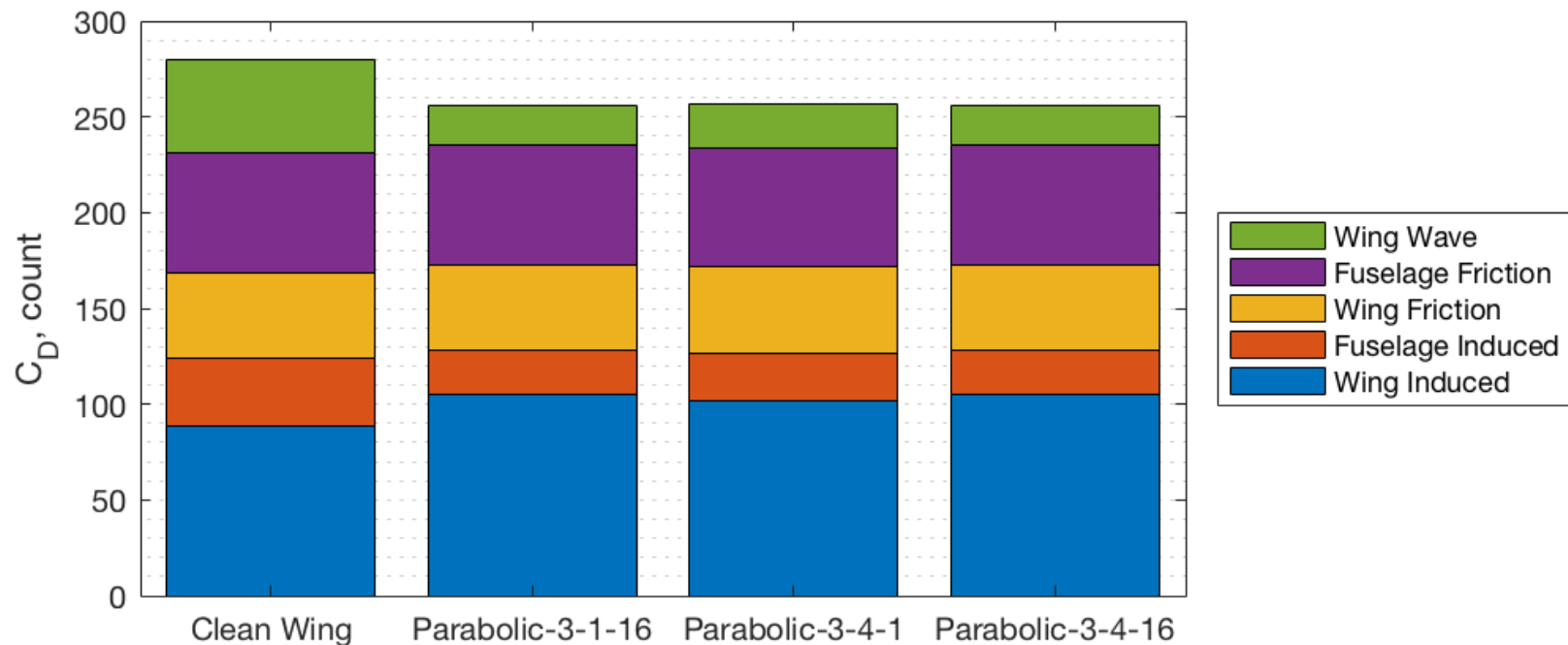
- Aeroelastic deformation shows little change in vertical bending, but increase in nose-down aeroelastic washout (ϕ_y measured positive nose-down).



Flap Optimization Analysis



- Total drag breakdown into source components (wave, induced, friction) is presented:

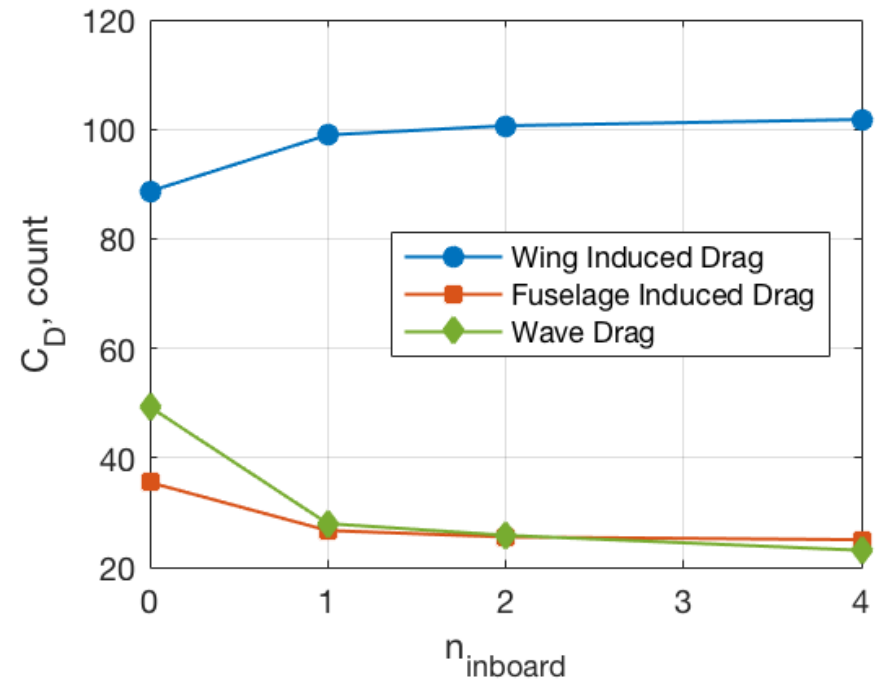
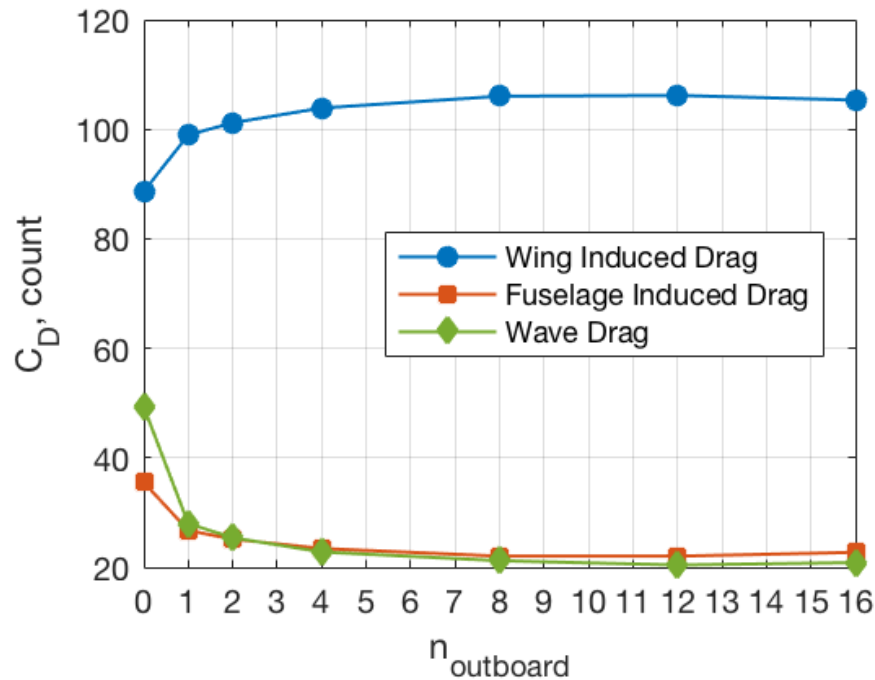


- Results demonstrate that the primary reduction in overall drag due to optimized VCCTEF deflections is due to reduction in wave drag.
 - Overall induced drag remains nearly same but is redistributed onto the wing.



Flap Optimization Analysis

- Induced and wave drag components are plotted along the subseries directions:



- Results are consistent with an overall reduction in wave drag while induced drag is transferred from the fuselage to the wing.
- Parabolic-3* configuration analysis is presented—all configurations demonstrated similar trends.

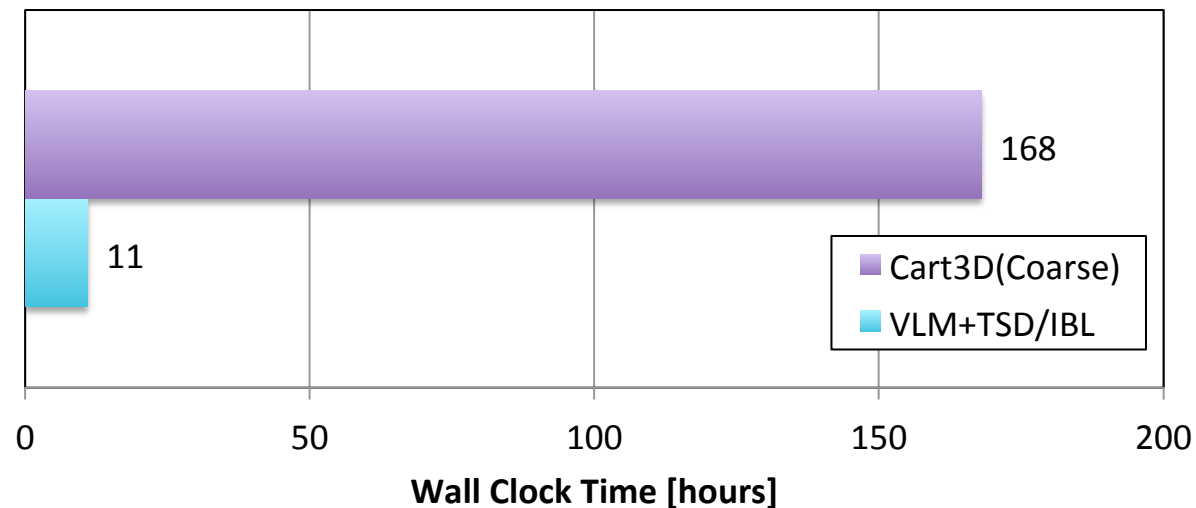
Computational Efficiency



- On a Linux Red Hat Enterprise 6.9 workstation, each optimization took around 11-14 hours.
 - 36 2.10 GHz cores
 - 96 GB of memory
 - On the order of 980 calls to the aero-structural model.
- A single Cart3D optimization would have taken an estimated 7-10 days to complete.



Projected Wall-clock Comparison of VCCTEF Optimization





Summary and Future Work

Summary



- Developed transonic and viscous potential flow framework for rapid design exploration and optimization of flexible wing transport aircraft
 - Modeled the GTM equipped with the VCCTEF
 - Frameworks show excellent agreement between MSES and TSD/IBL methods
 - Demonstrated close agreement with LAVA RANS solver with both rigid and flexible wings
 - Wall-clock time is orders of magnitude faster than Euler and RANS
- **The computational efficiency of the transonic and viscous potential flow method and close agreement with RANS make it well-suited for analysis of aeroelastic wings.**
- A drag optimization study is conducted on VCCTEF configurations equipped at the begin cruise, off-design flight condition.
 - Hybrid PSO-RLS framework used for optimization.
 - 45 VCCTEF configurations are examined
 - 5 deflection profiles
 - 9 flap section combinations
- Optimization results show best performance of the *parabolic-3* configurations
 - *Parabolic-3-4-16* configuration achieves the highest drag reduction of 8.95%



Summary

- *Parabolic-3* configuration has a highest drag reduction of 8.95%
 - *Circular-3* configuration has a highest drag reduction of 7.85%
 - *Parabolic-2* configuration has a highest drag reduction of 7.35%
 - *Plain* configuration has a highest drag reduction of 7.13%
 - *Circular-2* configuration has a highest drag reduction of 7.10%
- Results show that within 2% of highest drag reduction measured is generally achievable using only a single inboard flap.
- As the number of outboard flaps are increased, the drag reduction does not increase greatly past 4.
 - For the *parabolic-3* configuration, using 4 outboard flaps achieves ~7.95% drag reduction.
 - For the *parabolic-3* configuration, using 8 outboard flaps achieves ~8.63% drag reduction.
- Aerodynamic analysis of the results show the primary drag reduction mechanism is through a reduction of wave drag.
 - Lift distribution is redistributed such that induced is higher on the wing and lower on the fuselage (non-elliptical shape).
- **The rapid drag optimization study helps narrow the VCCTEF design space to viable candidates that can be further evaluated using MDAO with high fidelity aerodynamic tools including RANS.**



Future Work

- Enhance modeling capabilities
 - Incorporate VSPAERO steady state panel solver
 - Incorporate VSPAERO unsteady panel solver into aeroservoelasticity framework
 - Extend framework to capture transonic and viscous physics on fuselage and tail
 - Develop methodology for analyzing more complex configurations including the truss braced wing
- Initial exploration of VCCTEF configuration and layout design conducted and can be used to guide further studies. Additional optimization are planned:
 - Stiff wing optimization
 - 20% fuel case
 - Trim optimization
 - +30%/-30% lift coefficient case
- Eventual goal is to enable MDAO optimization:
 - Modeling of configuration changes that result in structural variations, weight penalties, and power requirements.
 - Actuator models included in VCCTEF
 - Addition of other objective functions in addition to drag minimization, including transonic flutter
 - Drag reduction numbers are expected to become more refined and lower than this aerodynamic-driven study.

References



- **The research summarized in this presentation are based on the following publications:**
 - Chaparro, D, Fujiwara, G. E. C., Ting, E., and Nguyen N., "Transonic and Viscous Potential Flow Method Applied to Flexible Wing Transport Aircraft", 35th AIAA Applied Aerodynamics Conference, AIAA 2017-4221, June 2017
 - Ting, E., Chaparro, D., and Nguyen, N., "Aero-Structural Optimization of Variable Camber Continuous Trailing Edge Flap Configurations Using Transonic and Viscous Potential Flow Method", 35th AIAA Applied Aerodynamics Conference, AIAA 2017-4220, June 2017

Acknowledgments



- **NASA ARMD and AATT Project for funding support.**
- **Boeing Research & Technology, Boeing Commercial Airplanes, and University of Washington for collaboration with NASA on the development of the variable camber continuous trailing edge flap concept**
- **NASA ARC Intelligent Systems Division and NASA Advanced Supercomputing Division for support of project execution**



Thank You



- **Aerodynamic/Aeroelasticity Modeling**

- Chaparro, D, Fujiwara, G. E. C., Ting, E., and Nguyen N., "Transonic and Viscous Potential Flow Method Applied to Flexible Wing Transport Aircraft", 35th AIAA Applied Aerodynamics Conference, AIAA 2017-4221, June 2017
- Nguyen, N., Ting, E., and Chaparro, D., "Nonlinear Large Deflection Theory with Modified Aeroelastic Lifting Line Aerodynamics for a High Aspect Ratio Flexible Wing", 35th AIAA Applied Aerodynamics Conference, AIAA 2017-4219, June 2017
- Chaparro, D., Fujiwara, G. E. C., Ting, E., and Nguyen, N., "Aerodynamic Modeling of Transonic Aircraft Using Vortex Lattice Coupled with Transonic Small Disturbance for Conceptual Design," 34th AIAA Applied Aerodynamics Conference, AIAA 2016-3418, June 2016.
- Denison, M., Housman, J. A., Ting, E., Nguyen, N., "Comparison of Viscous and Inviscid Loads in a Static Aeroelastic Model of the Variable Camber Continuous Trailing Edge Flap Concept in the Transonic Regime," 34th AIAA Applied Aerodynamics Conference, AIAA 2016-3571, June 2016.
- Fujiwara, G. E. C., Chaparro, D., and Nguyen, N., "An Integral Boundary Layer Direct Method Applied to 2D Transonic Small-Disturbance Equations," 34th AIAA Applied Aerodynamics Conference, AIAA 2016-3568, June 2016.
- Nguyen, N. and Ting, E., "Inertial Force Coupling to Nonlinear Aeroelasticity of Flexible Wing Aircraft," 15th Dynamics Specialists Conference, AIAA 2016-1094, January 2016
- Ting, E., Dao, T., and Nguyen, N., "Aerodynamic Load Analysis of a Variable Camber Continuous Trailing Edge Flap System on a Flexible Wing Aircraft," 56th AIAA/ASCE/AHS/ASC Structures, Structural Dynamics, and Material Conference, AIAA 2015-1407, January 2015
- Nguyen, N., Ting, E., and Lebofsky, S., "Aeroelasticity of Axially Loaded Aerodynamic Structures for Truss-Braced Wing Aircraft," 56th AIAA/ASCE/AHS/ASC Structures, Structural Dynamics, and Materials Conference, AIAA 2015-1840, January 2015
- Nguyen, N. and Ting, E., "Flutter Analysis of Mission-Adaptive Wing with Variable Camber Continuous Trailing Edge Flap," 55th AIAA/ASME/ASCE/AHS/SC Structures, Structural Dynamics, and Materials Conference, AIAA 2014-0839, January 2014
- Nguyen, N. and Urnes, Sr., J., "Aeroelastic Modeling of Elastically Shaped Aircraft Concept via Wing Shaping Control for Drag Reduction," AIAA Atmospheric Flight Mechanics Conference, AIAA 2012-4642, August 2012
- Nguyen, N., Trinh, K., Nguyen, D., and Tuzcu, I., "Nonlinear Aeroelasticity of a Flexible wing Structure Coupled with Aircraft Flight Dynamics," 53rd AIAA/ASME/ASCE/AHS/ASC Structures, Structural Dynamics and Materials Conference, AIAA 2012-1792, April 2012
- Nguyen, N., "Elastically Shaped Future Air Vehicle Concept," NASA Innovation Fund Award 2010 Report, http://ntrs.nasa.gov/archive/nasa/casi.ntrs.nasa.gov/20110023698_2011024909.pdf, Submitted to NASA Innovative Partnerships Program, October 2010



- **Multidisciplinary Optimization**

- Ting, E., Chaparro, D., and Nguyen, N., "Aero-Structural Optimization of Variable Camber Continuous Trailing Edge Flap Configurations Using Transonic and Viscous Potential Flow Method", 35th AIAA Applied Aerodynamics Conference, AIAA 2017-4220, June 2017
- Lebofsky S., Ting, E., and Nguyen, N., "Optimization for Load Alleviation of Truss-Braced Wing Aircraft With Variable Camber Continuous Trailing Edge Flap," 33rd AIAA Applied Aerodynamics Conference, AIAA-2015-2723, June 2015
- Kaul U. and Nguyen, N., "A 3-D Computational Study of a Variable Camber Continuous Trailing Edge Flap (VCCTEF) Spanwise Segment," 33rd AIAA Applied Aerodynamics Conference, AIAA-2015-2422, June 2015
- Rodriguez D., Aftosmis, M., Nemec, M., Anderson, G., "Optimized Off-Design Performance of Flexible Wings with Continuous Trailing-Edge Flaps," 56th AIAA/ASME/ASCE/AHS/SC Structures, Structural Dynamics, and Materials Conference, AIAA-2015-1409, January 2015
- Lebofsky S., Ting E., and Nguyen N., "Multidisciplinary Drag Optimization of Reduced Stiffness Flexible Wing Aircraft With Variable Camber Continuous Trailing Edge Flap," 56th AIAA/ASME/ASCE/AHS/SC Structures, Structural Dynamics, and Materials Conference, AIAA-2015-1408, January 2015
- Kaul U. and Nguyen, N., "Drag Optimization Study of Variable Camber Continuous Trailing Edge Flap (VCCTEF) Using OVERFLOW", AIAA-2014-2444, June 2014
- Lebofsky S., Ting, E., and Nguyen, N., "Aeroelastic Modeling and Drag Optimization of Aircraft Wing and Variable Camber Continuous Trailing Edge Flap," 32nd AIAA Applied Aerodynamics Conference, AIAA-2014-2443, June 2014
- Nguyen N., Trinh K., Reynolds, K., Kless, J., Aftosmis, M., Urnes, Sr., J, and Ippolito, C., "Elastically Shaped Wing Optimization and Aircraft Concept for Improved Cruise Efficiency," 51st AIAA Aerospace Sciences Meeting, AIAA-2013-0141, January 2013



- **Aeroelastic Flight Dynamic Modeling**

- Ting, E., Chaparro, D., and Nguyen, N., “Development of an Integrated Nonlinear Aeroservoelastic Flight Dynamic Model of the Truss-Braced Wing Aircraft,” 58th AIAA/ASME/ASCE/AHS/ASC Structures, Structural Dynamics, and Materials Conference, AIAA-2017-1815, January 2017
- Tal, E. and Nguyen, N., “Unsteady Aeroservoelastic Modeling of Flexible Wing Generic Transport Aircraft with Variable Camber Continuous Trailing Edge Flap,” 56th AIAA/ASME/ASCE/AHS/ASC Structures, Structural Dynamics, and Materials Conference, AIAA-2015-2722, June 2015
- Tal, E., Nguyen, N., and Ting, E., “Comparison of Unsteady Aerodynamics Approximations for Time-Domain Representation of Frequency-Independent Aeroelastic State-Space Models,” 56th AIAA/ASME/ASCE/AHS/ASC Structures, Structural Dynamics, and Materials Conference, AIAA-2015-1841, January 2015
- Nguyen, N., Ting, E., and Trinh, K., “Flight Dynamic Modeling and Stability Analysis of Flexible Wing Generic Transport Aircraft,” 55th AIAA/ASME/ASCE/AHS/SC Structures, Structural Dynamics, and Materials Conference, AIAA-2014-1040, January 2014

- **Adaptive Flutter Suppression**

- Nguyen, N., Hanson, C., Burken, J., and Schaefer, J., “Normalized Optimal Control Modification and Flight Experiments on NASA F/A-18 Aircraft,” AIAA Journal of Guidance, Control, and Dynamics, July 2016
- Nguyen, N., Drew, M., and Swei, S., “Adaptive Modal Identification for Flutter Suppression Control,” AIAA Infotech@Aerospace Conference, AIAA-2016-0400, January 2016
- Nguyen, N., Swei, S., and Ting, E., “Adaptive Linear Quadratic Gaussian Optimal Control Modification for Flutter Suppression of Adaptive Wing,” AIAA Infotech@Aerospace Conference, AIAA-2015-0118, January 2015
- Nguyen, N. and Balakrishnan, S. N., “Bi-Objective Optimal Control Modification Adaptive Control for Systems with Input Uncertainty,” IEEE/CAA Journal of Automatica Sinica, Vol. 1, No. 4, pp. 423-434, October 2014
- Nguyen, N., “Optimal Control Modification for Robust Adaptive Control with Large Adaptive Gain,” Systems & Control Letters, 61 (2012) pp. 485-494
- Nguyen, N., Krishnakumar, K., and Boskovic, J., “An Optimal Control Modification to Model Reference Adaptive Control for Fast Adaptation,” AIAA Guidance, Navigation, and Control Conference, AIAA-2008-7283, August 2008



- **Multi-Objective Flight Control**

- Nguyen, N., Ting, E., Drew, M., Chaparro, D., and Swei, S., “Multi-Objective Flight Control for Drag Minimization and Load Alleviation of High-Aspect Ratio Flexible Wing Aircraft,” 58th AIAA/ASME/ASCE/AHS/ASC Structures, Structural Dynamics, and Materials Conference, AIAA-2017-1589, January 2017
- Nguyen, N., Hashemi, Kelley, Yucelen, T., and Arabi, E., “Performance Optimizing Multi-Objective Adaptive Control with Time-Varying Model Reference Modification,” AIAA Guidance, Navigation, and Control Conference, AIAA-2017-1715, January 2017
- Nguyen, N. and Tal, E., “A Multi-Objective Flight Control Approach for Performance Adaptive Aeroelastic Wing,” 56th AIAA/ASME/ASCE/AHS/SC Structures, Structural Dynamics, and Materials Conference, AIAA-2015-1843, January 2015
- Swei, S., Zhu, G., and Nguyen, N., “LMI-based Multiobjective Optimization and Control of Flexible Aircraft Using VCCTEF,” 56th AIAA/ASME/ASCE/AHS/ASC Structures, Structural Dynamics, and Materials Conference, AIAA-2015-1844, January 2015
- Nobleheart, W., Chakavarthy, A., and Nguyen, N., “Active Wing Shaping Control of an Elastic Aircraft,” American Control Conference, June 2014
- Nobleheart, W., Chakavarthy, A., and Nguyen, N., “Optimal and Decentralized Controller Designs for an Elastically Shaped Aircraft,” 55th AIAA/ASME/ASCE/AHS/ASC Structures, Structural Dynamics, and Materials Conference, AIAA-2014-1042, January 2014
- Ippolito C. and Nguyen, N., “A Preliminary Study for Optimal Longitudinal-Mode Flight Control through Distributed Aeroelastic Shaping,” 55th AIAA/ASME/ASCE/AHS/ASC Structures, Structural Dynamics, and Materials Conference, AIAA-2014-1044, January 2014
- Nguyen, N. and Urnes, J., “Aeroelastic Modeling of Elastically Shaped Aircraft Concept via Wing Shaping Control for Drag Reduction,” AIAA Atmospheric Flight Mechanics Conference, AIAA-2012-4642, August 2012

- **Real-Time Drag Minimization**

- Ferrier, Y., Nguyen, N., and Ting, E., “Real-Time Adaptive Least-Squares Drag Minimization for Performance Adaptive Aeroelastic Wing,” 34th AIAA Applied Aerodynamics Conference, AIAA-2016-3159, June 2016